Lucas Hauser

New photoreactive materials for structural surface modification

PhD Thesis

Dissertation

zur Erlangung des akademischen Grades eines Doktors der technischen Wissenschaften

erreicht an der

Technischen Universität Graz

Betreuer: Assoc.Prof. DI Dr. Gregor Trimmel

Institut für chemische Technologie von Materialien

Technische Universität Graz

Juli 2011

Statutory Declaration

I declare that I have authored this thesis independently, that I have not used other than the declared sources / resources, and that I have explicitly marked all material which has been quoted either literally or by content from the used sources.

……. ……..

date (signature)

Abstract

The aim of this work was the synthesis and characterization of new photoreactive molecules for surface modification. Molecules for Self Assembling as well as photoreactive polymers have been synthesized. Two different kinds of photoreactions were investigated. The first one is the so called photo-Fries rearrangement, where an aromatic ester converts after illumination with UV-light to an *ortho*- or *para*-hydroxyketone. Two molecules with phosphonic acid groups as anchorgroups with different spacers have been synthesized. The second one is the spiropyran-merocyanine system, which is in difference to the photo-Fries group switchable, each form can be achieved by using UV or visible light. In this case, two molecules for Self assembling, one again with a phosphonic acid as anchor group, the other one with a trichlorosilane. The photoreaction was first investigated by FTIR. Then the SAMs were fabricated on SiO_x surfaces and characterized by contact angle, XRR, XPS and AFM measurements. For the photo-Fries based SAMs several postmodification reactions were carried out. In a further part of the work, a new photoreactive polymer based on the spiropyran system was synthesized via ring-opening metathesis polymerization. The reversibility of the photoreaction was investigated by FTIR and UV-vis measurements

Kurzfassung

Ziel dieser Arbeit war die Synthese und Charakterisierung von neuen photoreaktiven Molekülen für eine strukturierte Oberflächenmodifizierung. Sowohl Moleküle für selbstanordnende Monolagen (SAM) als auch photoaktive Polymere wurden synthetisiert. Zwei unterschiedliche Photoreaktionen wurden hierfür verwendet. Die Erste ist die Photo-Fries Reaktion, bei der sich durch UV-Belichtung aus aromatischen Estern ortho- und para- hydroxyketone bilden. Es wurden zwei Moleküle mit Phosphonsäuregruppen als Ankergruppen aber unterschiedlichem Spacer hergestellt. Die zweite Reaktion ist das Spiropyran-Merocyanine System, welches im Gegensatz zur Photo-Fries Reaktion komplett reversibel ist und durch den Einsatz von UV bzw. sichtbaren Licht in die jeweils andere Form geschaltet werden kann. In diesem Fall wurden zwei Moleküle einmal wiederum mit einer Phosphonsäuregruppe, einmal mit einer Trichlorosilangruppe als Ankergruppe dargestellt. Die Photoreaktion wurde zuerst mittels FTIR-Spektroskopie untersucht. In weiterer Folge wurden SAMs auf SiO_x Oberflächen hergestellt und mittels Kontaktwinkel, XRR, XPS und AFM Messungen charakterisiert. Im Falle der Photo-Fries-Moleküle wurden mehrere Postmodifikationen durchgeführt. Weiters behandelt die Arbeit auch die Synthese eines neuen photoreaktiven Polymers basierend auf dem Spiropyransystems mittels ringöffnender Metathesepolymerisation. Dessen reversible Photochemie wurde mittels UV- und FTIR-Spektroskopie untersucht.

To my family

Acknowledgement

During 3 years of work at the Institute for Chemistry and Technology of Materials (ICTM), I was accompanied and supported by many people.

First of all I would like to thank my supervisor Gregor Trimmel for his support and guidance during this time and Franz Stelzer for giving me the opportunity to carry out this PhD thesis at the ICTM.

Furthermore I would like to thank Dr. Petra Kaschnitz for support concerning the NMR-spectra, Ing. Josefine Hobisch for recording the GPC measurements, Heinz-Georg Flesch for XRR measurements and Quan Shen for AFM and FFM measurements.

Special thanks goes to a great co-worker, Marco Marchl and all the other guys from the Institute of Solid State Physics, we have been a fantastic team.

Of course great thanks to the whole ICTM team, especially to “the gang”, Bernd “Fuchsi” Fuchsbichler, Harald “Damg” Kren, Christoph “Risi” Stangl, Stefan Koller and Barbara “Babsi” Rupp for the companying during and after work. Also thanks to Christopher Fradler and my bureau colleagues, for broadening my horizon with pointless knowledge after each “question-round”.

Financial support by the FWF – Austrian Science Fond project: „Design and application of tuneable surfaces based upon photoreactive molecules” (S9702-N20) is gratefully acknowledged

Finally, a very grateful thank to Julia, for always being at my side and pushing me forward, even in not so good times and to my family, my sister Tanja, my brother Andy and my parents, Ulli and Andreas, a never ending wellspring of aspiration. Chief, this work is for you.

Table of contents

1. Introduction

Photochemical processes are a very common method for the modification of surface properties or to create functional or protective coatings on nearly any substrate. Through the application of photolithographic methods, patterning in a sub-micron range is possible. These techniques have already successfully been applied to self assembled monolayers or photoreactive thin layers. The combination of photolithography and SAMs allows the creation of highly ordered surface layers with different surface properties (e.g. polarity, wettability, chemical reactivity).

During the last years several persons in this working group have already worked on irreversible photoreactions. E.g. the SCN-NCS reaction and the photo-Fries reaction in polymers but also in SAMs were investigated. Thomas Griesser worked on thiol based SAMs on gold surfaces and Thomas Höfler on silane based SAMs on SiO_x surfaces, both using the photo-Fries reaction as photochemical part. [63,126]

The aim of this work was the synthesis of new photoreactive bifunctional molecules capable for forming SAMs and of new photoreactive polymers. The first part is dealing with the photo-Fries reaction like the two above mentioned co-workers, but this time with phosphonic acid based SAM molecules. Phosphonic acid as an anchorgroup for SAMs is known from literature to build up homogenous monolayers and no tendency for any multilayer creation is given.[104] After the synthesis and characterization of the molecules, SAMs on SiO_x were produced. After characterization of the SAM, some surface modification reactions were performed.

As a second photoreaction the spiropyran-merocyanine system was introduced. This system is completely reversible; each form can be achieved by using UV or visible light. This ability to switch between the spiropyran and the zwitterionic merocyanine makes this system in a polymer to a very interesting theme for optical or electronic applications or as switchable surface-modification as SAMs. Therefore two different bifunctional SAM molecules as well as a new photoreactive polymer have been synthesized and characterized. One SAM molecule was attached with a phosphonic acid as an anchorgroup and the other one with a trichlorosilane. The polymer was synthesized by ring-opening metathesis polymerization. The reversibility was proved

by continuing UV-vis measurements under different conditions. Finally the idea was to use this polymer as a switchable interfacial layer in an organic thin film transistor (OTFT).

2. Basics & Theory

2.1. Photochemistry, photoreactions

For the IUPAC, photochemistry is defined as the use of the chemical effects of light from deep UV to IR.[1] A photochemical reaction occurs by the absorption of photons, starting when a molecule is excited from the lowest ground state (S_0) to one of its vibrational levels of the excited single state (S_1). In this excited single state, a lot of different pathways are possible for the molecule. This excited state is achieved by the energy of the incoming light. Figure 1 shows the spectra of electromagnetic radiation. The range, which is colourful depicted, is the so called visible area, from 380 – 780 nm.

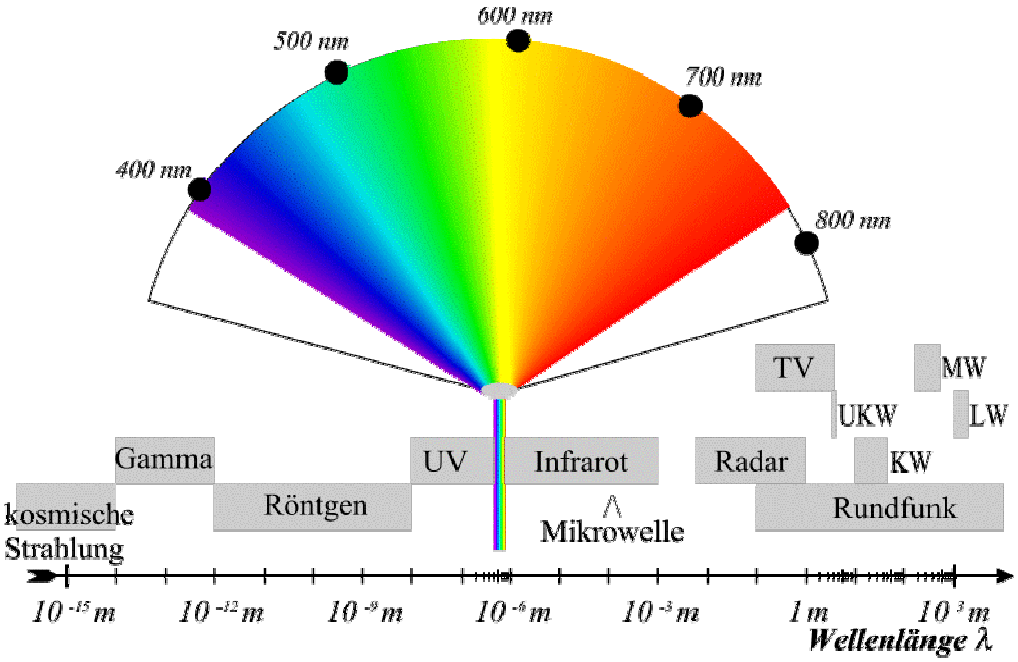

Figure 1. Spectra of electromagnetic radiation [2]

For photochemical investigations, the ultraviolet, X-Ray and the visible part of the light spectra are interesting due to fact that in this range enough energy is produced for photochemical reactions. [3,4]

This absorption is known as the First law of Photochemistry, the Grottus- Draper law (1):

(1) $R_0 \xrightarrow{h\nu} R^* \longrightarrow P$

The second one is the so called Stark-Einstein law (2). This law proclaims that the amount of radiation absorbed is limited to one quantum per molecule which takes part in the photoreaction. But some exceptions of this law have been observed during two-photon absorption processes.

(2) $1h\nu + {}^1R_0 = {}^1R^*$

The terms of quantum yield (Φ) (3), calculated out of the number of product molecules generated (n_A) per number of photons of the specific wavelength absorbed (n_Q), describes the efficiency of the radiation to the intended photoprocess.

(3) $$\phi = \frac{n_A}{n_Q}$$

A very good way for the depiction of nonradiative and radiative transitions is the so called Jablonski diagram, shown in Figure 2. After starting illumination, in the initial absorption, the excited electronically state is energetically unstable. These states of unstableness lead to a relaxation process, which can be divided into radiative or nonradiative decay processes. Examples for radiative processes are the fluorescence or the phosphorescence. In the Jablonski diagram, the three main informations, the absorption, the radiative and non radiative processes are marked with arrows. Examples for non-radiative processes are the internal conversion (IC) and the inter system crossing, (ISC), shown as waved lines in Figure 2. Internal conversion can appear when a vibrational state of a lower electronic state couples with a vibrational state of an excited electronic state. When a transition to a state with different spin multiplicity occurs, it is called inter system crossing. Through the information and results out of different photochemical investigations, like the

absorption spectra, luminescence studies or photophysical experiments, these diagrams can be constructed. [5]

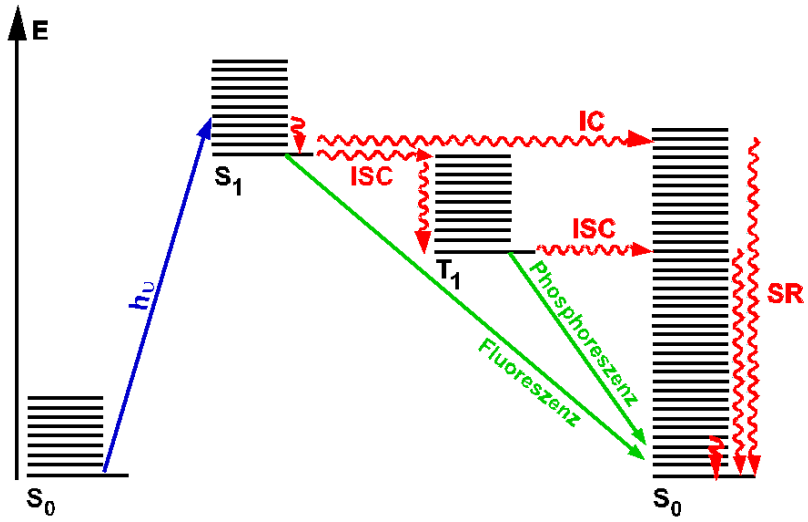

Figure 2. Simplified Jablonski diagram, where hν is the absorption or excitation, IC the internal conversion, ISC the intersystem crossing and SR the spin relaxation.[6]

It shows, that photochemical reactions occur when the internal conversion and the relaxation of an excited state leads to an excited vibrational state of another molecule. With this theoretical knowledge a lot of different photoreactions and applications were obtained in the last century and through the time people started using photoreactions as a way to photoassisted surface modification schemes. An interesting approach is the use of benzophenone functionalized siloxane layers as photolinker of polymer chains[7,8] and biomolecules[9] to the surface, where radicals are formed on the benzophenone unit. This group then reacts in a subsequent reaction with the molecules that have to be immobilized. Also interesting is the use of photoinitiators like azo-compounds[10,11,12] or dithiocarbamates[13,14], used to initiate polymerizations only in the irradiated areas of the layer ("grafting from"). Through this method, polymer can be patterned covalently to a surface. Another part of photochemistry is the application as photoprotecting group, for example ortho-nitrobenzylesters, which were used to mask amines and can be cleaved by irradiation with 364 nm light and give free amino groups at the surface.[15] Close to this system is use of photo acid generators (PAGs) or photo base generators (PBGs)[16]. PAGs are cationic photoinitiators, which have to fulfil several issues: They should have good radiation sensitivity for building enough acid groups, thermal stability and they should

include no metal atom[17]. Scheme 1 shows one type of this reaction. In this case, the PAG after illumination with UV-light builds up a free acid group and creates a 2-nitrobenzaldehyd as side product. This acid group can be used for further post-modifications.

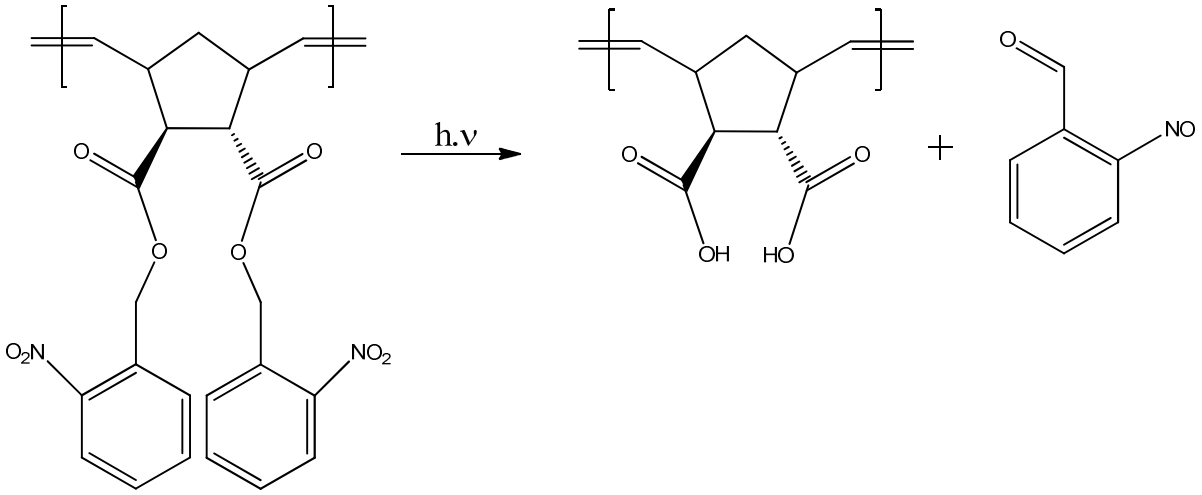

Scheme 1. Mechanism of a photo-acid generator

The next already well reviewed photoreaction is the benzyl-thiocyanate group, which undergoes after illumination a photoisomerization, leading to the corresponding isothiocyanate (Scheme 2).

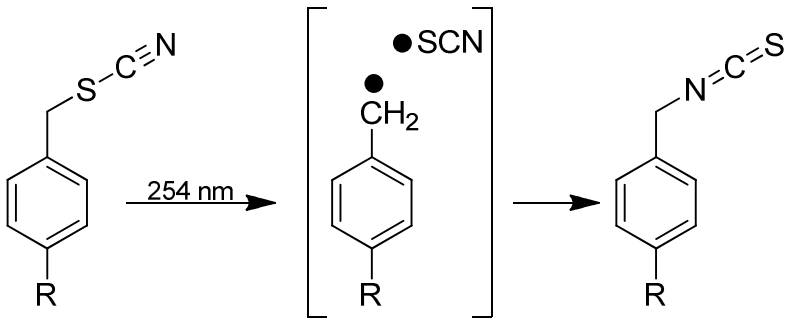

Scheme 2. Mechanism of the thiocyanate photoreaction

This photosensitive molecule can easily attached by using the corresponding rhodanide ions. Lex et al. described the use of this photoreaction for surface patterning by using trialkoxysilane as anchor group for thin-film technology[18].

Another interesting part of photochemistry is the photochromism. Photochromism is defined by IUPAC as a "*reversible transformation of a chemical species induced in*

one or both directions by absorption of electromagnetic radiation between two forms, A and B, having different absorption spectra." [19]

Photochromism bases on the reversible transformation of an isomer to another stable isomer. This transformation in the chemical structure also effects a lot of different properties, like the wettability, the dielectric constant, the redox potential, polarity, conductivity and so on. This special ability to change these parameters makes the photochromic materials an interesting part in a lot of different applications, like as gate dielectrics in organic thin film transistors, as selective ion sensors[20], full color rewritable films[21], for optical data recording and storage[22] or photo-induced magnetization in polymers.[23] Figure 3 shows some types of photochromic groups, used in today's technology.

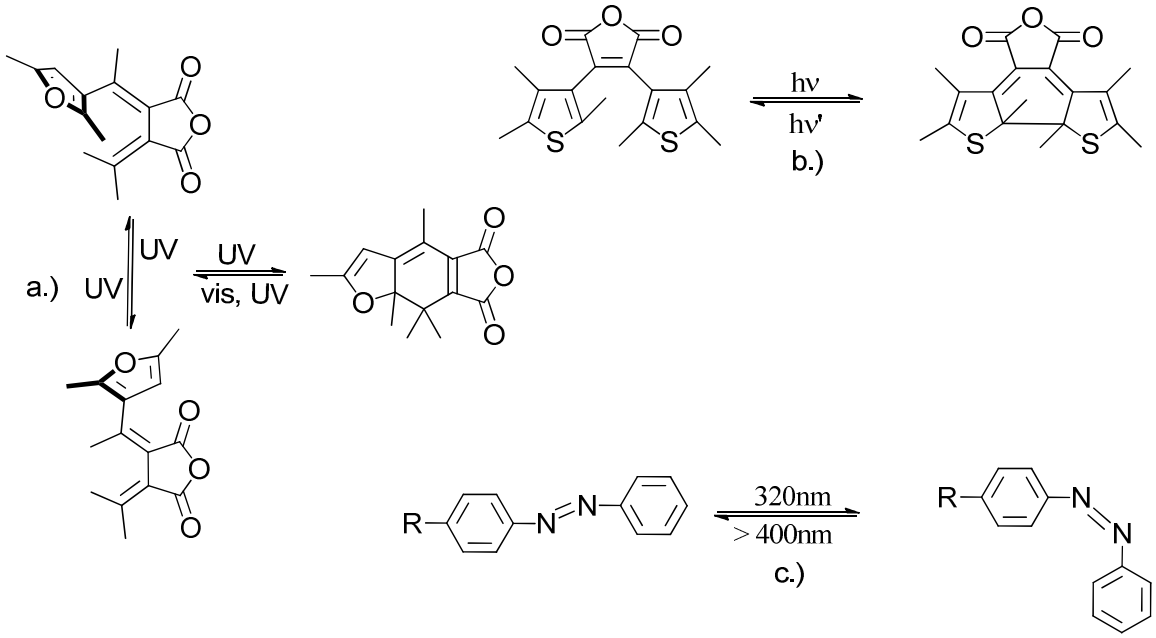

Figure 3. Three different types of photochromic reactions: (a) fulgides, (b) diarylethenes and (c) azobenzenes

On the top right diarylethenes are depicted, one of the most explored photochromic molecules, used for a lot of different applications. Down on the right, the isomerising azobenzene reaction is shown, very often used for data storage.[24] The third group are the so called fulgides, including a three state mechanism. In this work, one of the

most widespread group of the photochromic compounds was used, the spiropyrans, described in the next chapter.

2.1.1. Spiropyrans

The photochromic behaviour of spiropyrans was first reported by Fischer and Hirshberg in 1952 [25]. The reversible photochromism of this molecule involves two stable isomers, the neutral spiropyran and the zwitterionic merocyanine form, including two heterocyclic parts in different orthogonal planes, which are linked by a sp^3 carbon atom in the middle, depicted in Scheme 3. An important fact is that through the change in their molecular conformation, a change in their physical properties, like the wettability, refractive index or dipole moment can be observed.

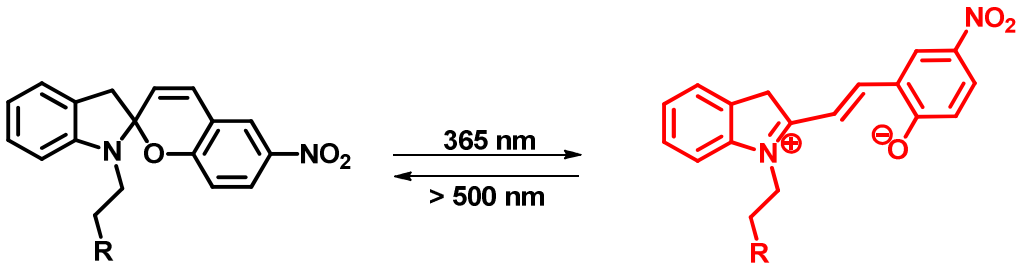

Scheme 3. Reversible photoreaction of spiropyran

The absorption spectrum of the closed molecule shows an actinic band in the range of 360 nm. Illumination in this range leads to a cleavage of the carbon-oxygen bond and switches the molecule to the coloured merocyanine isomer with an extended conjugation. Figure 4 shows a typical UV-vis spectrum of the molecule.

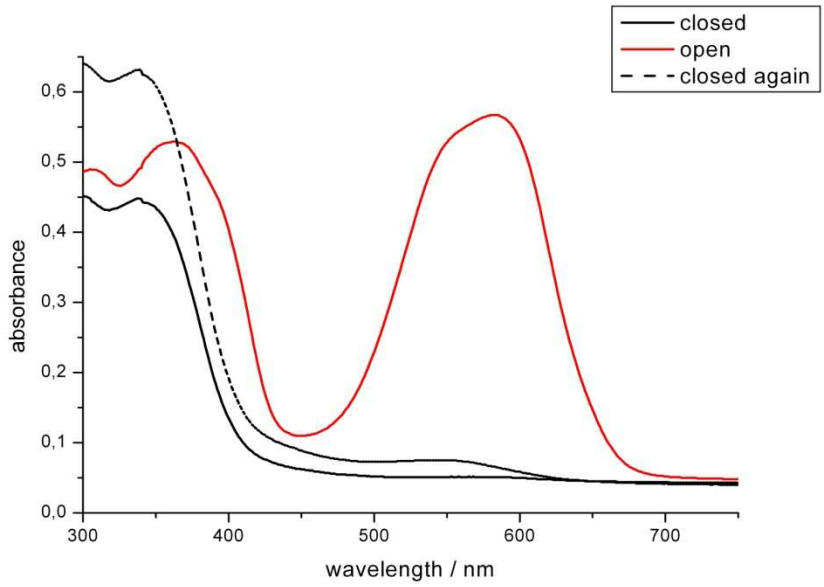

Figure 4. UV-vis Spectrum of a spiropyran molecule

Switching back to the spiropyran form can be performed by thermal or photochemical conditions. Too long illumination can lead to side products by photodegradation, for example through a radical process in combination with atmospheric oxygen[26]. This photochromism is depending on several aspects: The structure of the molecule, i.e. the positions of the substituents, the physical surrounding, temperature, pressure and of course the used medium. As an example, spiropyrans can be forced to a "negative" photochromism, where coloured solutions are obtained by keeping them in dark, whereas UV-illumination leads to the colourless solution. This effect can be achieved by different substituents, like free hydroxy, amino or carboxyl groups and is also extremely temperature depending.[27,28]

Already Hirshberg reported about the use of such compounds for erasable optical memory in 1956,[29] which can be seen as startpoint for an intensive research in the area of organic photochromism. Berkovic et al summarized the use of such compounds as photochromic liquid crystals, in non-linear optical applications as well as materials for real-time holography in his review.[30] The spiropyran ring system can be easily substituted and thus a lot of different compounds are synthetically accessible, what has been reviewed by Lukyanov and Lukyanova.[31]

In the late seventies and early eighties, scientist started to introduce spiropyrans into polymeric media, such as PMMA or PMA.[32,33] This was the starting point for the use

of spiropyrans in organic electronics and optics, but a lot of problems occurred. Due to the low stability and fatigue resistance of these photochromic materials, their practical application was limited.[34] Other problems are an appearing phase separation, crystallization, concentration gradients, most of them appearing at high amounts of the host gradient.[35] So a lot of different ways to attach covalently the photoreactive moiety to the polymer have been published.[36,37] One idea to solve the problem was to graft the photoreactive part to the backbone of the polymer.[38,39,40] Figure 5 shows one of this ideas, where at the beginning silicon based self assembled monolayers (SAMs) have been put on the surface, and afterwards through “Surface-Initiated Ring Opening Metathesis Polymerization” (SI-ROMP) a norbornene with a spiropyran side group was polymerized onto the SAM-base.

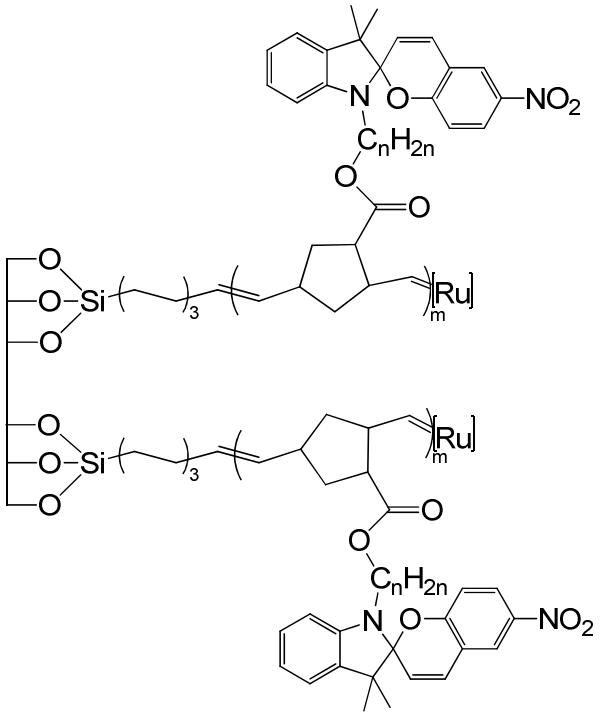

Figure 5. SI-ROMP of a spiropyran based monomer

Due to their ability of photochromic switching, the use of spiropyran-molecules as a part of optoelectronic devices[41,42,43,44,45], optical data storage[46], lipid membranes[47], nanoparticles[48], hybrid inorganic/organic matrices[49] or DNA-binding molecules[50] has grown over the last years. A very important fact for this increasing was the optimization of the lifetime stability of the system.[51,52,53] Also an interesting feature of spiropyrans are their ability to be used as a metal ion capper, which has a strong influence on their switching behaviour[54,55] and furthermore using this ability, as

photoswitchable $Fe^{2+,}$ Cu^{2+}, Ni^{2+}, Co^{2+}, Zn^{2+} selective sensors, caused by building of complexes of the zwitterionic merocyanine form with the divalent cations ($Fe^{2+,}$ Cu^{2+}, Ni^{2+}, Co^{2+}, Zn^{2+}) and unique UV-vis spectra allow to selectively analyze different metal ions with this material. [56,57]

2.1.2. Photo-Fries-Rearrangement

The second photoreaction used in this work is the so called photo-Fries rearrangement, first observed by Anderson and Reese in 1960.[58] Due to the fact, that in this photoreaction aromatic esters or amines undergo after illumination a rearrangement, the mechanism is named after the “classic” Fries- rearrangement. Anderson and Reese established in 1960 the photoreaction of phenylesters, three years later Elad et al.[59] published the same mechanism for aromatic amides.

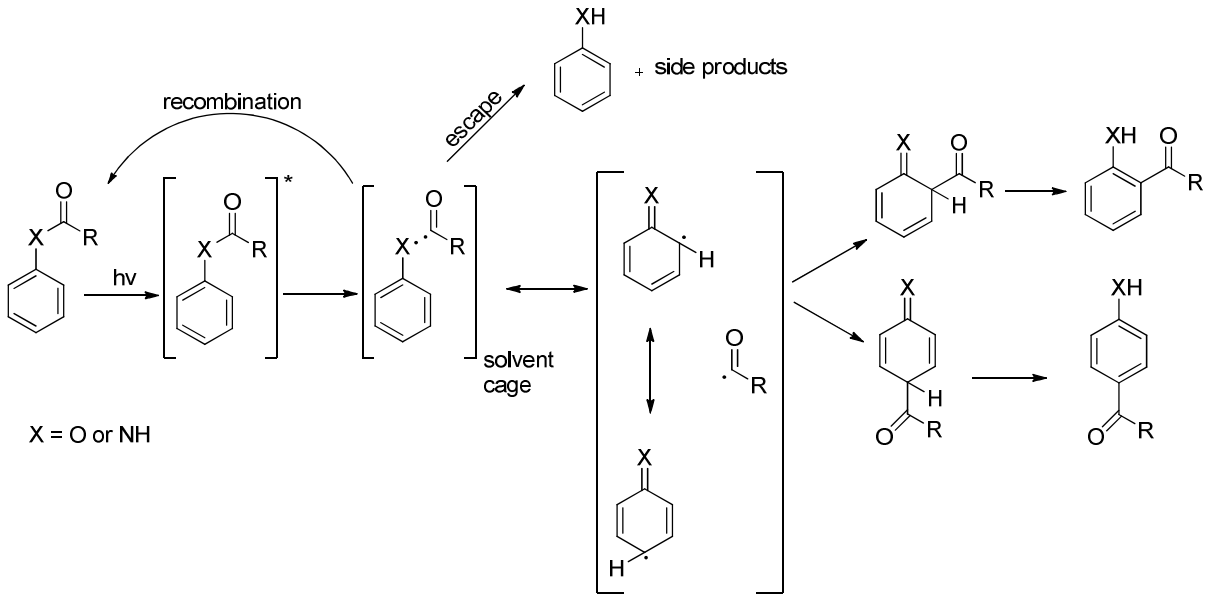

Scheme 4. Reaction mechanism of the photo-Fries rearrangement

Scheme 4 shows the typical pathway of the photo-Fries-rearrangement. In a first step after illumination, the molecule is in an excited form, leading to the cleavage of the C-O bond and the creation of two radicals in a solvent cage. In this state, two different types of reaction occur: on the one hand, escaping products can be observed; on the

other hand these radicals can recombine to derivates of cyclohexadienone, finally tautomerized to the desired product, the ortho and parahydroxyketones.

Two main types of escape reactions can occur: decarboxylation or decarbonylation. Knutsen and Finnegan[60] reported first on the creation of decarboxylation products during UV-irradiation, formed by an extrusion of CO_2 during the building of hydrocarbons out of aromatic esters. Another possibility is the decarbonylation of the acyl radical in the solvent cage caused by the diffusion of the radical pair out of the solvent cage. The yield of this side reaction is depending on the solvent: polar solvents favour the photo-Fries rearrangement, non-polar solvents advantage the creation of phenols through the promoting of the recombination out the cage.[61,62]

The creation of this ortho- and para-hydroxyketones including an intensive change in polarity and wettability of the surface makes these molecules to an interesting part of UV-light induced surface modification. In combination with self assembling monolayer technology, ultra-thin, photoreactive films can be produced and patterned.[63] As an example, several chemical post-modifications are possible through the hydroxy group, which is a very reactive part for a lot of different coupling reactions.

2.2. Self Assembling Monolayers (SAMs)

2.2.1. History

In the last two decades the interest in the field of self-assembled monolayers (SAMs) has grown enormous, although this system has a long background. Already in 1891, Pocket prepared first monolayers at an air water interface[64] and in 1917, Langmuir posted the first studies on floating monolayers on water.[65,66] In a next step, the Langmuir-Blodgett (LB) technique was invented by Langmuir and his partner Blodgett, where they started to build up thin layers on an air-water interface, by spreading them on the interface and through their hydrophobic tail they start to preassemble themselves. It took more than twenty years, till Zisman et al. could show, that it was possible to build up monomolecular layer by self assembling onto metal surfaces, using molecules with a polar group and a methyl group on the other end. This methyl group makes the surface through its upright position more hydrophobic.[67] In the eighties, the first articles about defined organosilane monolayers on SiO_2 by direct adsorption from solution[68] and alkanethiolates on gold by adsorption of di-*n*-alkyl disulfides from dilute solutions are published.[69] Through the inertness of the substrate and the simple preparation, thiol monolayers on gold are probably the most studied system. Even there are some disadvantages, alkylsilane based monolayers are also very common in today's SAM technology, especially when using silicon technology and they allow the use of different optical methods.[70] Through the huge amount of different anchor, spacer or endgroups, the field of self assembling found a new boost since the 1980's.[71]

2.2.2. Basics

Self assembled molecules should form highly ordered and oriented monomolecular layers that assemble spontaneously on suitable solid surfaces. They can be divided into three main parts[72]:

- Anchor or head group: It forms the chemical bond between surface atoms and molecule

- Alkyl chain: The inter-chain van der Waals interactions help to form ordered assembling and close packaging
- Surface or end group: This part determines the chemical and physical properties of the surface

Figure 6 shows the schematic picture of such molecules and the resulting monolayer on a substrate.

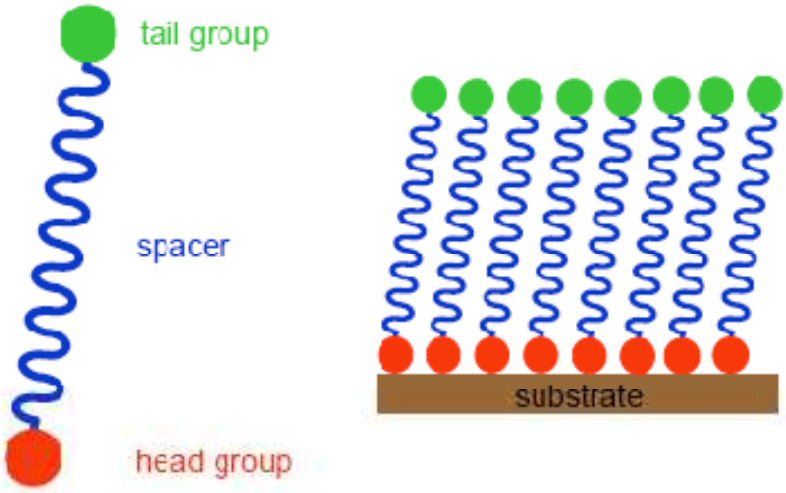

Figure 6. Scheme of a SAM forming molecule and a monolayer of the molecule assembled on a substrate.

During the last decades, SAMs have attracted much attention due to the opportunity to change surface properties, chemical or physical, of different substrates. These different substrates can be modified just by changing the anchor/head group of the molecule, e.g. silane, thiol or phosphonic acid based groups, even if they have the same spacer or end-group. When the substrate is chosen, the surface properties can easily be varied by changing the end/tail group. A hydroxy tail or other hydrophilic groups lead to a change of the wetting properties of the surface to more hydrophilic properties. Another great advantage is their preparation process, either by vapour-phase or solution deposition. For vapor-phase deposition the substrate is exposed to the vapor of a selected molecule in a closed chamber for a certain length of time. But only for certain molecules vapor phase deposition is the method of choice.[73,74,75] The common method is the solution deposition, where the substrate is immersed in a solution of the molecules in an appropriate solvent. The big advantage of this system is the huge variety of molecule/substrate combinations, which have already been

investigated including fatty acids on indium tin oxide (ITO)[76] or Al_2O_3[77,78,79], phosphonic acids on oxidic surfaces (ITO,[80] Al_2O_3,[81] TiO_2,[82] Ta_2O_5[83]), phosphates on titanium and titanium oxide surface,[84,85] carboxylic acids, alcohols and amines on mica[86,87,88] or selenols on noble metals as gold[89,90] and silver.[91] Even there are a lot of different possibilities, the two most investigated combinations for the preparation of SAMs are thiols on gold[92,93] and organosilanes on oxide surfaces like silicon oxide or glass.[94,95,96] The huge interest in this two systems is shown by the high number of review articles about them, e. g. the one of Ulman,[97] Schreiber[98] and Love et al.[99] for thiols on gold and of Onclin et al.[100] and Aswal et al.[101] for silanes on oxidic surfaces.

2.2.3. Parameters

As described in the chapter before, a lot of different reaction types between SAM molecules and surfaces are possible. This leads to a lot of different reaction types and mechanisms and finally reproducibility is a great problem for SAM fabrication. These differences are directing to other problems- different molecules and different surfaces need other parameters. So for each molecule/surface combination different parameters have to be checked. The most important are summed up on the next few pages:

water content

Silberzan [102] and Angst and Simmons[103] have shown that the essential role of the water content on the surface for the formation of a complete monolayer. Angst and Simmons prepared a tightly packed monolayer on a fully hydrated oxidized silicon wafer, whereas reaction with a dry silicon wafer gave a disordered monolayer with a lower surface coverage.

solvent

For the growing of organophosphatic films a lot of different solvents can be used, depending on the selected method and of course the surface. Schwartz et al., the creator of the in the next chapter described “T-Bag” formation, used THF as a solvent for growing on SiO_x surfaces. Due to the fact that THF can easily evaporate out of the used box this solvent is predestined for this method. [104] When using other substrates, like Al_2O_3, Nb_2O_5 or ZrO_2, Spencer et al. proposed the use of phosphate ammonium salts in aqueous solutions, yielding to well characterized SAM formations.[105] In a third approach, Wang et al. used ethanol as a solvent for the “T-Bag” formation, again utilizing the evaporation of the alcohol.

deposition time

Regarding the optimum deposition time, again no consent exists in the community. For evaporation, normally 4-6 hours are required. Other formation methods, like the before described method of Spencer, are requiring at least 48 hours.

Not only the deposition time differs, also the duration of annealing afterwards is varying, again depending on the method. Schwartz et al. are baking the wafer at 140℃ for 48h under nitrogen atmosphere, followed by a carbonate rinsing, where arising multilayers are removed by sonication in a K_2CO_3 solution, whereas Spencer et al. are only drying the wafer with a simple CO_2-stream.

temperature

In difference to silane based molecules, where temperature is an important parameter since it can affect the rate of reaction itself as well as the solubility parameter of the trichlorosilane molecules in the solvent, for organic phosphonic acid based SAM molecules the temperature has nearly no influence. For silane based molecules the threshold temperature below which an ordered monolayer is formed

was found to be a function of the chain length of the alkyl groups.[94] This critical temperature (T_c) is directly dependent on the chain length of the assembling molecules.[106,107] E.g. T_c rises from 10 ℃ for undecyltrichlorosilane (UTS) to ~ 28 ℃ for OTS. This behaviour is explained by the competition between the reaction of hydrolyzed (or partially hydrolyzed) trichlorosilyl groups with other such groups in solution to form a polymer, and the reaction of such groups with surface Si-OH moieties to form a SAM. As the temperature decreases, the preference of surface reaction decreases. Moreover, as the temperature decreases, reaction kinetics decreases as well, resulting in the diminution on the thermal disorder in the forming monolayer, the increase of the formation of an ordered assembly, and the gain of Van der Waals energy. The only aspect for phosphonic acids which should be observed is that the temperature should be in the range of the solubility of these compounds, which is normally room temperature.

chain length and composition of the compound

Another strong impact on the surface quality and composition at the end of the reaction has the chain length and the presence of a terminal group.[108] But in difference to silane or thiol based SAM molecules, there is no difference for phosphonic acid based molecules, if there is an alkyl or aliphatic spacer, even by “T-Bag” formation the same results were observed.

other

But not only the above mentioned parameters such as water content, type of solvent, deposition time and temperature have an effect on the monolayer building. Also the substrate type, the cleaning procedure of the substrate before immersing, the precursor concentration and of the course the age and purity of the synthesized molecule and solution are of crucial importance for the formation of well ordered monolayers.

To get a well defined thickness of the layer, a reference of only the silicon substrate with the oxidic layer has to be measured and the thickness of the oxide is subtracted

from the obtained value of the “double-layer” system to get the thickness of the SAM. Whereas with XRR larger areas can be measured and so an average thickness over the whole sample (sample size used in this thesis: 2x2 cm^2) of the layer is obtained. Another advantage is the possibility to measure multilayer systems in only one step and to determine the roughness.

For investigating the chemical composition of a SAM, X-ray photoelectron spectroscopy (XPS) is the most frequently used technique. Fourier-transform infrared (FTIR) spectroscopy can be used to identify special functional groups and additionally reactions in the SAM can also be followed by FTIR spectroscopy. The best method to get an overview of the morphology of the monolayer surface is atomic force microscopy (AFM) which provides a direct image of the structure of the layer. Nevertheless, AFM takes local probe images of the sample and so different areas of the SAMs have to be analyzed to get representative results. Other features, such as wetting behaviour and surface energy, can be characterized by contact angle (CA)-measurement, which is a very good fast check for the SAM quality and surface wettability.

There are quite a lot of different characterization possibilities for SAMs which were not used in this work, like second ion mass spectroscopy (SIMS), near-edge X-ray absorption fine structure spectroscopy (NEXAFS) and scanning tunnelling microscopy (STM).

2.2.4. Phosphonic acid based molecules

As already mentioned above, alkanethiols on gold and alkylsilanes on silica are the most studied systems for self assembling. But in the last two decades, even more and more different classes of SAMs have been developed. Due to the fact, that different metals were used as substrates, a lot of functional groups have been investigated. As metals tantalum, titanium or aluminium oxides were used coated with alkylsilanes, phosphonates, carboxylic acids thiols and more.[109,110,111] This work focuses on the phosphonic acid system. Phosphonic acid or phosphonate bearing molecules have been shown to form nicely ordered self-assembling monolayers on metal oxides due to the strong interaction between the hydroxyl groups of the metal oxides and the used anchor group. Figure 7 shows a schematic representation of the bonding between the phosphonic acid and the metal oxide surface.

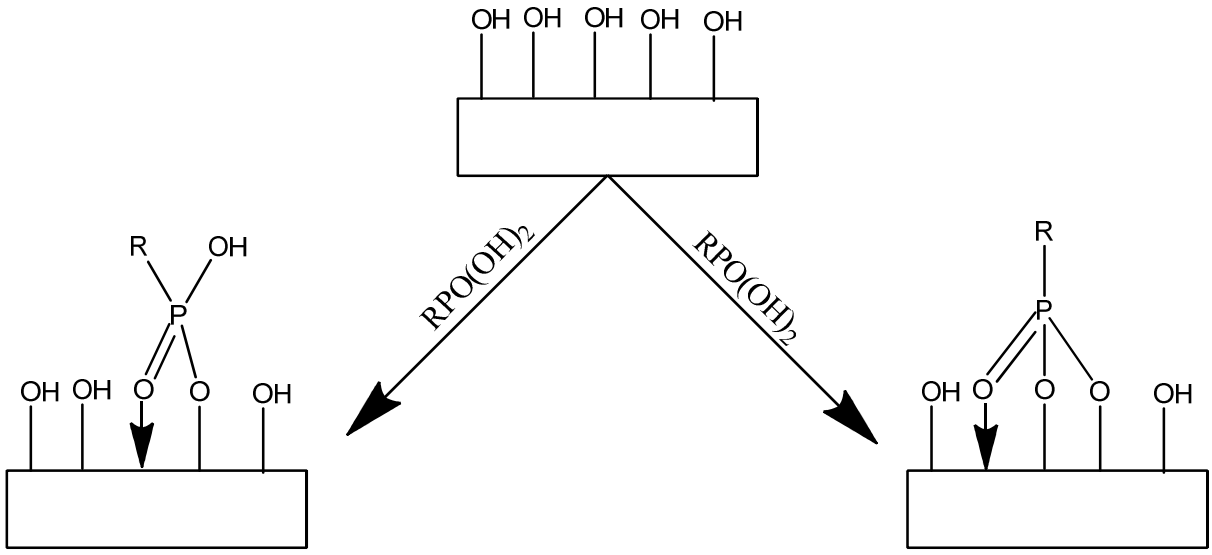

Figure 7. Schematic bonding of phosphonic acids on metal oxide surfaces

As can be seen from figure 7, phosphonic acids and phosphonates normally need a high concentration of hydroxyl groups on the surface to build up a proper bonding. That is why under normal aqueous conditions, phosphonic acids bind to for example TiO_2 but not to SiO_2 surfaces.[112] Because SiO_2 is the state of the art in today's technology, many different pathways to use these molecules for SAMs had to be

investigated. The first very important one is to use silicon wafers (100) with coated films of Al, Ta or Ti. After the coating step, the wafers were immersed into a solution of the molecule in ethanol at room temperature for 24h and finally dried.[113] In this case, they could observe that molecules with longer alkyl chains are better orientated then molecules with shorter ones, starting with low surface coverage and island building. Another approach was performed by the group of Schwartz in 2003, where they could bind organophosphates on the native oxide surface of SiO_2.[114] Herein they presented a new method, called T-BAG (tethering by aggregation and growth). The SiO_2 substrate was held in an upright position in a solution of the organo phosphonic acid below its CMC and the solvent is allowed to evaporate. So the meniscus moves slowly down and the phosphonic acid is transferred to the surface like an inverse LB-film. Therefore it might be an advantage that some kind of organized aggregation of the dissolved phosphonic acid amphiphile at the surface-air interface occurs. After heating at 140℃ to convert the surface adsorbed ph osphonic acid to a surface-bound phosphonate, in a last step, the wafer is “carbonate rinsed”, to remove possible formed multilayers. Figure 8 shows the principle of this work.

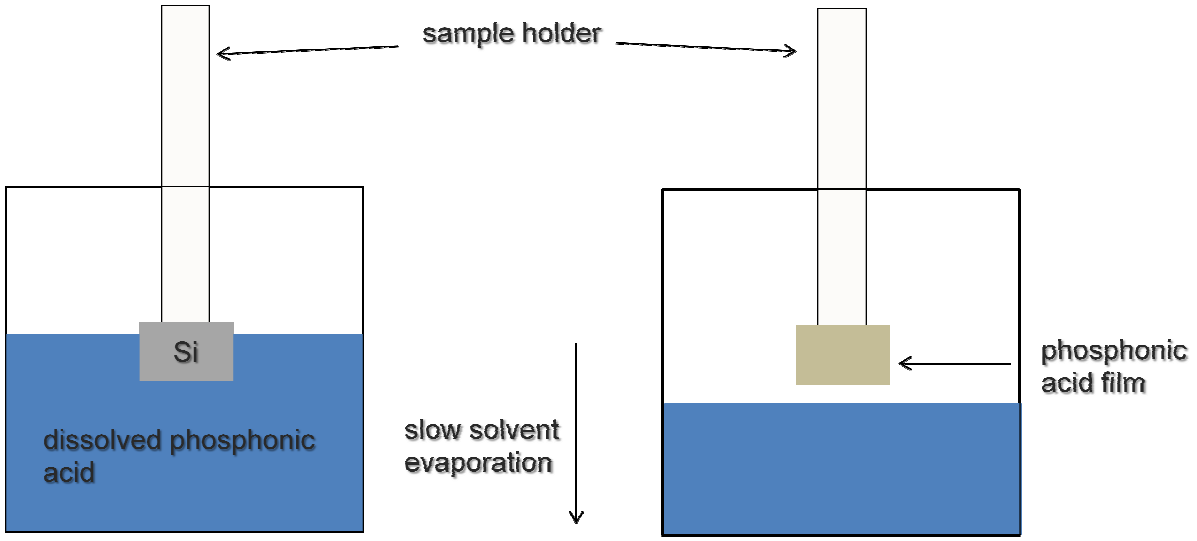

Figure 8. Method of T-BAG surface modification

In this work, the SiO_x surface was treated by piranha solution or plasma etching with followed water rinsing, both methods leading to a high concentration of hydroxyl groups on the substrate.

2.2.5. Applications of SAMs

The system of self assembled monolayers has experienced an enormous boost in the last years, although there are still problems with the reproducibility of the monolayers. Nevertheless they seem to play a very important role in today's thin film technology, where everything has to be smaller, thinner and of course without any lose of the abilities. Although most of the studies are dealing with thiols or silane based molecules, there are some publications containing phosphonates or phosphonic acid groups.

The most interesting part of the molecule is the end group. This part is the essential factor for the specific chemical and physical properties by controlling the wetting, corrosion inhibition, prevention of bio-fouling or protein adsorption.[115] This variation leads to a huge amount of applications. Talham et al. reported about the use of monolayers for supported oxidation catalysts, using manganese(III) porphyrins.[116] Another approach was the use for nanochemical patterning surfaces for biological applications, through protein capping layers.[117] The tunability of the wetting and electronic behaviour of surfaces was shown by the group of Armstrong, where they tried to modify Indium-Tin-Oxide (ITO) electrodes by using phosphonic acid based SAMs.[118] Based on this work, and on the knowledge, that phosphonic acid based SAMs form dense, robust and structurally well-defined functional monolayers, Jen et al. presented SAM based gate dielectrics for organic thin-film transistors (OTFTs).[119] Through this film, they could improve the gate leakage current, the on/off current ratio and slope down the threshold voltage in comparison to transistors without this thin film. Also the use of these phosphonic based monolayers for passivation of metal surfaces seems to be very interesting, for example for biochip applications in molecular diagnostics.[120]

In this work, the aim was the use of SAMs for photoinduced patterning and surface modification induced by UV-light.

2.3. Ring Opening Metathesis-Polymerization (ROMP)

The possibility of living polymerization and a lot of new catalysts increased the interest for the ring opening metathesis polymerization in the last decades. In the year 1971 Chauvin[121] was the first who proposed the mechanism behind the polymerization (Scheme 5) and together with Schrock and Grubbs he was awarded the Nobel-prize in 2005.

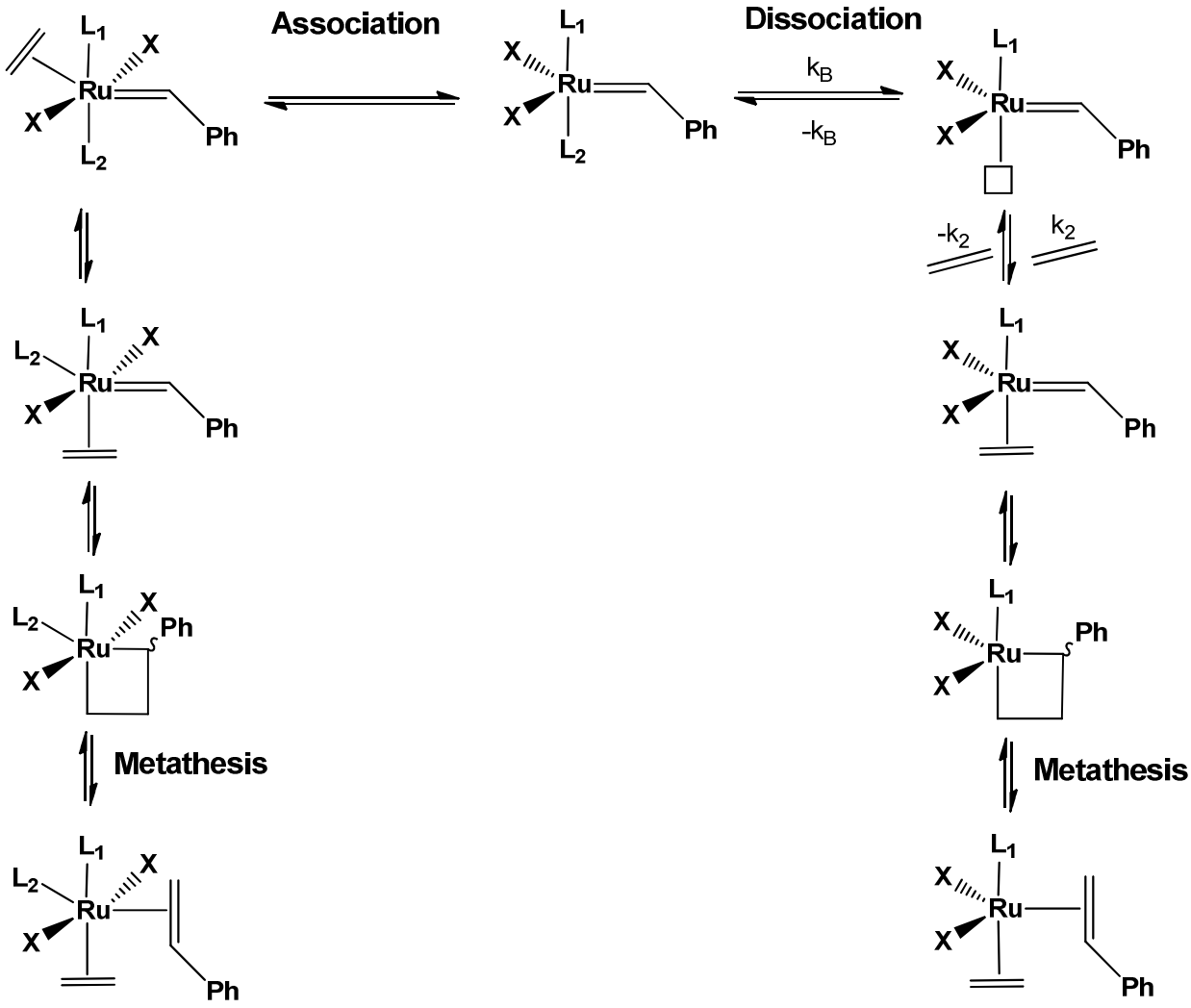

Scheme 5. Schematic pathway of a metathesis reaction

Two main pathways for the metathesis are depicted, differing in the starting reaction: To the left, starting with the association of the olefin, to the right, the dissociation of

the second ligand, which is followed by coupling of the olefin, leading to a cyclobutane intermediate. Then the metathesis takes place, until no olefin is left or the polymerization gets terminated. To move the equilibrium reaction in the last step to the product side, a molecule with a high ring strain is normally used. Typical monomers having this ability are norbornenes, norbornadienes or 7-oxanorbornenes.[122] But not only the type of monomer affects the polymerization process, also the temperature, solvent or other additives.[123] During the last years, a lot of studies concerning the initiator have been performed. Today's standard initiators are ruthenium based carbene complexes, with a high stability towards air or water, or molybdenum based carbene complexes, with sensibility against air or water. These new initiators allow a controlled living polymerization, leading to the desired molecular weights. As an example, Scheme 6 shows two initiators, Grubb's 2nd and 3rd Generation ruthenium catalysts, used during this work.[124]

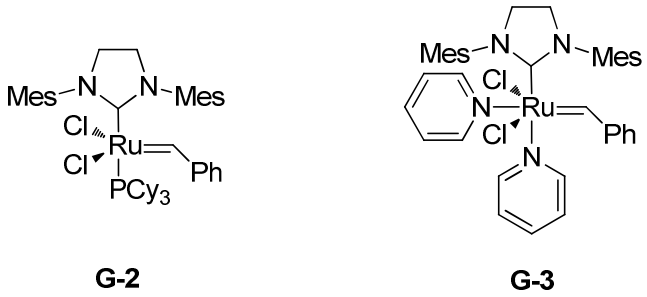

G-2 **G-3**

Scheme 6. G-2: Grubb's 2nd generation and G-3: Grubb's 3rd generation catalyst

As already mentioned above, norbornene monomers are one of the most prominent representatives in the metathesis polymerization. Scheme 7 demonstrates the ROMP with a norbornene derivate. Due to the fact that a lot of different norbornene-derivates are available, they are a good starting point for varying synthesis pathways and therefore a bicyclo[2.2.1]hept-5-ene-2,3-dicarbonyl dichloride was used during this work.

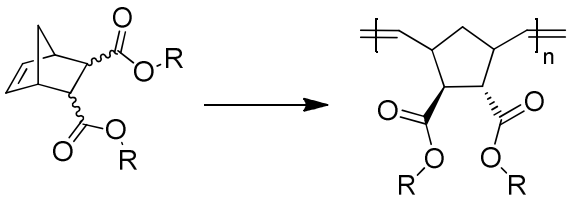

Scheme 7. ROMP of a norbornene derivate

3. Results and Discussion

3.1. Synthesis of the SAM- molecules

For realizing a photoreactive SAM molecule, first of all an anchor group has to be chosen. During the last years, two types of anchor groups have been tested in our working group. T. Griesser worked on the assembling of thiol on gold[125], whereas T. Höfler and A. Lex worked on silane based molecules, like $SiCl_3$ or $Si(OMe)_3$.[126,127] In this work, the phosphonic acid group was chosen as anchor group and SiO_x wafers as surface. Therefore four different types of molecules for self assembling have been synthesized, based on two photoreactions. Two of them have as an irreversible photoreactive end group a phenyl ester, capable to undergo the photo-Fries reaction and a phosphonic acid as anchor group. They only differ in the spacer, where one molecule (SAM-1) has a long aliphatic spacer and the other molecule a short aromatic spacer (SAM-2). The aim was to show if there is a difference in the behaviour and structuring of the assembling process.

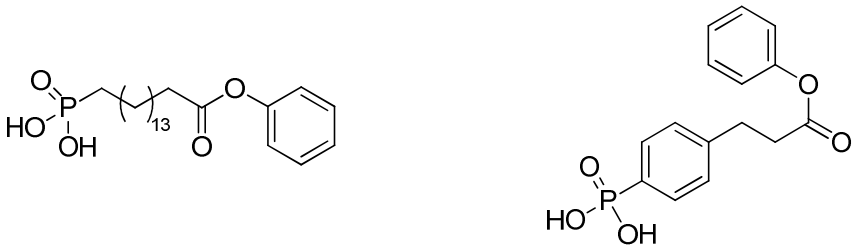

Scheme 8. Molecular Structure of the two synthesized photo-Fries SAMs, SAM-1 (left) and SAM-2 (right)

The other two molecules have a reversible photoreactive end-group, a so called spiropyran. This reversible photoreaction should allow a switchable tuning of the monolayer by illumination with UV or visible light. One molecule has a phosphonic acid as anchor-group (SAM-4), like the two photo-Fries based SAMs. SAM-3 has got the same spacer and the same photoreactive endgroup, but as an anchor group a trichlorosilane was used.

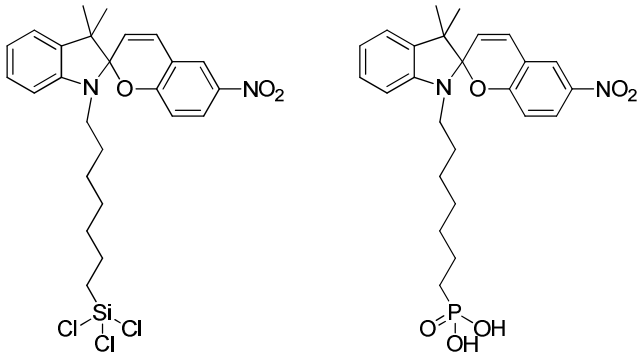

Scheme 9. Molecular Structure of the two spiropyran based SAMs, SAM-3 (left) and SAM-4 (right)

The next chapters will give some details about the different synthesis pathways, how they have been optimized and some explanations to the spectral characterization data.

3.1.1 Exploring the synthesis pathway for the Photo-Fries based SAMs

3.1.1.1 Introduction of the photoreactive part

For the introduction of functional groups to the SAM molecules, several steps have to be realized. A lot of different reaction steps have been tested to receive the best yield and performance.

During this work, for both, the anchor and the photoreactive group, at least three different reaction variations were investigated.

The first reaction which was investigated was the introduction of the photoreactive phenyl-ester to a long chain alkyl spacer with a bromide end-group. The first experiment was a direct coupling of a phenol group to the acid group using DCC. This reaction leads to a very clean product, but with a low yield, between 30-40%.[139] Therefore another reaction pathway was tried.

1.) 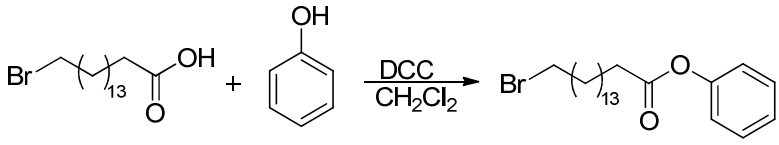

In a second reaction variant, an intermediate product was synthesized for the coupling of the phenol group. This was realized by using thionyl chloride to receive a reactive acid-chloride as coupling partner. Finally the phenol was added with pyridine as solvent and co-reagent. This version leads at the beginning to a very good yield (79%), but even after cleaning by column chromatography, there is still a small amount of the educt left in the product and the yield goes down to about 60%, which is acceptable, but the overall yield for five steps would decrease

.

2.) 

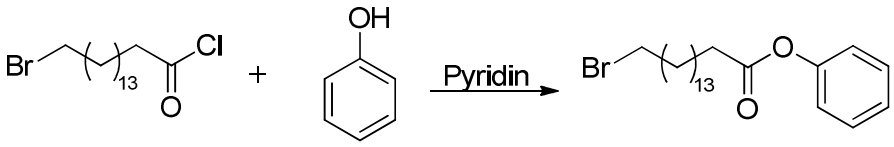

Due to the fact, that in this synthesis method the yield was higher than in the first one, a modification of this reaction was tested. Instead of pyridine, triethylamine and BHT (Butylhydroxytoluol) as a catalyst were used. The advantage of this system is the decreased reaction time caused by the catalyst. Removing of the excess phenol and triethylamine can be done quite easy by extraction and no further column chromatography was needed. This mechanism leads to a yield of 80-90%.

3.) 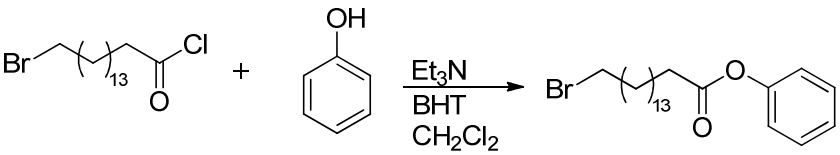

3.1.1.2 Introduction of the anchor group

After optimization of the reaction route for the photoreactive group, several reaction types for the attachment of the anchor group were performed.

Instead of the often applied Michaelis-Arbuzov reaction[128,129], phosphorylation was done in a first experiment using diethyl phosphite and a palladium catalyst. The advantage of this system is the lower reaction temperature and an easier work up procedure, a simple flash column chromatography. But the disadvantage after this reaction step was the extreme low yield, below 30%.

1.)

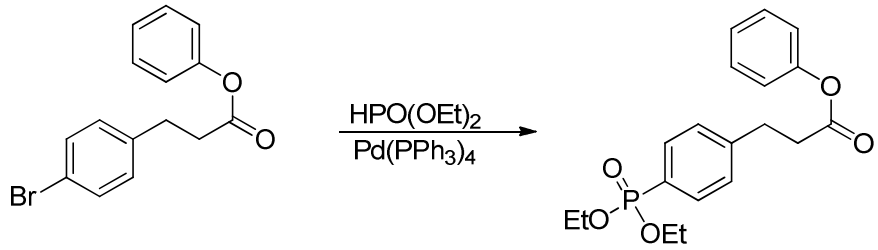

Due to the fact, that in the previous experiment the yield was low, a variation of Michaelis-Arbuzov reaction was tested. Triethylphosphite was mixed with the synthesized molecule and refluxed for 24h in chloroform as solvent. After extractions and a column chromatography, there was still an excess of triethylphosphite in the product, shown by ^{31}P-NMR measurements in Figure 9.

2.)

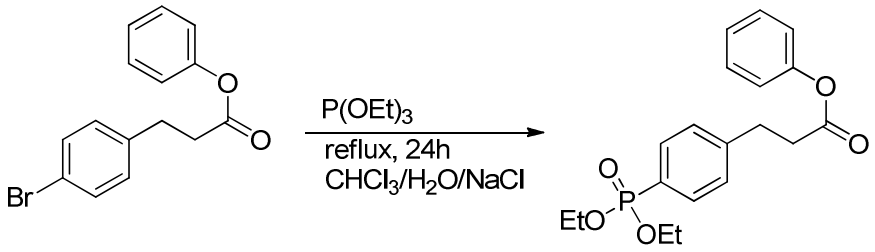

.

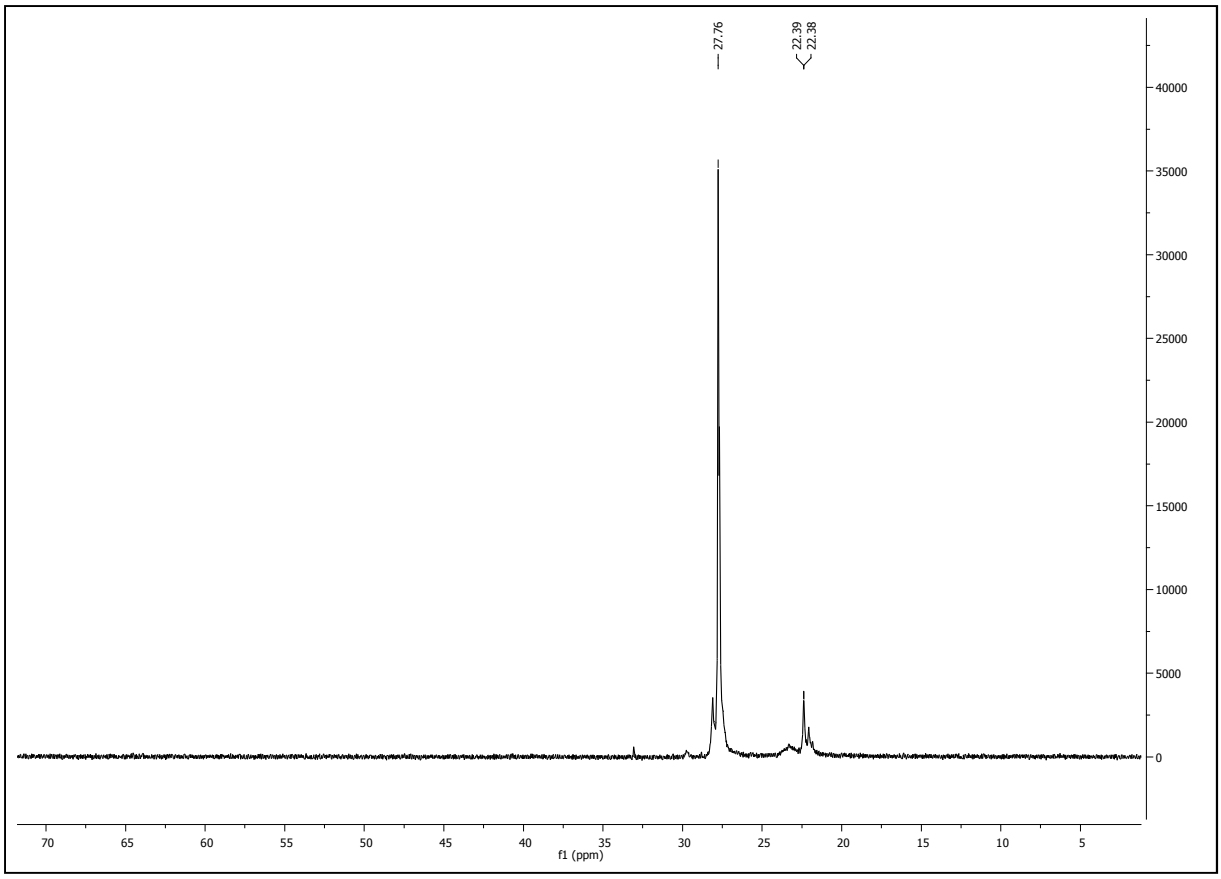

Figure 9. ^{31}P-NMR spectrum of the not complete converted phosphonic acid

In the picture above it is shown, that there is next to the product peak at 27.76 ppm still a residue of the educt at about 22 ppm left. Therefore the Michaelis-Arbuzov reaction was carried out under different reaction conditions. This time no solvent was used and the reaction time was limited to 2h. After reaction time the excess of triethylphosphite was removed via vacuum distillation. This step leads to a clean product in a high yield of about 75%.

3.)

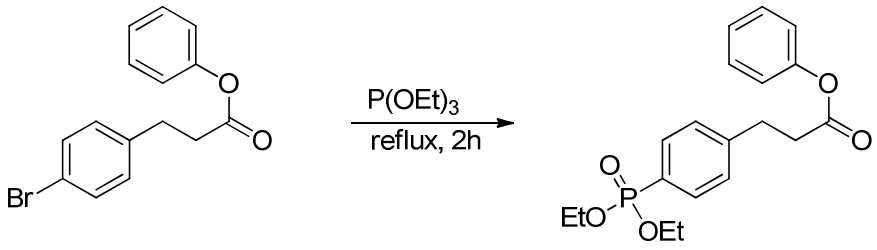

3.1.2 Synthesis of SAM-1

(16-oxo-16-phenoxyhexadecyl)phosphonic acid

In a first step the hydroxyl group of 16-hydroxy-hexadecane acid was converted to a reactive bromide for phosphorylation (1). In the second step, the acid end group was converted with thionyl chloride, leading to an acid chloride (2). For esterification, the acid chloride was treated with phenol, introducing the photoreactive photo-Fries part (3).

In the next step, the end group, at the moment a bromide group was substituted by a phosphonic ester via Michaelis- Arbuzov reaction (4) and finally after silylation and hydrolysis, the target phosphonic acid end-group as anchor group was obtained in a good yield (SAM 1).

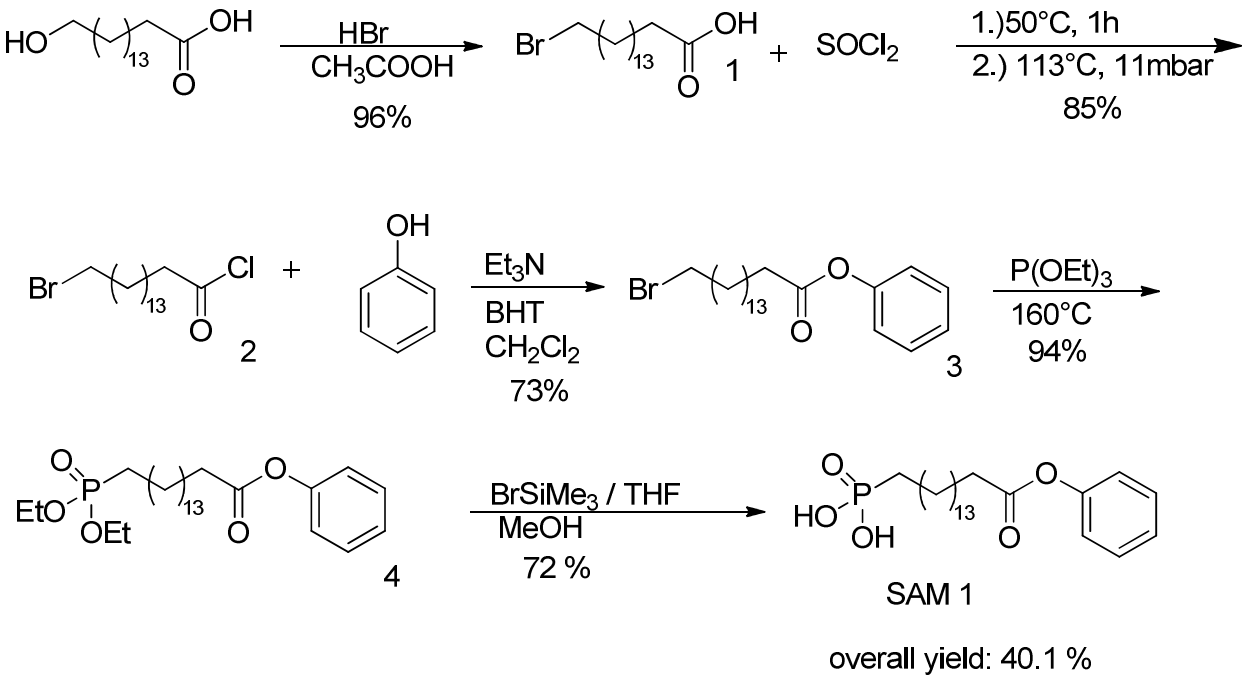

The spectroscopic data of (1), (2), and (3) are in accordance to the literature.[125] The ^{1}H-NMR spectrum of SAM 1 is divided into several parts: between 1.1 and 1.8 the peaks for the aliphatic spacer, at 2.2 the CH_2 peaks before the ester unit, at 4.8 a broad peak with 2H for the phosphonic acid group and finally the aromatic-ester between 7-7.5. As can be seen in the yields of each step, every single reaction has a

yield of over 70 %, which gives an overall yield of 40 %. This is a quite good percentage for 5 reaction steps, especially as various cleaning steps like column chromatography or extraction have been performed.

3.1.3 Synthesis of SAM-2

(4-(3-oxo-3-phenoxypropyl)phenyl)phosphonic acid

3-(4-Bromophenyl)-propionic acid was treated with thionylchloride to get the reactive acid chloride (5). Esterification was done with phenol, triethylamine and BHT as a catalyst (6). Adding of the phosphonic acid anchor group was done analogous to the reaction of 4 and SAM-1, leading to the desired phopsphonic ester 7 and finally to the targeted molecule SAM 2.

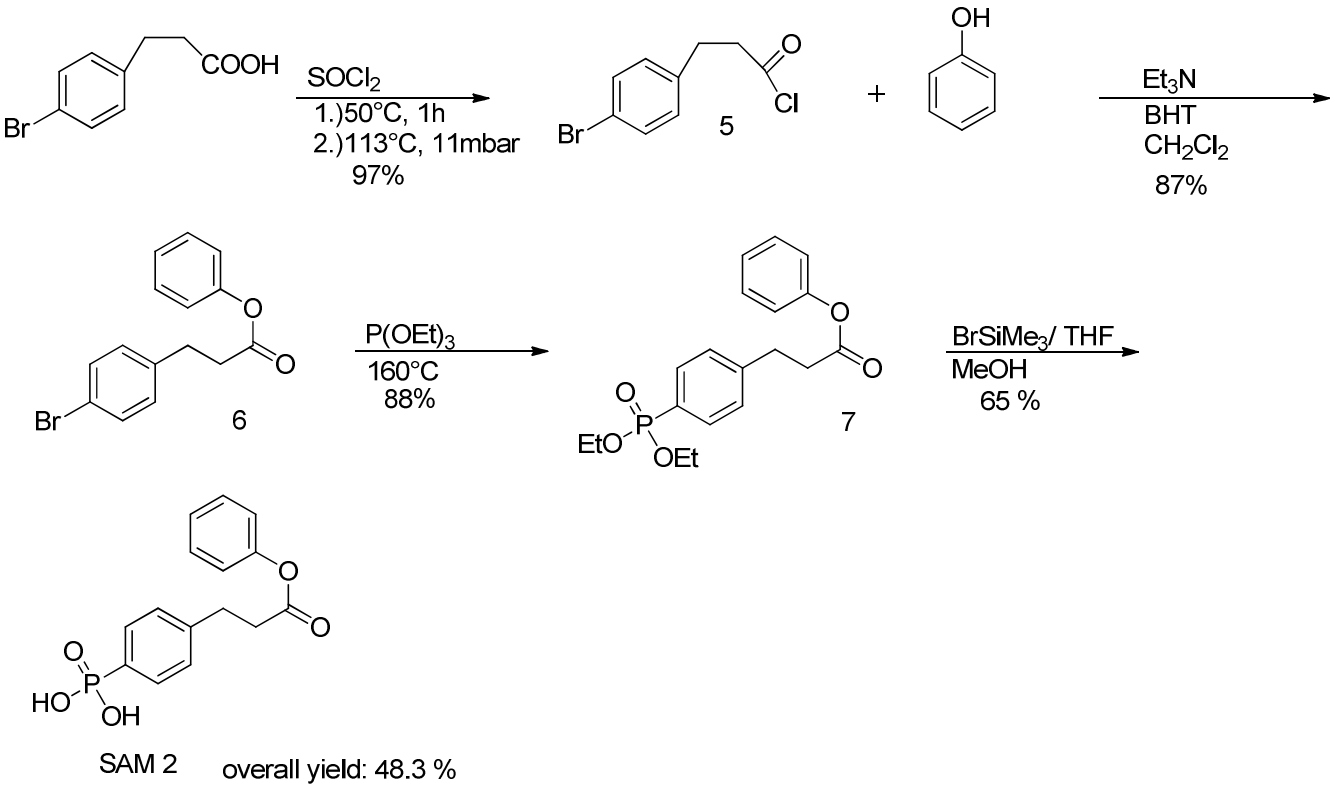

This time, starting from (6) there are no known NMR spectra in the literature for the obtained products. The ^{1}H-NMR spectrum of (6) shows the expected peaks for the aromatic units and for the CH_2-CH_2 units in the spacer

Figure 10 shows the ^{1}H-NMR spectrum of (7), the phosphonic ester. As can be seen, there are several important peaks: Between 2.5 and 3.0 the CH_2-bond between the aromatic groups, and at 4.2 the ester peaks of the phosphonic acid. Finally the aromatic peaks between 7.0 - 7.5 can be observed. Solvent residual peaks are marked by a star (*).

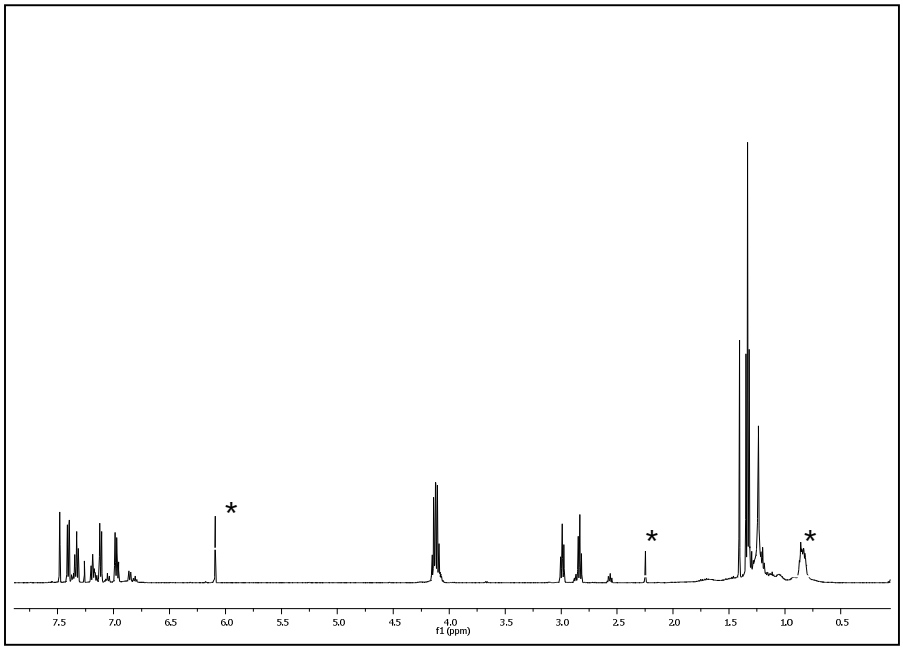

Figure 10. ^{1}H-NMR spectrum of 7, solvent residual peaks are marked by a star

The ^{1}H-NMR spectrum of SAM 2, shown in Figure 11, confirms the desired product. The spectrum gives information about the structure of the important parts of the molecule: The aromatic groups between 6.8 and 7.5, the phosphonic acid at 2.09 and the four hydrogen peaks of the CH_2-CH_2 in the middle of the molecule between 2.8 and 2.9 ppm. Solvent residual peak is marked by a star (*).

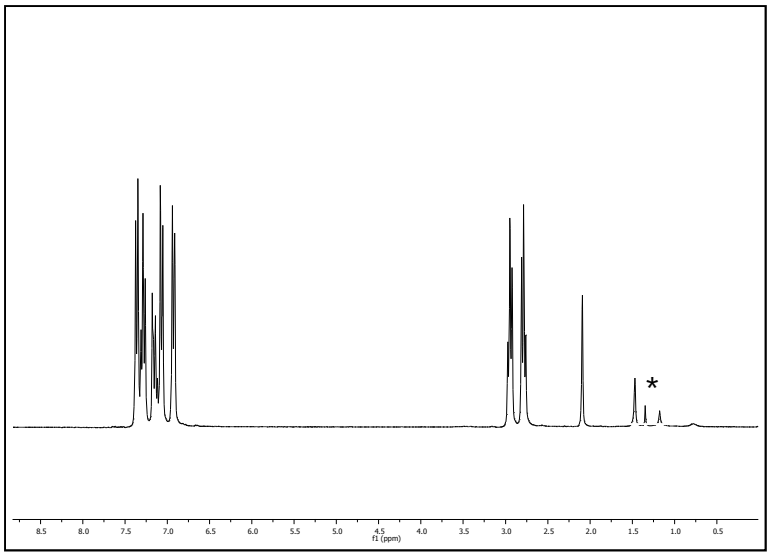

Figure 11. ^{1}H-NMR of SAM-2

A remarkable shift in the ^{31}P-NMR could be observed after the last reaction step. Figure 12 shows the ^{31}P-NMR spectra of (7) and SAM-2, the change from the phosphonic ester peak at 39.117, to the free acid group at 33.775.

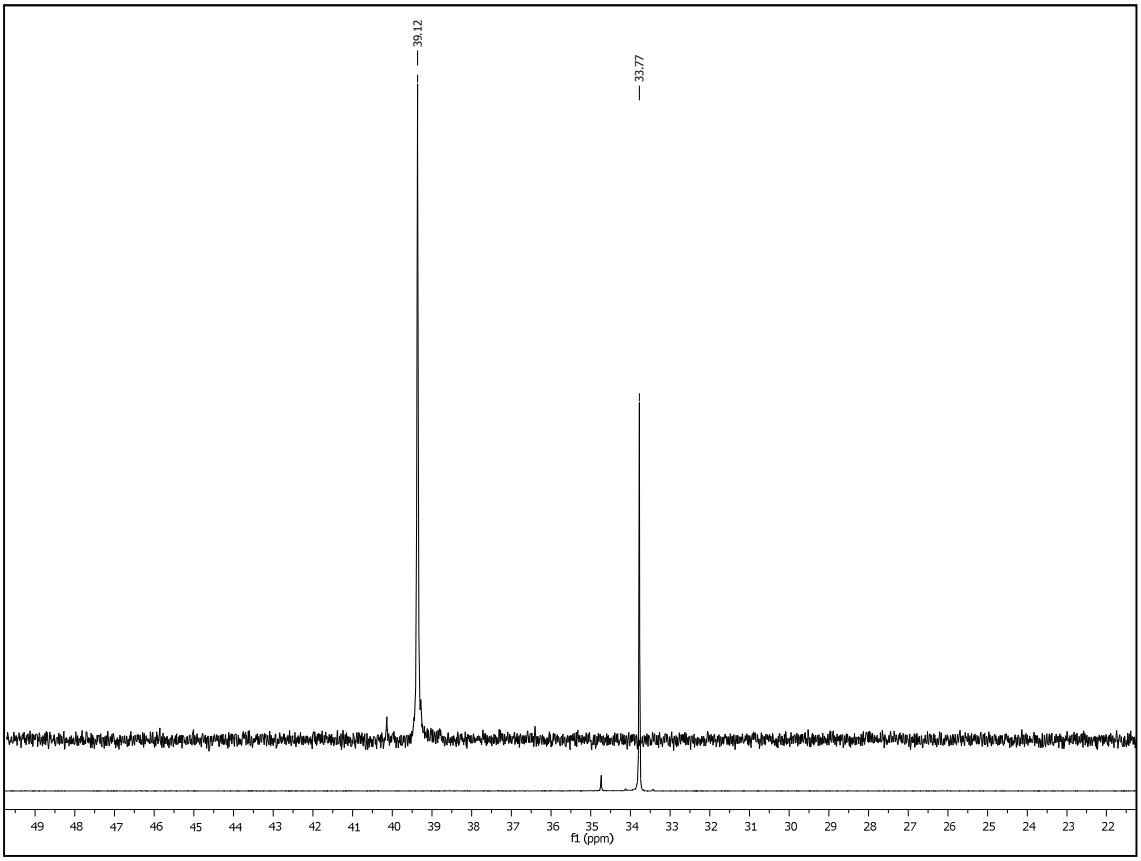

Figure 12. ^{31}P-NMR spectra of the phosphonic ester (up left) and the phosphonic acid (down right)

3.1.4 Synthesis of Spiropyran SAMs

The use of spiropyrans in self assembling systems is not very common, although the photoreaction is one of the best investigated in today's chemistry as already mentioned in the Basics. Nevertheless, the combination of SAMs and spiropyrans has not been investigated very well in the last decades.[130] The task was to find a proper anchor group and the right spacer between the photoreactive part at the end of the molecule and the anchor group, which should bind the molecule to the desired surface.

During this work, two different types of anchor groups were introduced to the same photoreactive molecule. This molecule contains a spiropyran group as the photoreactive end group, a spacer containing an alkyl chain and one of the two different head groups as an anchor groups. It is known from literature that true monolayer formation when using silane based anchor groups is difficult due to the possibility of a multilayer formation[127], whereas phosphonic based anchor groups are known for a well defined monolayer formation.[131]

Therefore, the first molecule was coupled via a trichlorosilane group, whereas in the second molecule the already known phosphonic acid group was introduced.

3.1.4.1 Synthesis of SAM-3

(3',3'-dimethyl-6-nitro-1'-(10-(trichlorosilyl)decyl)spiro[chromene-2,2'-indoline]

For the silane based SAM molecule, in a first step a spacer was introduced to 2,3,3-trimethylindolenine with an alkene end-group (8). Afterwards the photoreactive group was finalized by a reaction with nitrobenzaldehyde (9), leading to the spiropyran with an alkene spacer. Using this terminal alkene, the anchor-group was added via hydrosilylation by trichlorosilane and a platinum catalyst (SAM-3) in an overall yield of 44.8 %. The ^{1}H-NMR spectra of (8) and (9) are according to literature.[132]

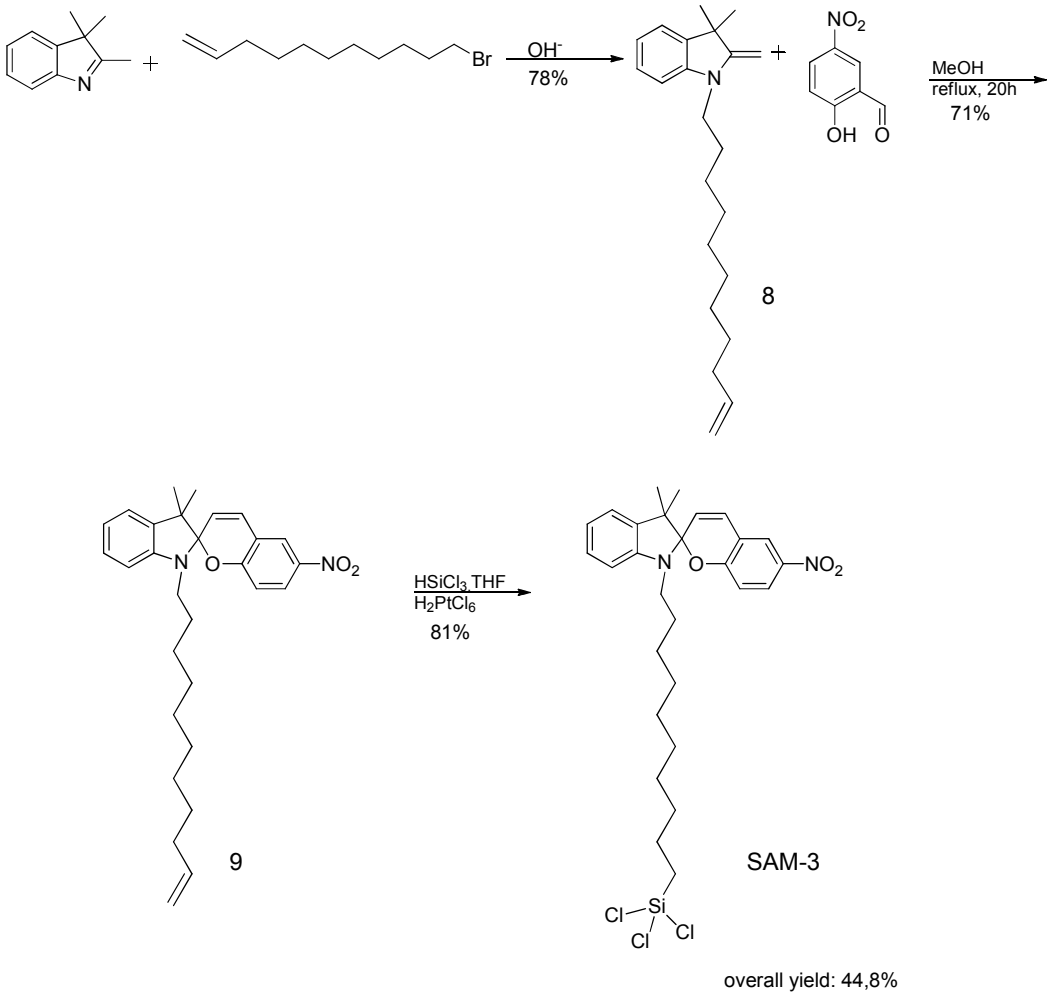

overall yield: 44,8%

^{1}H-NMR spectrum of SAM-3 shows following important data: between 6.8- 8.1 the aromatic peaks for the photoreactive group, at ~3.1 the CH_2 group next to the amine

and finally at ~2.5 2H for the CH_2 group next to the silane. The overall yield of 45 % is quite high for this reaction steps.

3.1.4.2 Synthesis of SAM-4

(7-(3',3'-dimethyl-6-nitrospiro[chromene-2,2'-indolin]-1'-yl)heptyl)phosphonic acid

This synthesis is similar to the reaction before, but the introduction of the phosphonic acid group needs more steps. Instead of an terminal alkene, here a bromide group was needed, this was done by a reaction of 2,2,3 trimethylindolenine and 1,7-dibromoheptane, leading to compounds (10) and (11).

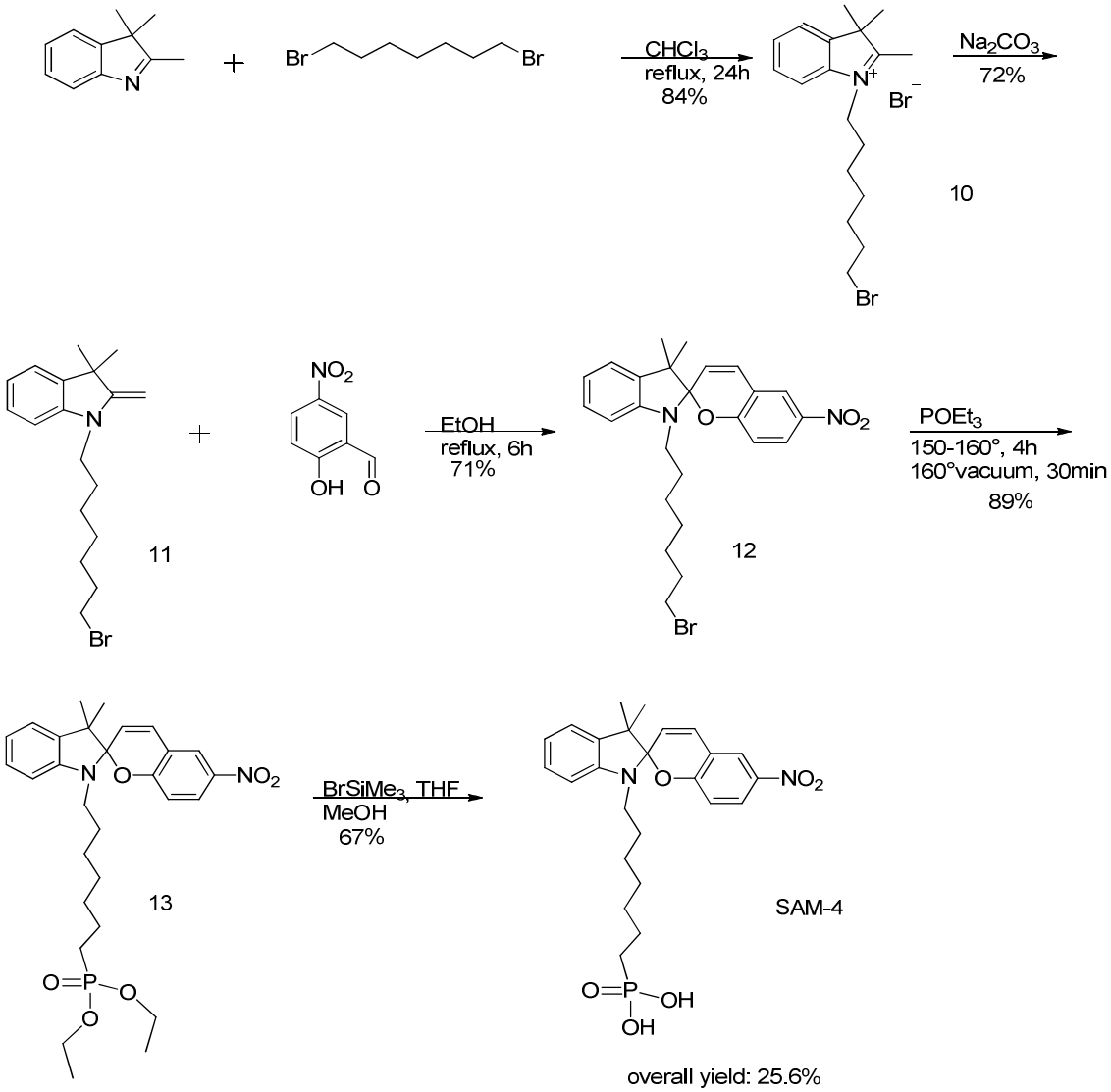

The spiropyran was finished by adding a nitrobenzaldehyd group (12). The observed peaks of the ^{1}H-NMR and ^{13}C-NMR of compound (10)(11)(12) are according to the literature.[133] After attaching of the photoreactive group, the bromine endgroup was substituted via Michaelis-Arbuzov reaction to a phosphonate (13), which was finally converted via silylation and hydrolization to the phosphonic acid (SAM-4). The NMR-peaks for (13) and SAM-4 are showing all the known peaks for spiropyrans like in molecule SAM-3, plus the OH- peaks of the phosphonic acid at ~5.6 ppm. The ^{31}P-NMR spectrum shows a singlet peak at 27.73 ppm for the phosphonic acid-group. An overall yield of 25 % is quite acceptable due to the fact that this synthesis includes five difficult steps, each with a yield over 67 %.

.

3.2 Synthesis of the photoreactive monomer

For the synthesis of the photoreactive monomer, in a first step again an alkyl-spacer, 7-bromo-heptanol, was introduced to a 2,2,3 trimethylindolenine group (14). In a second step, the photoreactive group was finished by adding an ortho-nitro-benzaldehyde (15). For coupling with a polymerizable molecule, the spacer was equipped with a hydroxyl group. The observed peaks of (14) and (15) are according to literature.[134]

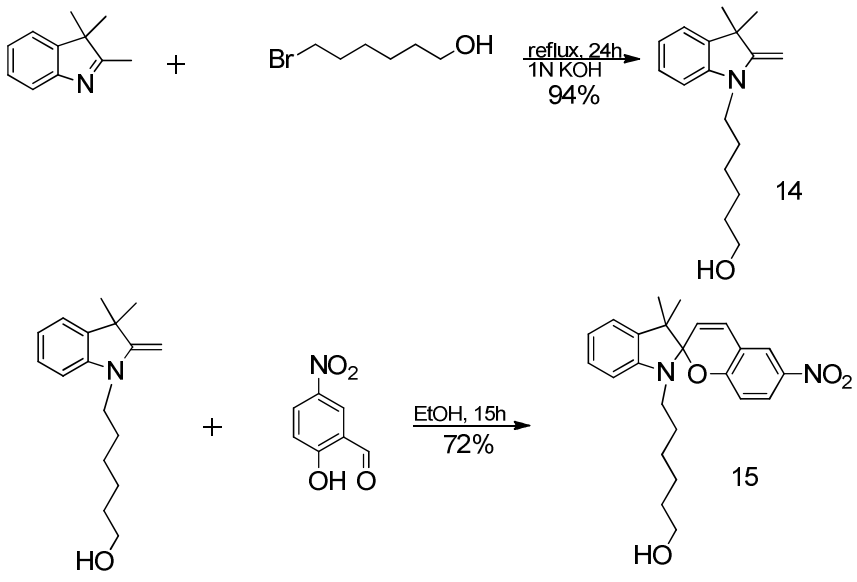

Two reaction steps with an overall yield after all cleaning processes of 68% are showing that the reaction has worked very well. In the next reaction step, a norbornene-di-acid-di-chloride was introduced as a polymerizable backbone.

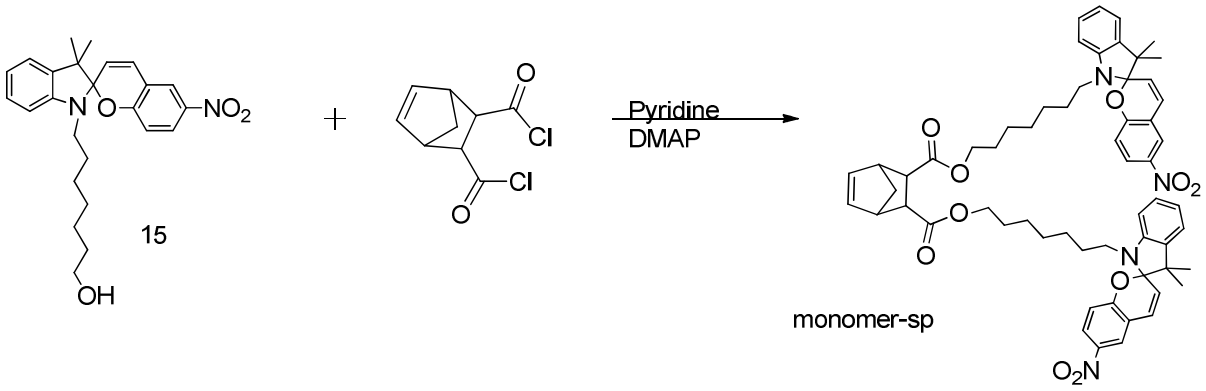

This coupling, with a yield of about 50-60% was like all other steps before, kept in dark to avoid photoreactions. The ^{1}H-NMR of the photoreactive monomer is showing following important peaks: From 6.9-8.1 ppm the aromatic part of the spiropyran, between 6.0-6.2 ppm the norbornene double bond and at ~4.1 ppm the CH_2 group next to the norbornene. Finally the spacer from the norbornene to the photoreactive spiropyran could be observed, 24H from 1.1-1.6 ppm.

3.3 Synthesis of the photoreactive polymer

The polymer was synthesized using ring opening metathesis polymerization (ROMP). The spiropyran monomer was dissolved in dichloromethane and the also in CH_2Cl_2 dissolved Ruthenium-Initiator, *$(H_2IMes)(py)_2(Cl)_2Ru{=}CHPh$,* (Grubbs 3rd generation) was added.

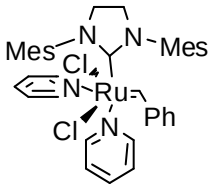

After complete conversion, the reaction was stopped with ethylvinylether and, finally, the polymer was recrystallized several times in cold methanol. After drying, the molecular weight was measured via GPC. An average polydispersity-index (PDI) of 1.84 occurred, which could be due to the sterically exigent side-groups of the monomer. ^{1}H-NMR studies of the polymer showed already known spiropyran peaks and between 5.0-5.8 the typical double bond peaks of the polymer.

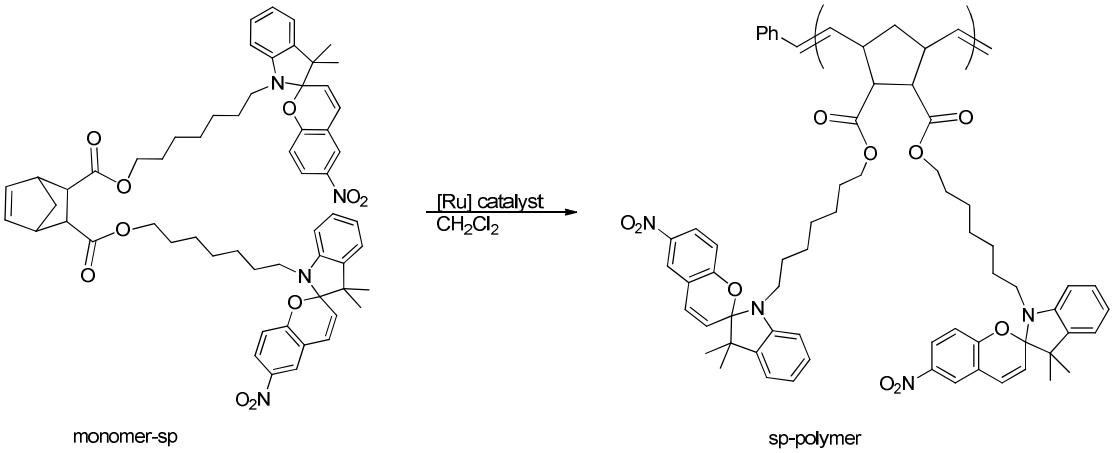

3.4 Investigation of the phosphonic acid based photo-Fries SAMs

For FTIR investigation, thin films of the molecule have been spin coated onto CaF_2 discs. For all other measurements, monolayers have been produced on thin silicon wafers, using different types of anchor coupling methods. Using the photo-Fries rearrangement, it is possible to change surface polarity, reactivity or tension just by illumination with UV-light at a certain wavelength and gives the possibility for some modification reactions.[126]

3.4.1 Preparation of SAMs on SiO_x surfaces

For the preparation of self assembling monolayers a lot of different studies are available. During this work, three different types of manufacturing have been tested. Scheme 10 shows as an example, how this self assembling system should work. The phosphonic-acid anchor group should bind covalently on the hydroxy-group covered surface and so called “self assembling monolayers” should stand in an upright position on the substrate. At the end of these SAMs, the photoreactive group, in this case the aromatic esters should be ready for the photo-Fries rearrangement. After illumination, ortho- and para- hydroxyketones are expected to be formed.

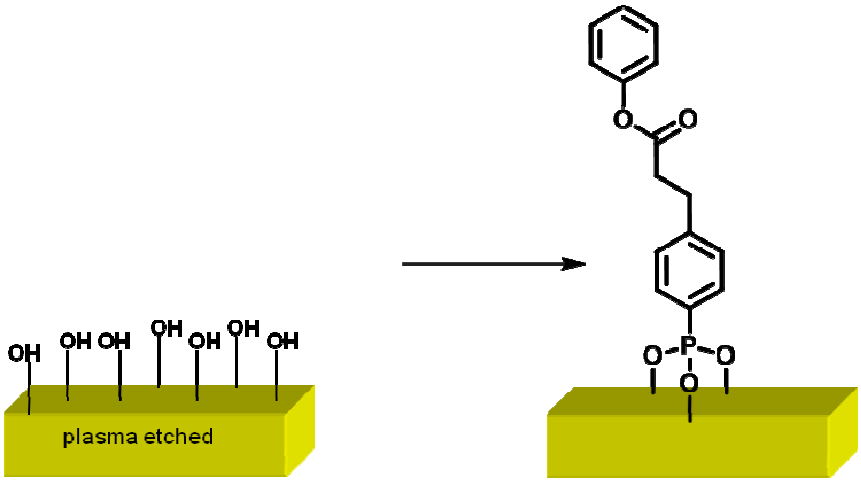

Scheme 10. Principle of SAM-capping

The first one is the already mentioned “T-BAG” type, where the oxide wafer are standing in an upright position in solution of the SAM molecule in THF for a couple of hours, till the solvent evaporates and the meniscus is below the wafer. After this step, the wafer have been dried in a N_2-stream and finally “baked” under vacuum for 48h at 140℃ to remove any solvent. Although this type of preparation is very common, in this work island-growing occurred.

In a second experiment the configuration was the same, but now the vessel was covered and the solvent was not allowed to evaporate during the exposition time. After the vacuum drying step, this time the wafers were sonicated with a K_2CO_3 solution and water to remove any multilayer on the wafer. Due to this step, the removing of any salts and any multilayers, a monolayer formation should be possible.

With the knowledge from these two different types of fabrication, a new preparation type was tested. The first steps are again similar to the already known one: The Silicon-Oxide were O_2 plasma etched for 3 min, sonicated two times in Milli-Q water and finally in deionized water, to receive a homogeneous and with hydroxyl anchor groups covered surface. After drying in a nitrogen stream, the wafers were transferred into a glove-box and put into a 5 mmol solution of the samples, but not in THF as before, here a 2-propanol solution was used. Again the vessels were covered, but now the reaction time was increased to 48 hours. Finally the substrates were dried on a hot plate at 60℃ for one hour unde r ambient conditions.

3.4.2 FTIR

Because of the fact, that SAMs are extreme thin films and that highly doped silicon wafers were used for SAM- fabrication, no direct FTIR measurements were possible to carry out. Therefore the photoreaction was investigated in liquid films on CaF_2 discs, using drop coating method.[125]

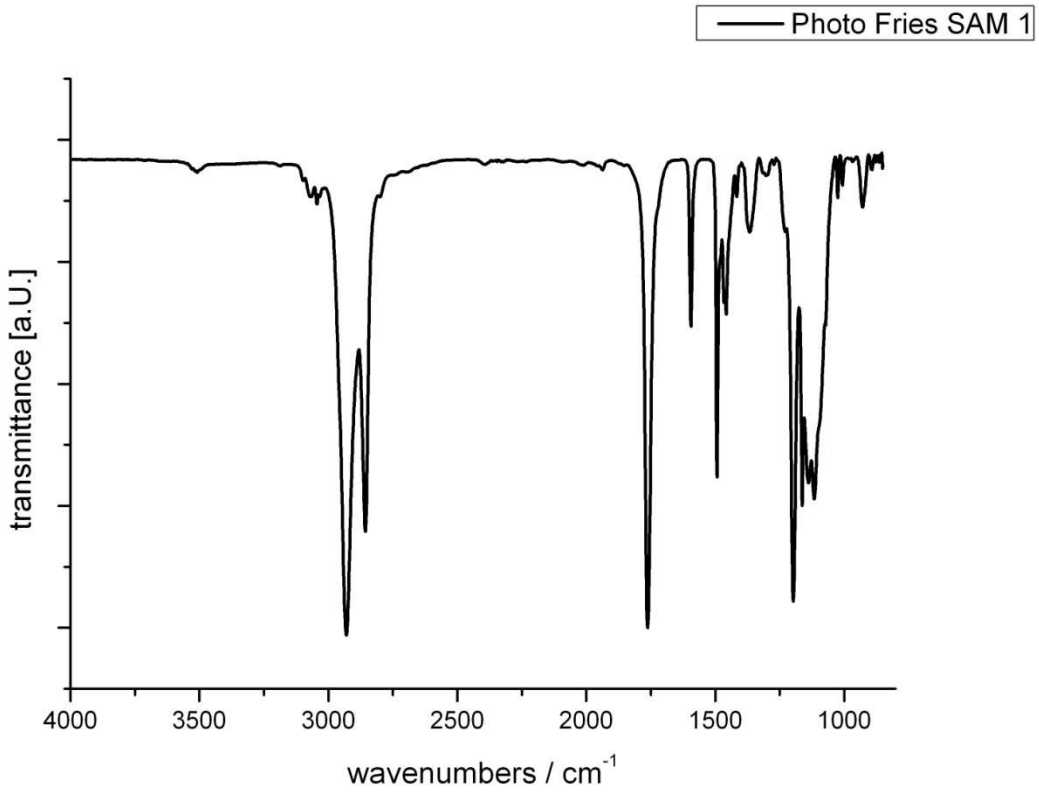

Figure 13. FTIR spectrum of a liquid film of SAM-1 before illumination

Figure 13 shows the FTIR spectrum of the Photo Fries SAM-1 before illumination. In the spectrum the signals at 1751 (C=O stretch) and at 1197 cm^{-1} (asym. C-O-C stretch) are typical for the ester units. The position of these two bands exactly meets the expectation for esters R_1-(C=O)=R_2 with R_1 being an aliphatic unit and R_2 being a phenyl ring.

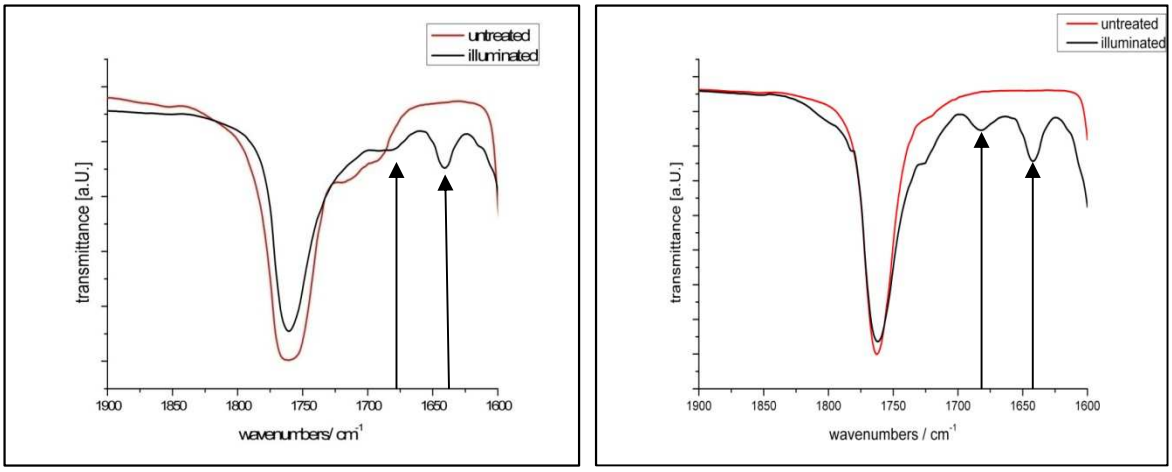

Figure 14. part of the FTIR spectra of a liquid film of SAM-2 (left) and SAM-1 (right) before and after illumination

Figure 14 shows a part of the FT-IR spectra of a liquid film of the SAM molecules before and after monochromatic irradiation of 254 nm. The spectrum of the non-irradiated film (red curve) shows a signal at 1751 cm^{-1}, the C=O stretch band, which is typical of the ester units. After UV irradiation (black curve), significant changes are observed in the FT-IR spectrum of the molecule. The signal of the phenyl ester group at 1751 cm^{-1} has decreased and a new band is observed at 1640 cm^{-1}. This signal indicates the formation of an ortho-hydroxyketone which is the expected photo-Fries product and a small peak at 1677 cm^{-1} shows the building of the para-hydroxyketone, a side product of the photo-Fries reaction.[126]

3.4.3 Contact angle measurements of SAMs

Contact angle measurements are an easy way to prove polarity changes on a surface. The substrates were prepared as described in chapter 3.4. After each step the change in the contact angle of the surface was measured with two test liquids, water and diiodomethane. As a result of this measurement method, the surface tension IFT_s with its polar $IFT_{s,P}$ and dispersity $IFT_{s,D}$ part can be observed. From these results, the polarity of a surface could be obtained.

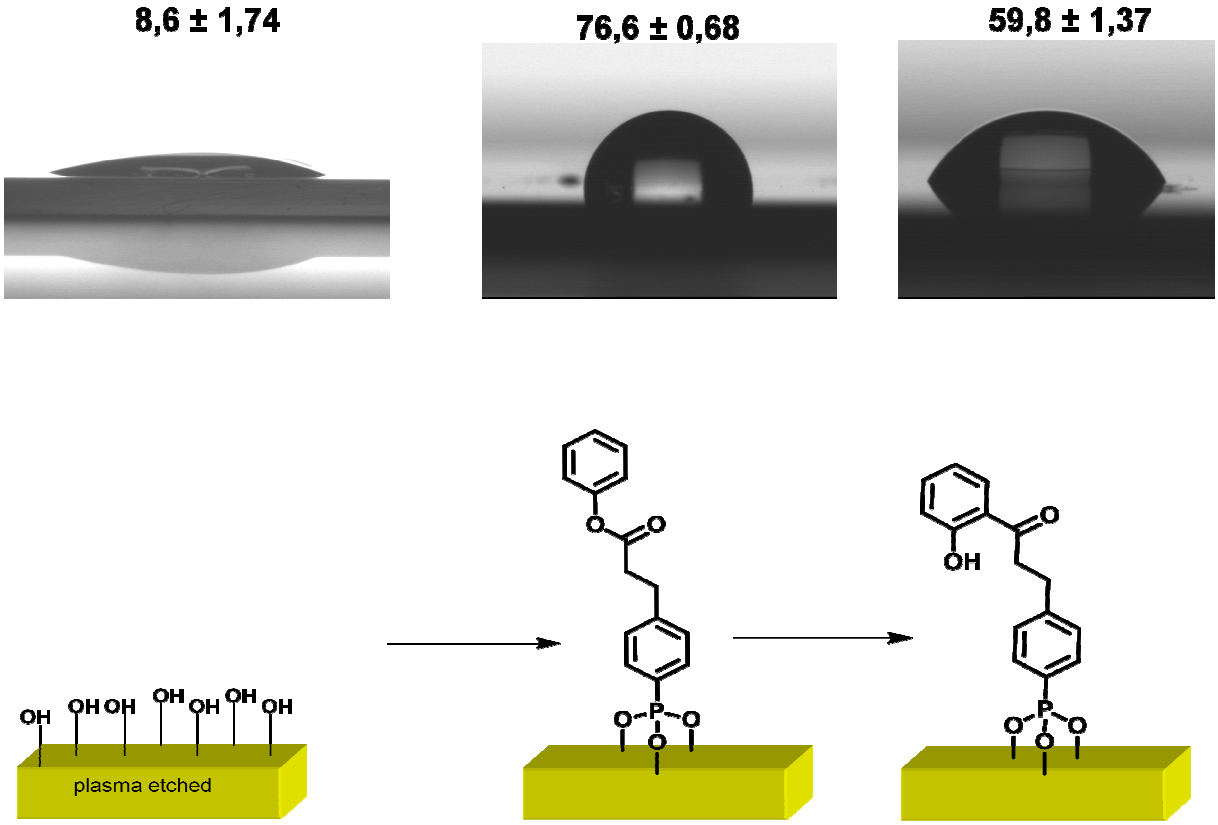

Figure 15. Depiction of the wettability change before and after illumination of SAM-2

After plasma-etching and sonicating in MilliQ-water, the contact angle of water is going down to ~8°, caused by the hydroxyl groups on the surface. In the next step the SAM molecule is bond on the surface, which makes the substrate more hydrophobic through the ester groups on the top of the molecule. Finally, after illumination with UV-light at 254 nm, when the photoreaction takes place, the contact angle decreases. This is caused by the building of the new hydroxyketones on the

surface through the photo-Fries reaction. Figure 15 shows pictures of the wettability change of the surface with water as test liquid.

Table 1. CA-measurements before and after illumination of SAM-1 and SAM-2 on a silicon wafer

	H_2O	CH_2I_2	$IFT_{s,D}$ [mN/m]	$IFT_{s,P}$ [mN/m]	IFT_s [mN/m]	Polarity [%]
Untreated SAM-1	78.4 ±1.1	38.1 ±0.4	40.6±0.1	3.8±0.0	44.4±0.1	8.6
Illuminated SAM-1	63.7 ±0.6	44.4 ±1.8	37.3±1.2	11.3±0.7	48.6±1.9	23.3
Untreated SAM-2	76.6 ±0.7	36.8 ±1.1	41.2±0.0	4.3±0.0	45.5±0.0	9.4
Illuminated SAM-2	59.8 ±1.4	49.7 ±0.8	34.4±0.1	14.6±0.1	49.0±0.2	29.8

Table 1 summarizes the measurement results before and after illumination. The decreasing of the dispersity part and the increasing of the polarity part of IFT_s are caused by the more hydrophilic surface of the illuminated side, shown by lower the contact angle of water and the higher contact angle of the more apolar diiodomethane. The calculation of the surface polarity shows a treble rising of the polarity after illumination.

3.4.4 XRR

X-ray reflectivity is a good method to determine thickness and roughness of a surface. For this measurement, (4-(3-oxo-3-phenoxypropyl)phenyl) phosphonic acid (SAM-2) was used, the measurements of SAM-1 failed due to the roughness of the layer. The XRR results in Figure 16 are showing a surface thickness of 1.35 nm with an aberration of 0.46 nm, close to the calculated molecule length of 1.38 nm. This measurement also proves that a monolayer was build and not a multilayer, which are known e.g. for silane molecules.

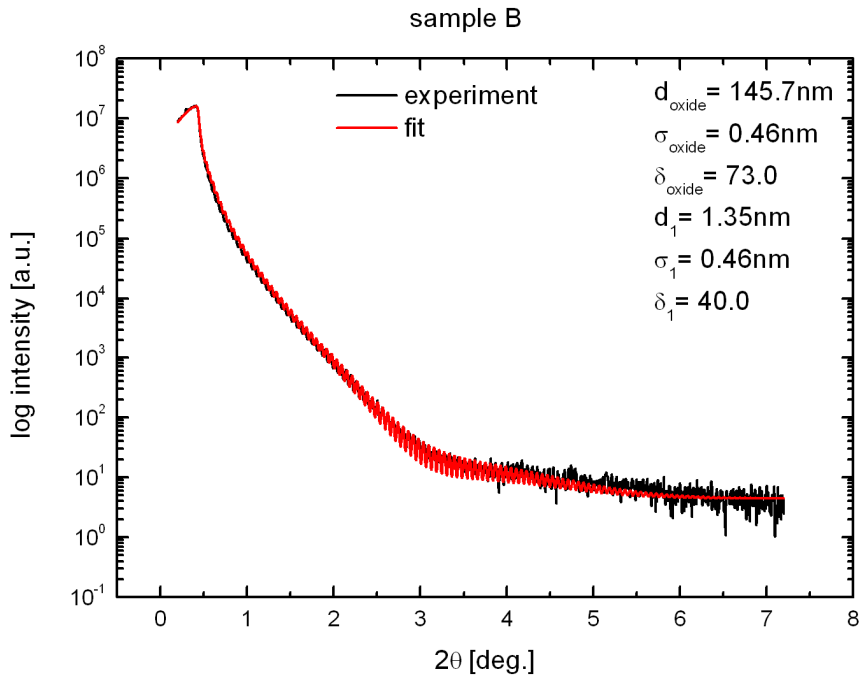

Figure 16. XRR measurement of SAM-2 on a SiOx wafer

3.4.5 AFM

Through Atomic force microscopy (AFM) information about surface roughness and coverage can be observed. Figure 17 shows a small section of a SiO_x wafer covered with a self-assembling monolayer, again SAM-2.

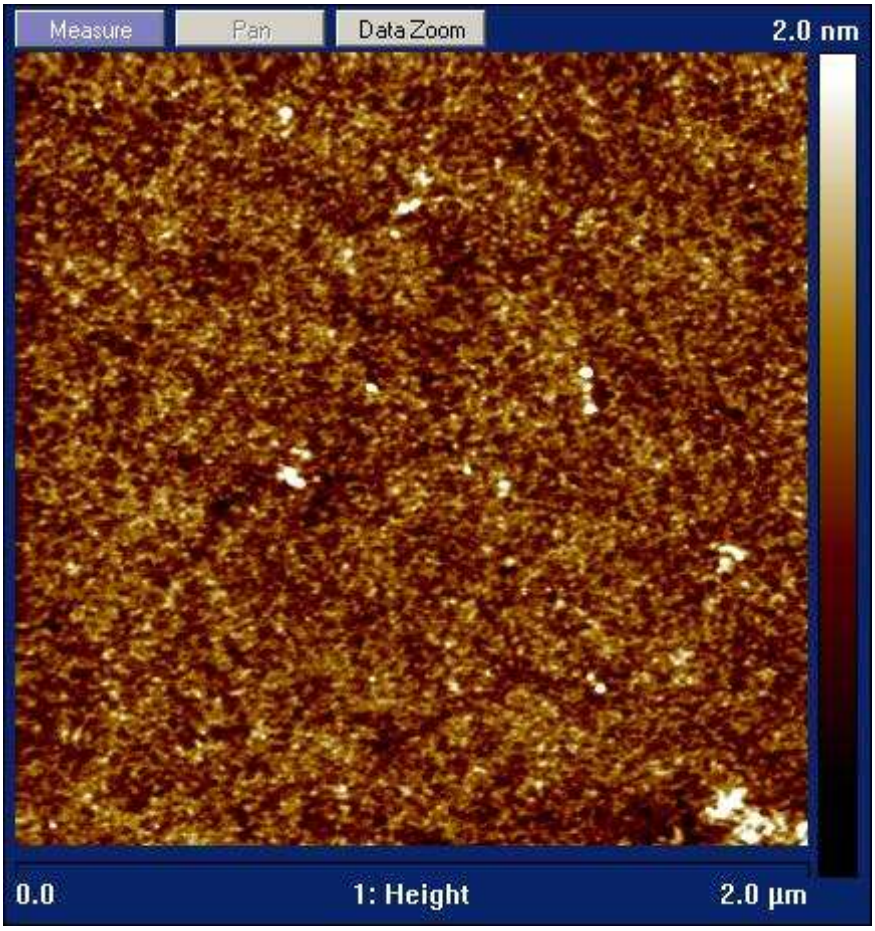

Figure 17. AFM image of SAM-1

A certain roughness occurs, but only in small range between 1.2 nm and 2 nm. The picture also shows a good coverage on the substrate with only a few contaminations, depicted as high white parts on the substrate

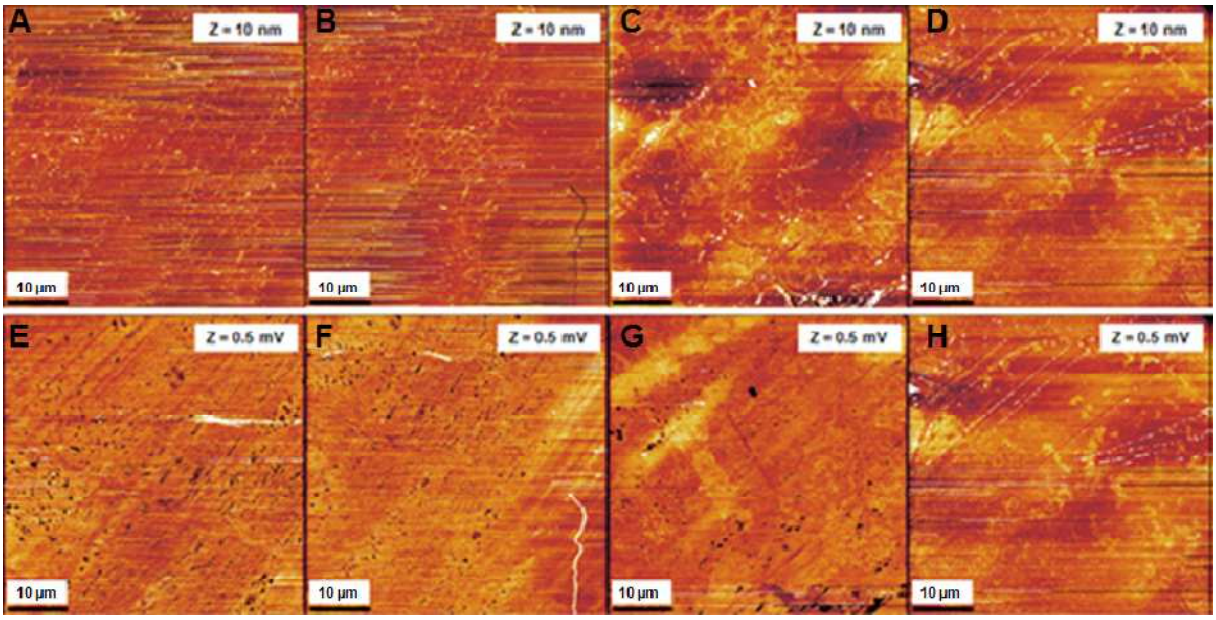

Figure 18. FFM measurements after surface patterning of SAM-1 with a 10µm mask. A-D are showing the morphologic, E-H the FF contrast.

After characterization of the plain SAMs, first attempts of patterning were carried out. Figure 18 shows the resulting FFM images using the photo fries SAM-1 molecule with an average high of 2.3 nm. For Friction Force Microscopy (FFM) which is also called Lateral Force Microscopy (LFM), the fast scan direction is set perpendicular to the long axis of the cantilever. In addition to the deflection signal normally recorded in contact mode, also the horizontal deflection of the laser beam on the four-quadrant PSD is recorded. During the FFM measurement, both topography and friction force data are recorded simultaneously. As can be seen in the pictures above, a certain roughness occurs, similar to the XRR results. In the pictures, A-D are the morphological and E-H the Friction Force (FF) contrasts. Although slightly changes through patterning can be detected, a lot of defects are determinable. These defects can have a lot of different reasons and therefore the UV-illumination has to be optimized.

3.5 Postmodification of SAMS

Based on the results of the previous photochemical measurements, some postmodification reactions were carried out, i.e. to bind substances on the surface to change surface properties like the polarity or wettability. This postmodification reaction were investigated using SAM-2

To achieve comparable surfaces, only one half of the wafer was illuminated, the other side was covered with aluminium-foil. After illumination, the substrate was immersed into a solution of the chosen molecule in dichloromethane for a couple of minutes. The aim of this treatment was to obtain two different surface properties on one substrate. This half/half illumination makes it easier to compare between the treated and non treated side. For investigation, two types of measurements have been performed: CA- measurements for determination of surface polarity, wettability and tension; and XPS measurements. Through XPS measurements changes in the elemental composition can be detected, which should only be observed on the illuminated substrate side.

3.5.1 Modification with ethylendiamine

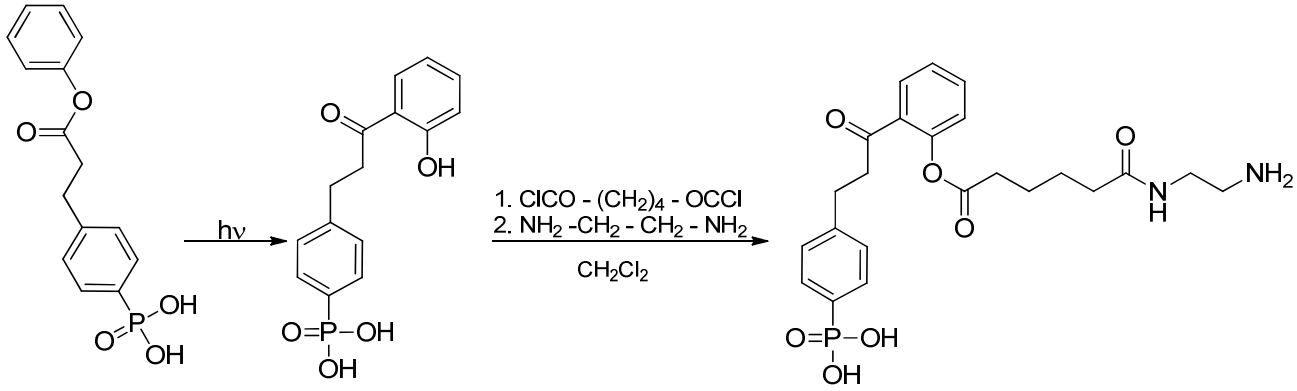

Scheme 11. Postmodification with ethylendiamine

CA-measurement:

Table 2. CA-results after postmodification with ethylendiamine

			$IFT_{s,D}$	$IFT_{s,P}$	IFT_s	Polarity
	H_20	CH_2I_2	[mN/m]	[mN/m]	[mN/m]	[%]
Untreated	76.6±0.7	36.8±1.1	41.2±0.0	4.3±0.0	45.5±0.0	9.5
Illuminated	58.7±1.5	50.1±1.0	34.5±0.1	14.6±0.1	49.0±0.2	29.8
Modificated	43.5±3.5	49.7±0.0	34.5±0.0	24.6±0.4	59.0±0.4	41.7

For this modification, the wafer was treated after half/half illumination in a first step with a mixture of adipoylchloride, triethylamine and dichloromethane for 60 min. After rinsing with pure dichloromethane, the wafer was immersed into a solution of ethylendiamine in dichloromethane for 10 min. After each step, contact angle measurements were performed with water and diiodomethane as test liquids and finally the surface tension IFT_s and their dispersive and polar components $IFT_{s,D}$ and $IFT_{s,P}$ were calculated. Starting from the very hydrophobic untreated SAM surface, the contact angle of water decreases through illumination with UV-light at 254 nm, caused by the development of the new hydroxy group. These new hydroxyl groups make the surface more hydrophilic and the polarity is increasing from 9.5 to 41.7%.

After modification with ethylendiamine, the surface gets even more hydrophilic caused by the capped terminal amino groups.

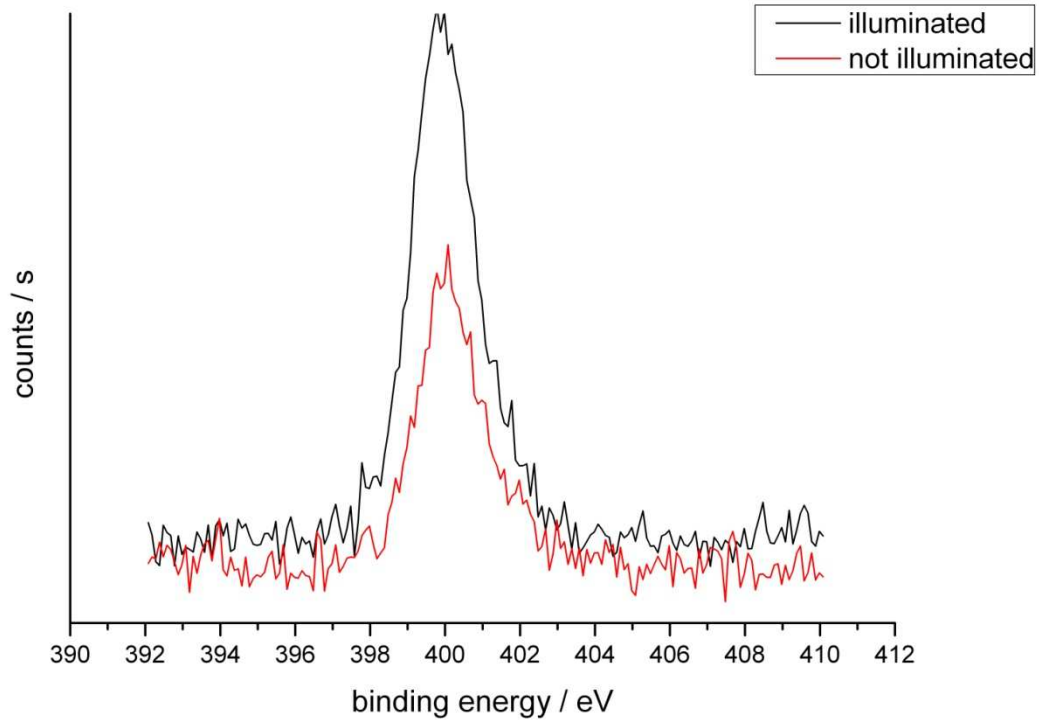

Figure 19. XPS N1s spectra of nitrogen on the untreated side (red) and the modified side (black)

The XPS measurements in Figure 19 show the nitrogen peak on the untreated (red) and on the modificated (black) side. As can be seen, there is already a small amount of nitrogen on the untreated side, nearly half of the amount of the treated side. This can have some reasons. Maybe the wafer was not very well covered during illumination and thus a small part of the “untreated” was photochemically converted.

3.5.2 Modification with perfluorobutyrylchloride

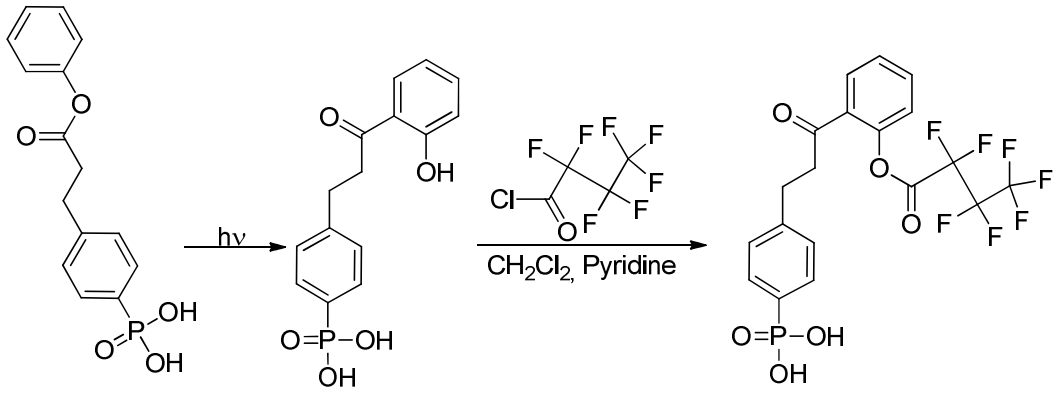

Scheme 12. Postmodification with perfluorobutyrylchloride

CA-measurement:

Table 3. CA results after postmodification with perfluorobutyrylchloride

			$IFT_{s,D}$	$IFT_{s,P}$	IFT_s	Polarity
	H_20	CH_2I_2	[mN/m]	[mN/m]	[mN/m]	[%]
Illuminated	59.9±1.4	49.7±0.7	34.4±0.1	14.5±0.1	49.0±0.2	29.6
Modificated	80.5±2.3	50.8±2.0	33.8±0	5.0±0.1	38.8±0.2	12.9

In this case, shown in Scheme 12, the half illuminated wafer was immersed into a solution of perfluorobutyrylchloride in triethylamine and dichloromethane for 10 min. As can be seen in Table 3, the contact angle measurement results, modification with perfluorobutyrylchloride after illumination makes the surface more hydrophobic and oleophobic, caused by terminal fluorine molecules on the SAM. Even if there are no changes for the apolar diiodomethane, the contact angle of water is shrinking over 20%. Through the decreasing of the polar part, the surface tension is going down from nearly 50mN/m to 39mN/m and the whole surface polarity is decreasing from 30% to 13%.

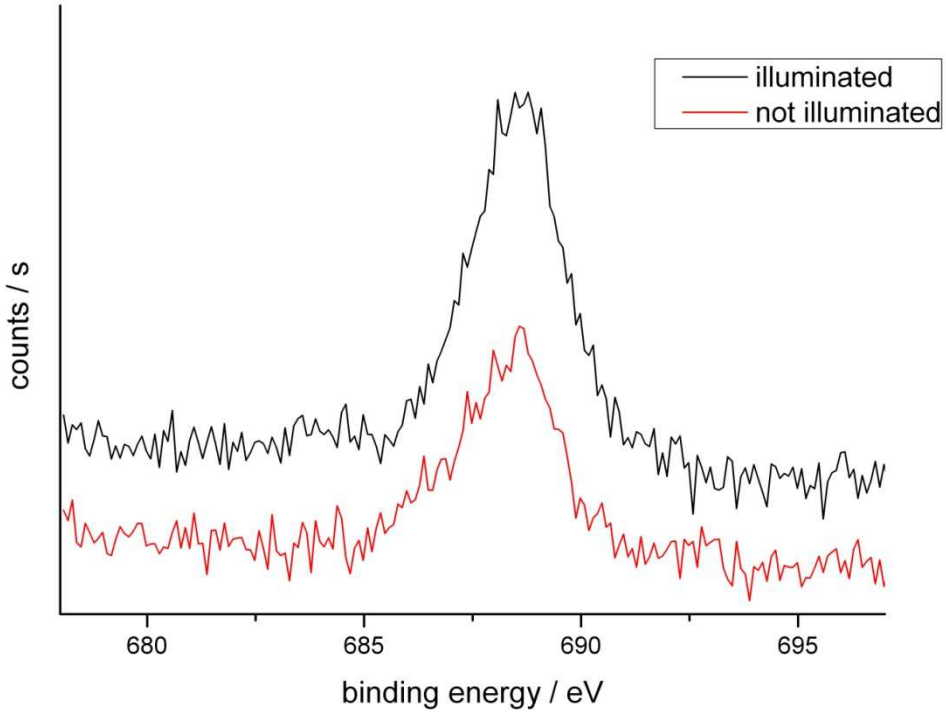

Figure 20. XPS results of flourine on the untreated side (red) and the modified side (black)

In Figure 20, the XPS F1s spectra for the not illuminated and the illuminated side are shown. As can be seen, the fluorine molecule has capped very well on the illuminated side, but also a small amount on the covered side. Nevertheless on the treated side is three times more fluorine capped than on the untreated. The problem can be a transesterification effect, which occurs during the coupling of this fluorine molecule or the illumination has not worked perfect. To realize a complete conversion and no modifications on the untreated surface, this system has to be optimized by further investigations.

3.5.3 Modification with CDI und histidin

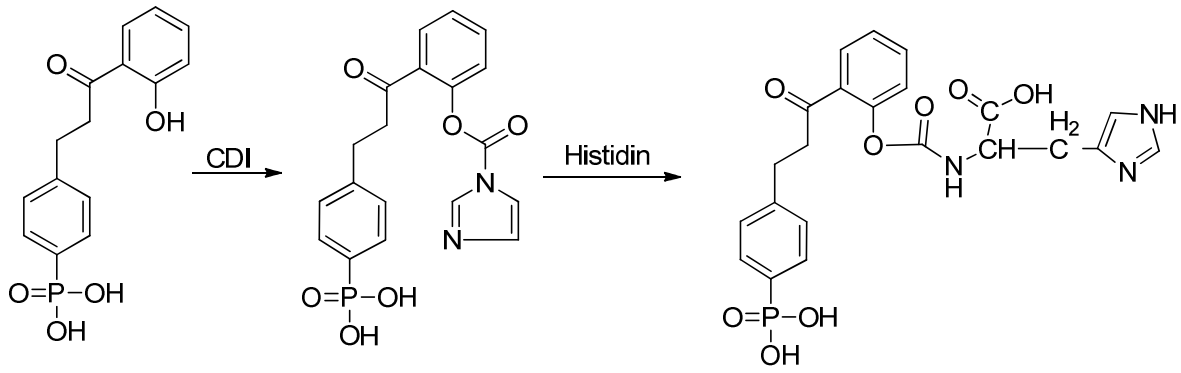

Scheme 13. Postmodification with histidine

CA-measurement:

Table 4. CA results after postmodification with histidine

	H_20	CH_2I_2	$IFT_{s,D}$ [mN/m]	$IFT_{s,P}$ [mN/m]	IFT_s [mN/m]	Polarity [%]
Illuminated	60.2±1.9	48.6±0.8	34.8±0.1	14.0±0.2	48.9±0.2	28.6
CDI-modified	51.6±3.5	58.1±0.3	29.7±0.1	22.1±0.4	51.8±0.4	42.7
HIS-modified	72.6±2.5	47.3±0.3	35.8±0.1	7.3±0.2	43.1±0.3	16.9

Because it is not possible to cap amino acids directly after illumination on the surface, a special amine group catcher was introduced, shown in Scheme 13. In this case, 1,1-Carbonyldiimidazole (CDI), was used[135]. CDI is a well-known, cheap and often used amine capper, which also gives a huge change in surface polarity, caused by the aromatic nitrogen. This capped CDI can now react with the dissolved amino acid histidin. As seen in Table 4, the end standing amine groups make the surface more hydrophilic and the surface tension is decreasing too. The capping of the histidin group also causes a decreasing of the surface polarity, down to 17%.

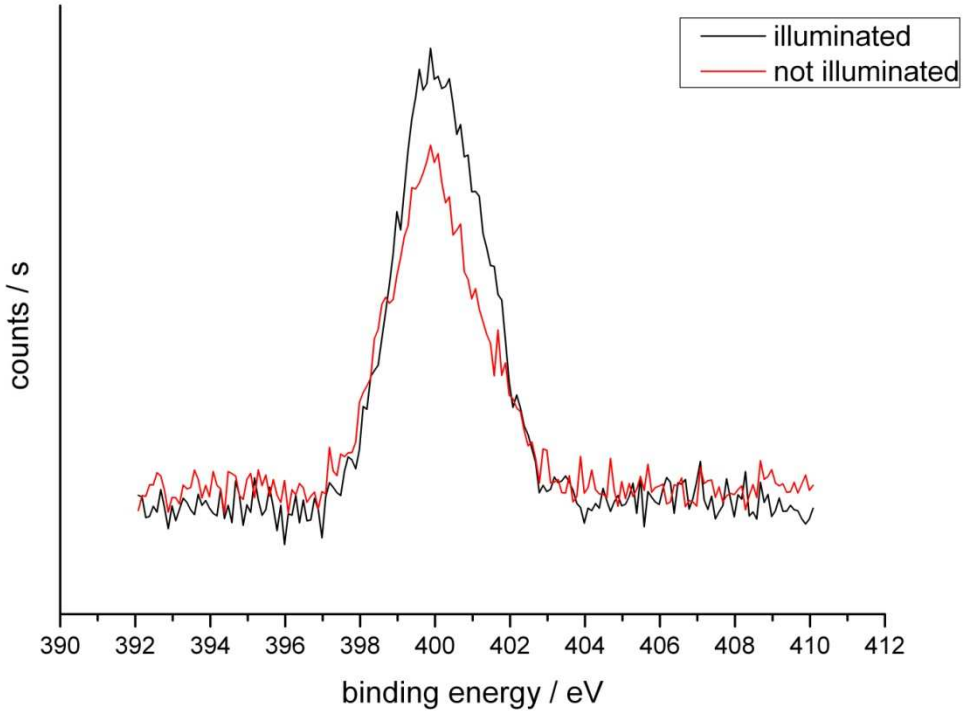

Figure 21. XPS results of nitrogen on the untreated side (red) and the modified side (black)

In Fig 21, the XPS N1s spectra of nitrogen, nearly no difference between the modified and the untreated side can be observed. The intensity is quite low, which means that the coupling of the amino-molecule is not in a direct connection with the illumination and modification, the molecule is just covering the whole wafer. This can have several reasons. One can be that the amino-group catcher, the CDI, has bound to some part of the untreated surface, like in the case of the ethylenediamine reaction and so no direct conclusion can be made.

3.5.4 Modification with CDI und Fe_3O_4

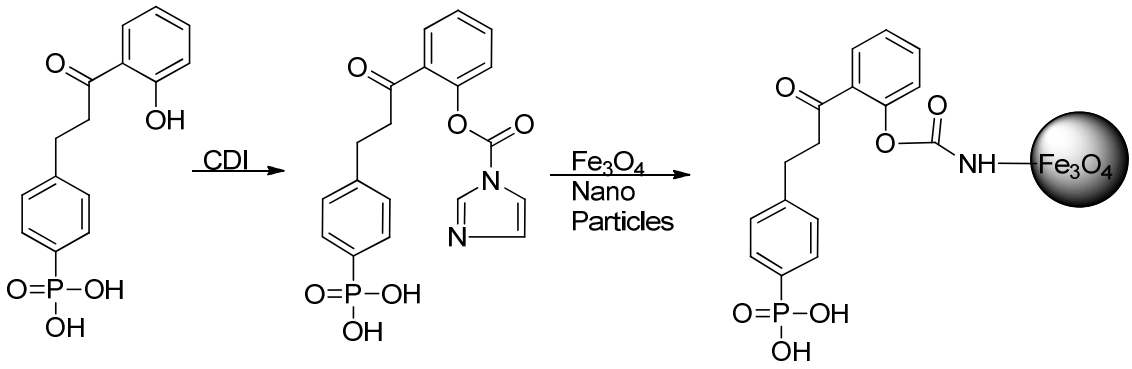

Scheme 14. Postmodification with iron-nanoparticles

Table 5. CA results after postmodification with iron-nanoparticles

			$IFT_{s,D}$	$IFT_{s,P}$	IFT_s	Polarity
	H_20	CH_2I_2	[mN/m]	[mN/m]	[mN/m]	[%]
Illuminated	58.9±0.8	50.3±0.4	33.6±0.2	15.2±0.1	48.8±0.3	31.1
Modificated	44.5±0.5	44.8±0.7	36.2±0.1	23.8±0.2	60.0±0.3	39.7

In this case again CDI was used, now to cap nanoparticles to the surface, shown in Scheme 14. In this experiment, Fe_3O_4 nanoparticles, covered with amine groups, were used. These amine groups made it possible to perform this surface modification. In addition to the change in wettability, shown in Table 5, a visible change on the treated side, a dark grey covering on the substrate, can be observed. In difference to the reactions before, in this case not only the contact angle of water changes, the contact angle of diiodomethane decreases too.

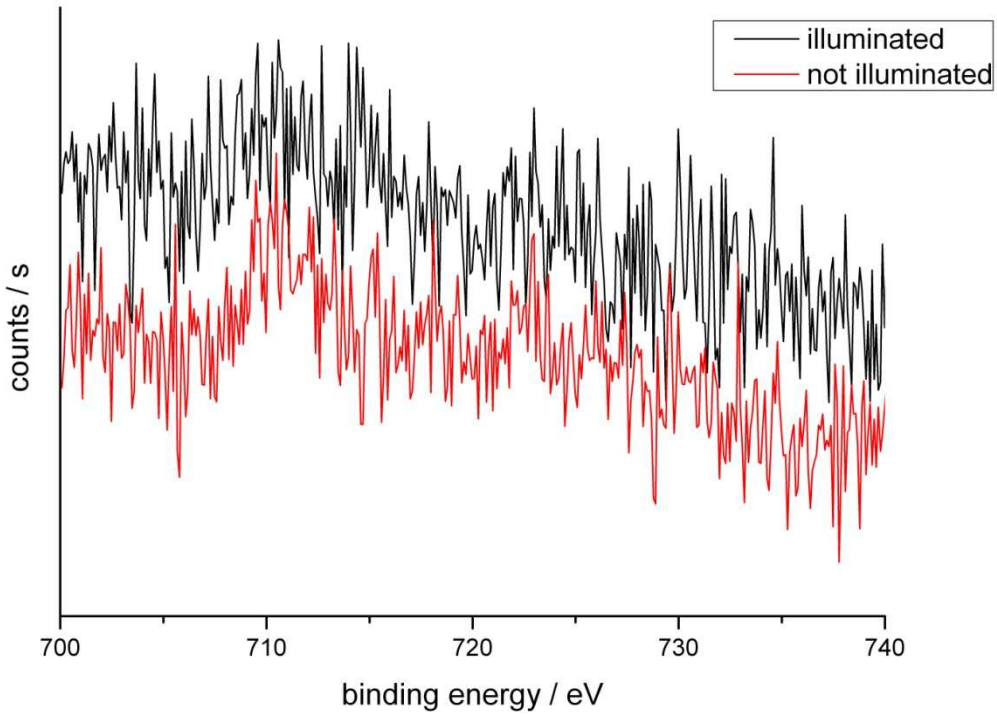

Figure 22. XPS results of iron on the untreated side (red) and the modified side (black)

In Figure 22 the XPS Fe2p spectra of iron can be seen. Due to the fact that this iron-nanoparticle capping is depending on the CDI caption from the step before, no direct conclusions can be drawn for these nanoparticles because the intensity is too low to give further information. The before obtained changes in the CA-measurements could be caused by the CDI-caption in the first step or by the covering amino groups. Due to the fact that a visible change on the illuminated side was observed, this system seems to work but has to be optimized.

3.6 FTIR and CA-measurements of SAM-3 and SAM-4

For FTIR measurements again a thin liquid film of the molecules in $CHCl_3$ was dropcoated onto a CaF_2 disc. For CA-measurements monolayers were produced on silicon-oxide wafer as described in Chaper 3.4. UV-illumination time was 2 min, using EXFO EFOS Novacure with 6500mW/cm^2, visible light illumination was performed using a tungsten 60 W lamp for 20 min.

3.6.1 CA- measurements of SAM-3 and SAM-4

For CA-measurements, monolayers with SAM-3 and SAM-4 have been fabricated. For each SAM the contact angles were measured three times, before, after illumination at 365 nm and again after illumination with visible light to proof the reversibility of the system. As test liquids, water and Diiodomethane were used. Table 6 shows these measurement results.

Table 6. CA- results of SAM-3 and SAM-4 before and after illumination

			$IFT_{s,D}$	$IFT_{s,P}$	IFT_s	Polarity
	H_2O	CH_2I_2	[mN/m]	[mN/m]	[mN/m]	[%]
Untreated SAM-3	96.3 ±1.1	17.0 ±0.4	48.6±0.2	0.0±0.0	48.6±0.2	0.0
Illuminated SAM-3	80.5 ±1.3	24.8 ±1.3	46.2±0.1	2.2±0.2	48.5±0.3	4.5
Untreated SAM-3	95.7 ±1.8	20.7 ±0.4	47.6±0.1	0.0±0.0	47.6±0.2	0.0
Untreated SAM-4	90.9 ±0.1	17.8 ±0.4	48.4±0.2	0.2±0.0	48.6±0.2	0.0
Illuminated SAM-4	79.8 ±0.5	26.6 ±0.5	45.6±0.3	2.5±0.1	48.1±0.4	5.2
Untreated SAM-4	92.9 ±1.2	22.8 ±1.9	46.9±0.5	0.1±0.0	47.0±0.5	0.0

As can be seen in Table 6, a slightly change in the polarity occurs due to the building of the zwitterionic merocyanine. Due to the apolar spiropyran, the surface polarity is close to 0%, caused by the hydrophobic part of the molecule. The ring opening to the zwitterionic merocyanine makes the surface a bit more hydrophilic, shown by the decreasing of the water contact angle from about 90-96° to ~80°, which can also be observed by the increasing of the surface polarity up to ~5%. The contact angles of diiodomethane do not show any strong differences.

Very interesting is that the enormous change in the water contact angle has no influence on the surface dispersity, where only changes from ±2 can be observed and the low surface polarity, also with changes in the same range.

3.6.2 FTIR measurements of SAM-3 and SAM-4

The FTIR- spectra of SAM-3 and SAM-4 in Figure 23 are showing the expected conversions for the spiropyran-merocyanine system.

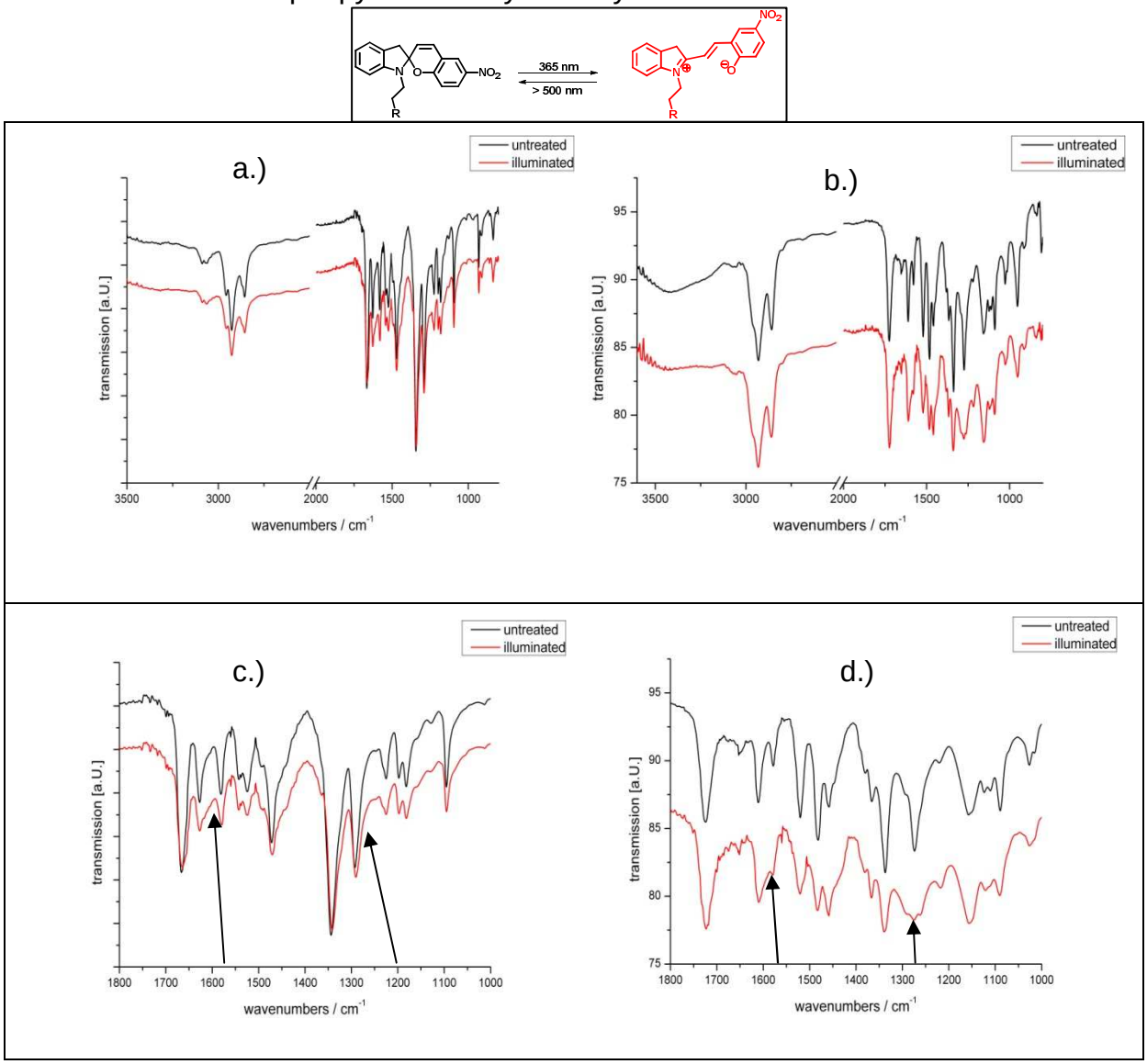

Figure 23. FTIR spectra of SAM-3 (a) and SAM-4 (b) before (black) and after (red) illumination. (c) and (d) are showing detailed parts of these spectra

On the top right picture (b) from 3000-3500 cm^{-1} the acid group of the phosphonic acid can be observed. (c) and (d) are showing the most important part of the FTIR spectra, the broadening of the peak at 1277 cm^{-1} can be detected, caused by the building of the new $C=N^{+}$ bond and the peak at 1597 cm^{-1}, the new double bond in the middle of the merocyanine.

3.7 Photochemical Investigations and CA-measurements of the polymer

For photochemical investigations, a thin film of the polymer was prepared on glass substrates using a doctor blade. Illumination with UV-light turns the closed spiropyran to the open zwitterionic merocyanine, which gives not only a change in the colour and the UV- absorption, but also in the FTIR spectrum and the polarity of the surface, measured by CA-measurements.

Figure 24 shows 1.5:1 cm picture of the film on the glass substrates, starting from the slightly yellow spiropyran (A), changing to the colourful red merocyanine (B). After the next illuminations step, the backreaction to the yellow spiropyran (C), a mask was used for a patterning with the emblem of the TU-Graz, where the rest of the substrate was completely covered (D). This patterning is also shown in picture (E), with a tenfold magnification.

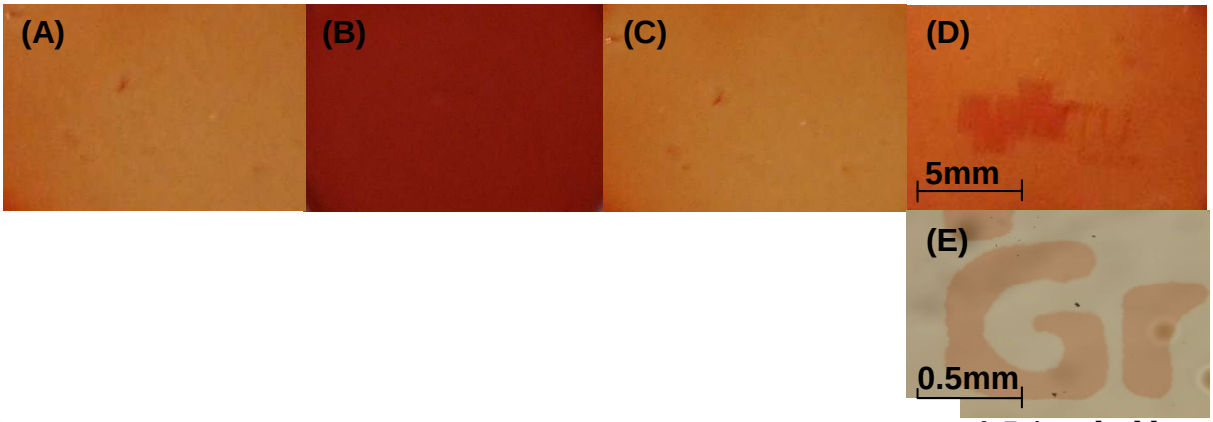

, A-D in a double

3.7.1 FTIR

As depicted in Figure 25, three main differences in the FT-IR-spectra of the spiropyran and the merocyanine can be observed. The first one is the broadening of the peak after illumination at 1276 cm^{-1}, through the building of the new $C=N^{+}$ bond in the merocyanine form. The second one is the building of a new peak at 1422 cm^{-1}, the forming of the $C\text{-}O^{-}$ bond in the merocyanine and finally the peak at 1595 cm^{-1}, generated by the new C=C double-bond in the middle of the molecule, which disappears in the closed spiropyran form.

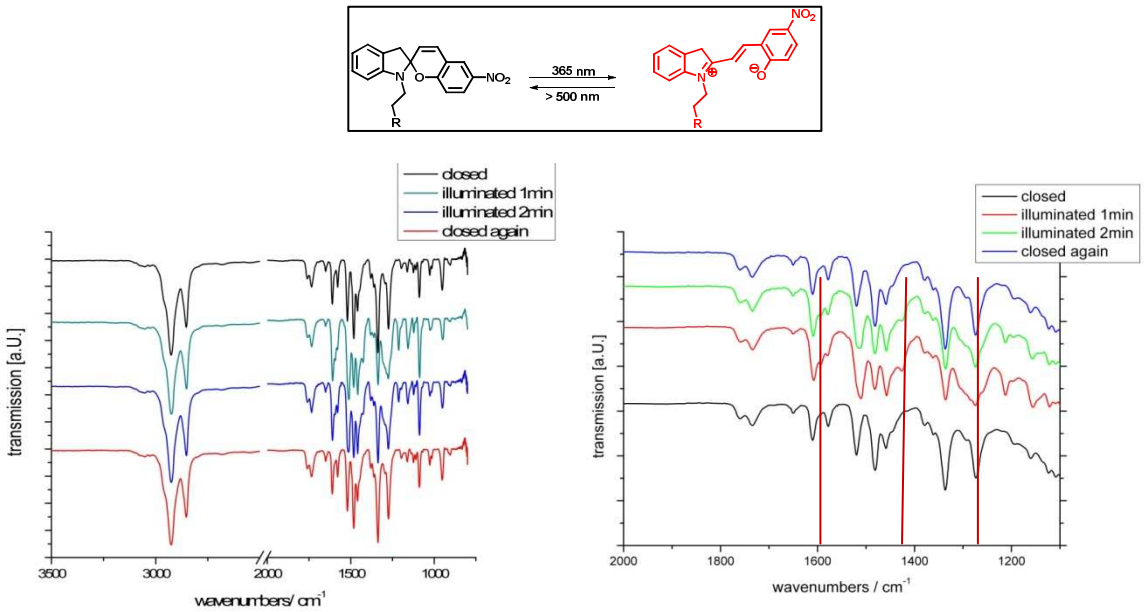

Figure 25. FTIR spectra of the spiropyran polymer before and after illumination (left) and a detailed part out of it

3.7.2 UV-vis

As already known from other spiropyran derivates, the absorption spectra of the slightly yellow spiropyran polymer shows a maximum at about 360nm, which is related to the internal charge-transfer transition in the molecule. After illumination with UV light, the spiropyran switches to the dark-violet zwitterionic merocyanine. Through the cleavage of the C-O bond and especially the formation of the $C=N^-$ bond, the conjugation between the aromatic rings increases and a new maximum absorption bond at 572 nm appears. Just by treatment with visible light, merocyanine isomerizes back to the ring-closed spiropyran and again the original maximum in the absorption spectra at 365 nm was observed, which is shown in Figure 26.

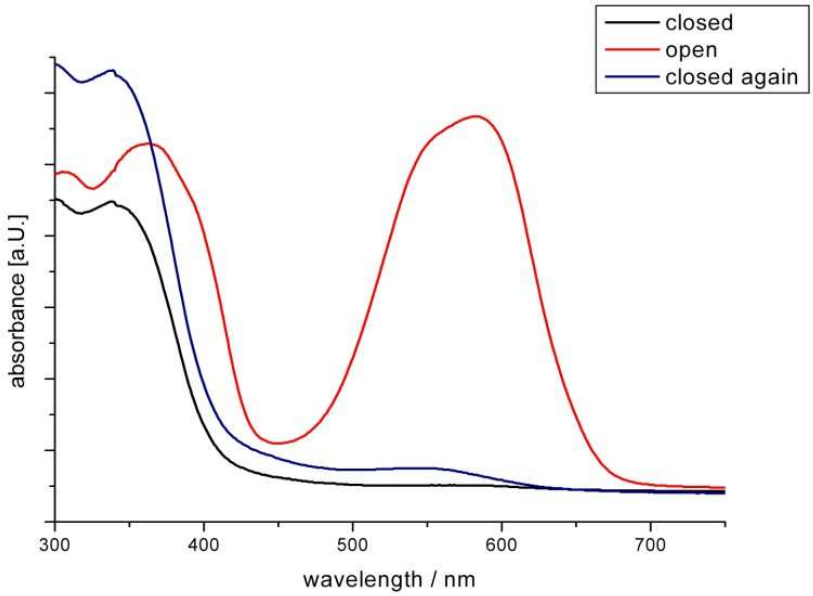

Figure 26. UV-vis spectra of the spiropyran polymer before and after illumination

To visualize the photochemical reversibility of the spiropyran system, repeating measurements were performed to compare the relationship between illumination under argon and illumination under air. The results of this measurement should also give some information about the cycle stability of this polymer. For this experiment, a thin polymer film was coated on a glass substrate by using a doctor blade. Afterwards it was illuminated with UV-light at 365 nm (EXFO EFOS Novacure) for 5 minutes and measured within 1 minute. Direct after measuring the substrate was illuminated with

a standard tungsten lamp for 30 min to rebuild the spiropyran from the open merocyanine form.

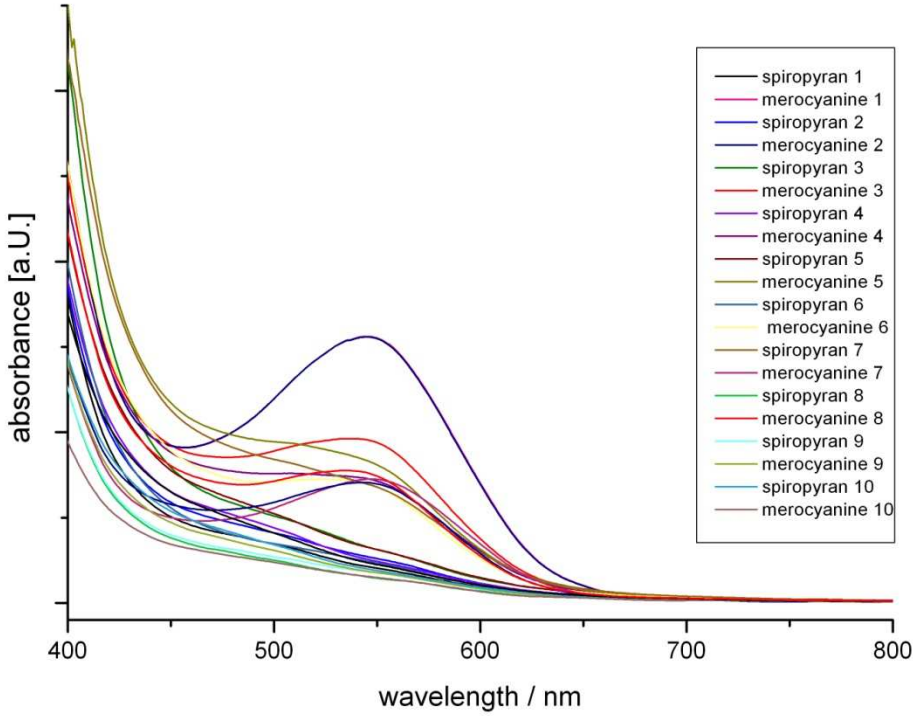

Figure 27. UV-vis spectra of reversibility tests on the polymer under O_2 atmosphere

Figure 27 shows the cycle stability of this polymer under air-illumination. The closed, slightly yellow spiropyran was illuminated for 5 minutes as already mentioned above to convert to the zwitterionic merocyanine, with his new absorption maximum at 560 nm, for the backreaction the illumination time was settled for 20 min. After two cycles, there is nearly no change in reversibility. But after the third illumination, there is a huge change in the intensity of the merocyanine, which means that nearly only fifty percent of molecules could have been converted into the zwitterionic form. This is maybe due to the occurring instability of the open zwitterionic form, but also many other impacts could explain this behaviour. On the one hand, just a small amount of the ruthenium-initiator, left in the polymer even after several cleaning steps, could catalyse some oxidation effects in the polymer during illumination. One the other hand, when illuminating under air atmosphere, the UV-light can react with oxygen in

the air and disturb the more complex reaction from the stable spiropyran to the open merocyanine form.[136]

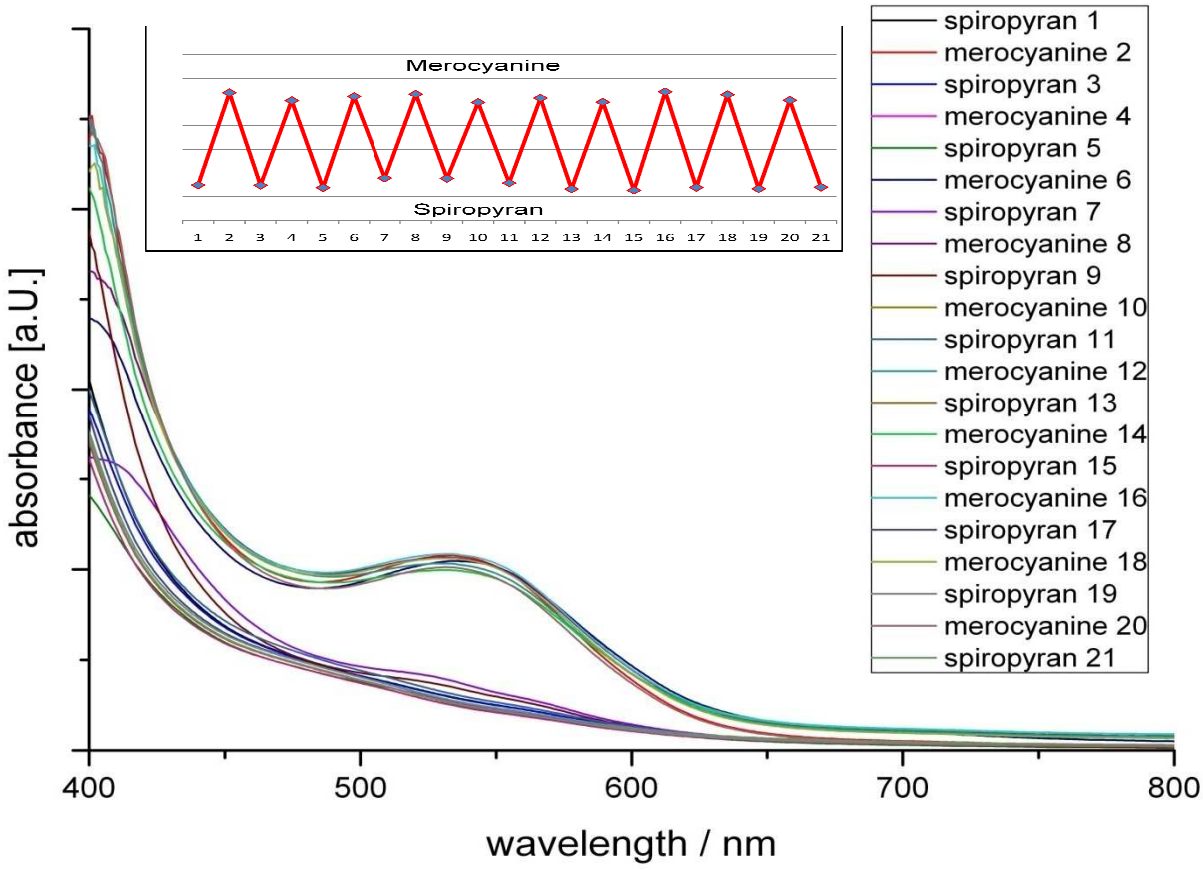

Figure 28. UV-vis spectra of reversibility tests on the polymer under nitrogen atmosphere

In a second experiment, the UV-illumination was carried out under inert atmosphere, to get some information about the stability of the polymer under nitrogen atmosphere. As Figure 28 shows, now the photoreaction is stable over several cycles. Even after ten cycles, there is nearly no difference in the absorbance of the merocyanine form. The graph in Figure 28 is showing the absorbance at 545 nm after each illumination step to depict the cycle stability of this system. With these results, it is now clear that only interactions with air during UV-illumination are disturbing the photoreactive effect of the polymer.

3.7.3 Contact angle measurements

Another proof for the reversibility of the system is the difference in the change of the wettability on the surface. This can be performed by contact angle (CA) measurements, using water as test liquid.

Table 7. CA results before and after illumination

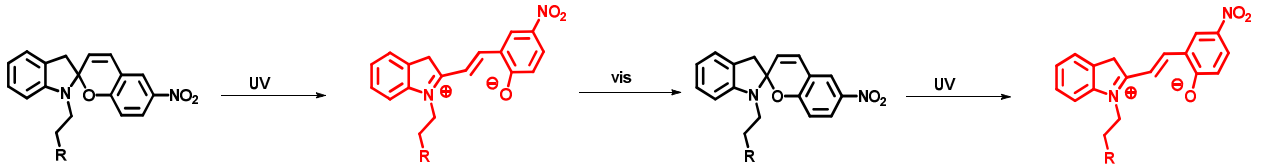

untreated	365 nm	572 nm	365 nm
106,0 ± 1,32	91,9 ± 0,53	105,4 ± 1,43	93,4 ± 1,12

Table 7 shows the change in the wettability after illumination and after ring-closing. The closed spiropyran is very hydrophobic, starting with 106° angle for water. After illumination with UV-light at 365 nm, the contact angle decreases, making the surface a bit more hydrophobic. This change in polarity is complete reversible, shown by subsequent repetitions of the illumination.

3.8 Electrochemical measurements

To check the electrochemical properties of the polymer and its behaviour before and after illumination, cyclovoltammogramm investigations were performed. As shown in Figure 29, two main differences can be observed between the closed spiropyran and the open merocyanine form. In the range of 0.2 V the peak is increasing after illumination, which can be assigned to a single electron transfer from the C-N-C bond to the $C=N^+$ bond in the centre of the molecule. The second one is the increasing of the peak at -0.8 V. This one can be assumed to the easier reducibility of the nitro-group at the end of the molecule by the creation of the new O^- group after illumination.

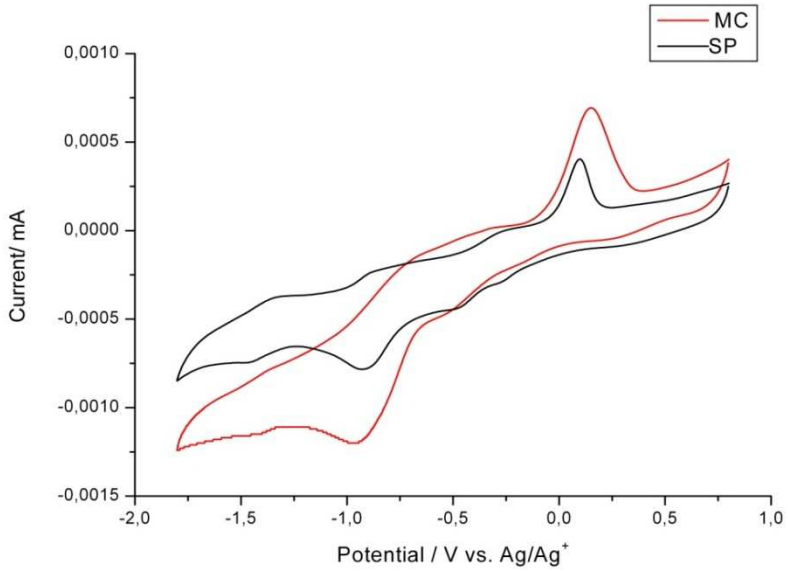

Figure 29. CV of the polymer against a Ag/Ag^+ counter electrode

3.9 Solvatochromic behaviour of the spiropyran-polymer

The spiropyran-merocyanine system shows a strong solvatochromic effect.[137,138,139,140] In a simple experiment we want to show the different behaviour of the system before and after illumination in four different solvents. As the pictures in Figure 30 show, the untreated polymer is absorbing in different colours, according to the polarity of the solvent. Now, just by adding small amounts of water, the colour of the liquid changes immediately.

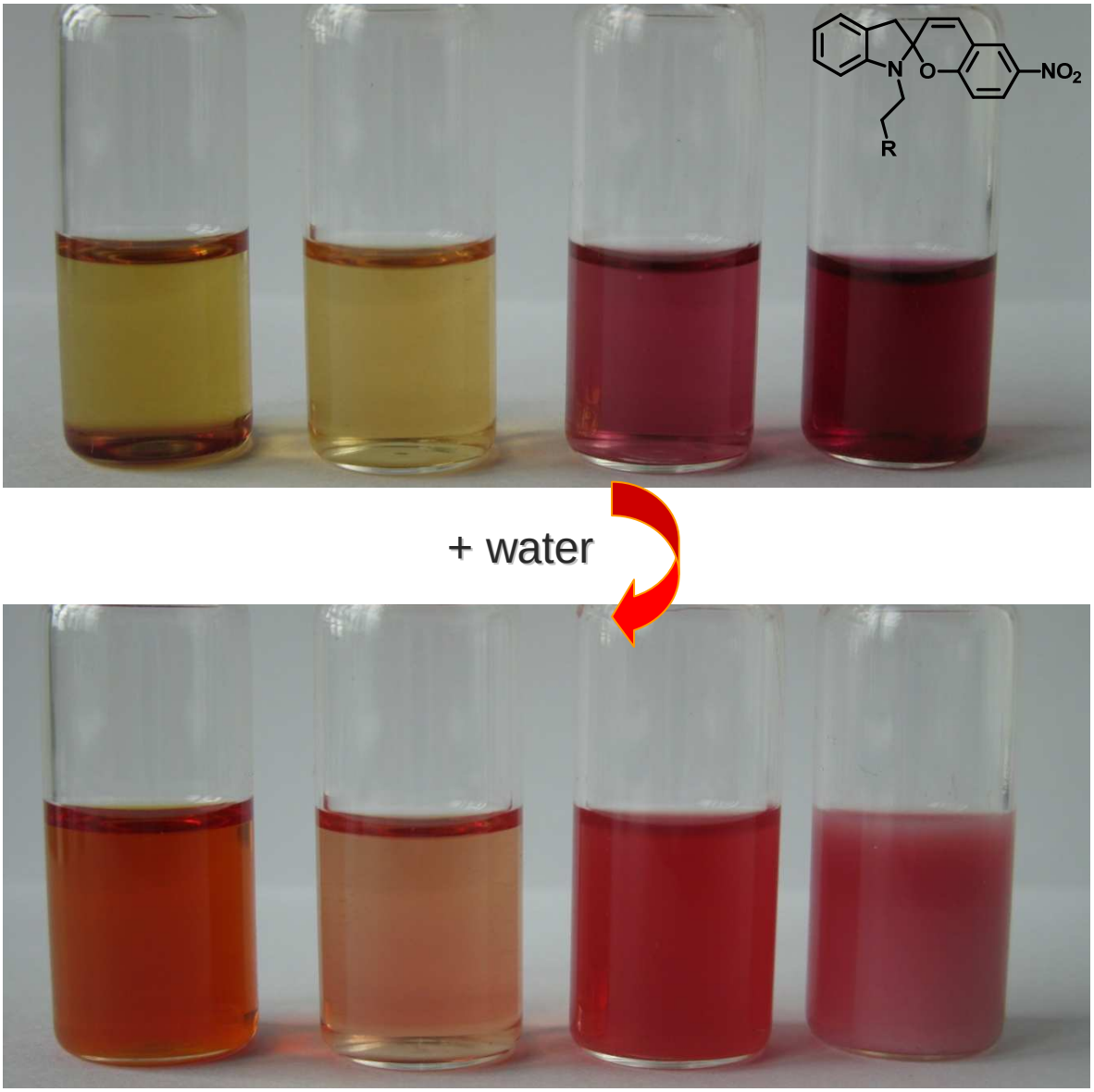

Figure 30. Pictures of solvatochromic test on the untreated polymer in different solvents

In each glass tube 2ml of the solvent were used and finally 8 drops of water were added. An intensive colour change could be observed for pyridine, whereas for THF nearly no change could be observed. Acetone turned faintly and acetonitrile turned completely cloudy, caused by the precipitation of the water-insoluble spiropyran polymer

In a second try, the same test was performed, but now after 3 min illumination of the polymer in the sample. Figure 31 shows the results of this measurement.

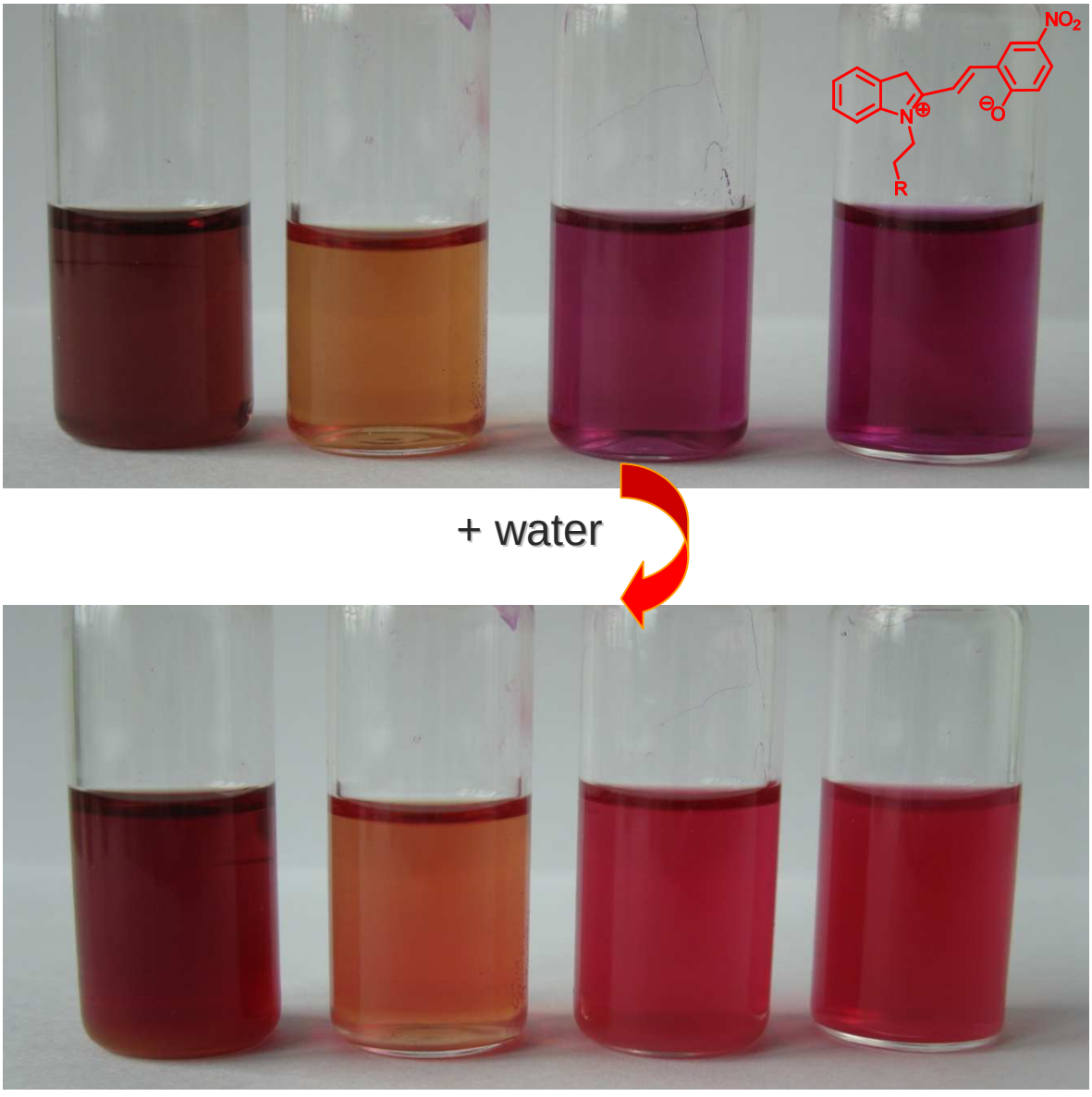

Figure 31. Pictures of solvatochromic test on the illuminated polymer in different solvents

In comparison to the not illuminated samples it can be seen that there is a huge difference especially for the acetone and the acetonitrile. In these two cases due the change in polarity after illumination, the solvents did not turn cloudy after adding the small amount of water, caused by the zwitterionic merocyanine which makes the polymer more water-soluble.

3.10 Preparation of OTFTs using the polymer SP-1

After characterization of the photochemical and electrochemical properties of the molecule, this polymer seemed to be interesting as an interfacial layer in an Organic Thin Film Transistor (OTFT).

The purchased SiO_2 wafers were unpacked in a laminar flow box and after several cleaning steps (CO_2 spray, sonicating..) the wafers were treated in an ultrasonic bath in ultra-pure water to achieve a defined chemical composition on the surface. Now the polymer solution (10mg polymer/ml $CHCl_3$) was spin-coated onto the surface. Afterwards the wafers were locked into a glove box, where the active material, pentacene, and the Au-source and drain electrodes were evaporated onto the transistor. For comparison-measurements, a typical pentacene transistor was constructed in the same way.

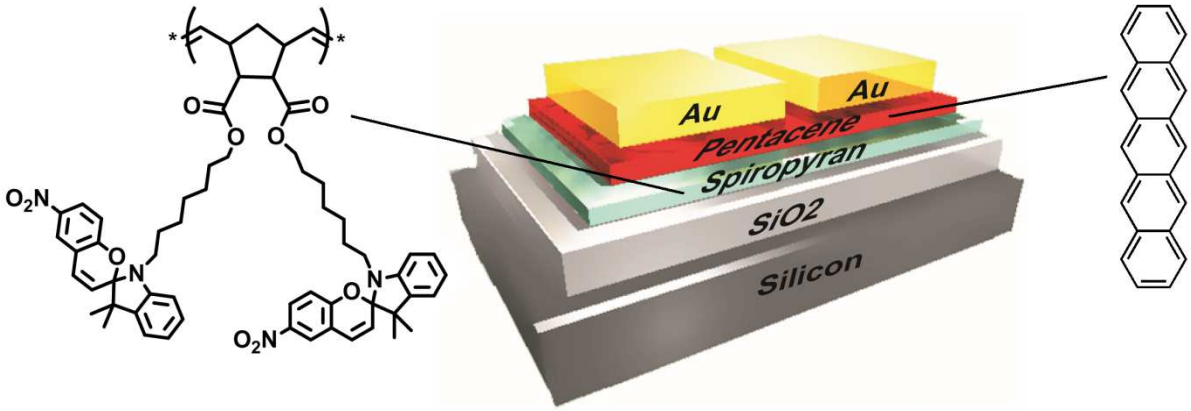

Scheme 15. Depiction of the OTFT setup bearing a spiropyran gate-dieletectric

3.11 Transistor characteristics of the SP-1 transistor

Here the source, drain and gate electrodes were contacted with needles and characterized with a parametric analyser. Through this setup, transfer and output characteristics were measured and finally analysed (Figure 32). Additionally bias stress and long time measurements by a Keithley source meter and special analyzing software were performed by Stefan Kirnstötter.

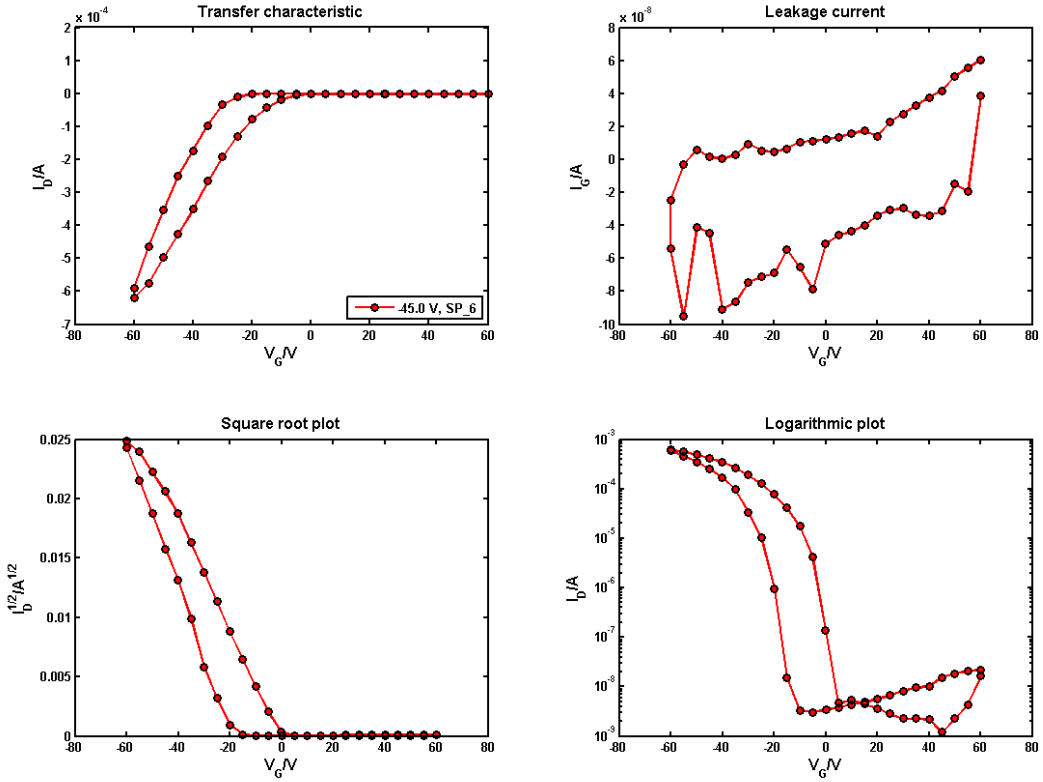

Figure 32. Transfer and output characteristics of the spiropyran based OTFT

Figure 33 shows the transfer characteristics of the transistor before and after illumination. As can be seen, the curves show a reversible shift of the threshold voltage to even more negative values after illumination.

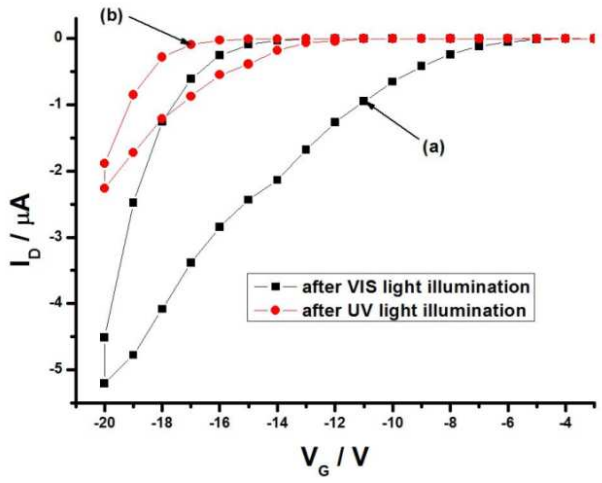

Figure 33. Transfer characteristics before and after illumination

Also problematical is a huge bias stress, which occurs just by changing the threshold voltage-range, shown in Figure 34. Long-time measurements and different control experiments confirmed that this negative shift appears even after several circles of switching between the spiropyran and merocyanine form.

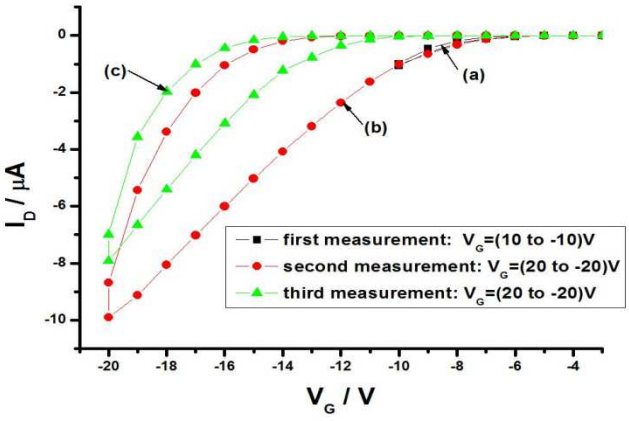

Figure 34. Bias Stress effect of the transistor

Better working transistors should be possible to create, maybe using the polymer not as an interfacial layer, as shown in Figure 35 by Guo et al. with a similar molecule. [141]

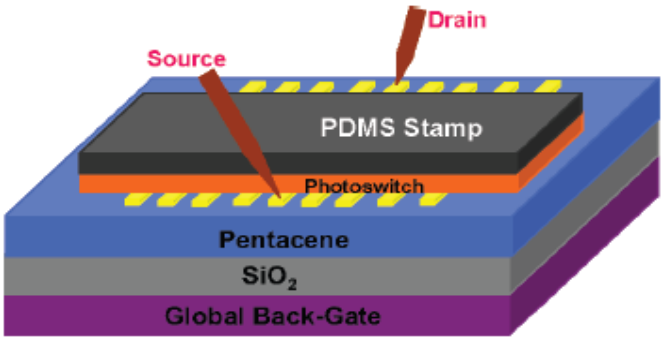

Figure 35. OTFT with a spiropyran/PDMS stamp on the top

Instead of using the spiropyran as an interfacial layer, a PDMS/Spiropyran stamp was put on the top of the transistor. Here the spiropyran produces the electrostatic environment, which can function as a negative gate voltage to increase the electrical conductivity in p-type devices.

4 Conclusion

The aim of this work was the synthesis and characterization of new photoreactive molecules for surface modification. During the last years several persons in this working group have already worked on irreversible photoreactions. E.g. the SCN-NCS photoisomerisation reaction and the photo-Fries reaction in polymers but also in SAMs were investigated. Thomas Griesser worked on thiol based SAMs on gold surfaces and Thomas Höfler on silane based SAMs on SiO_x surfaces, both using the photo-Fries reaction as photochemical part. In this work, first this photo-Fries reaction was now transferred to molecules bearing phosponic acid groups as new anchor groups. These groups strongly bind to metal oxide/hydroxyl surfaces and are known to form real monolayers. Therefore two new molecules, SAM-1 and SAM-2 have been designed both bearing a phenyl ester capable to undergo the photo-Fries reaction. Secondly, 2 SAM-molecules bearing the reversible spiropyran moiety have been synthesized. One of them has again the phosphonic acid group as anchor group, the other one, a trichlorsilyl group. These four different photoreactive molecules for the use as self assembled monolayers (SAMs) are shown in Figure 36.

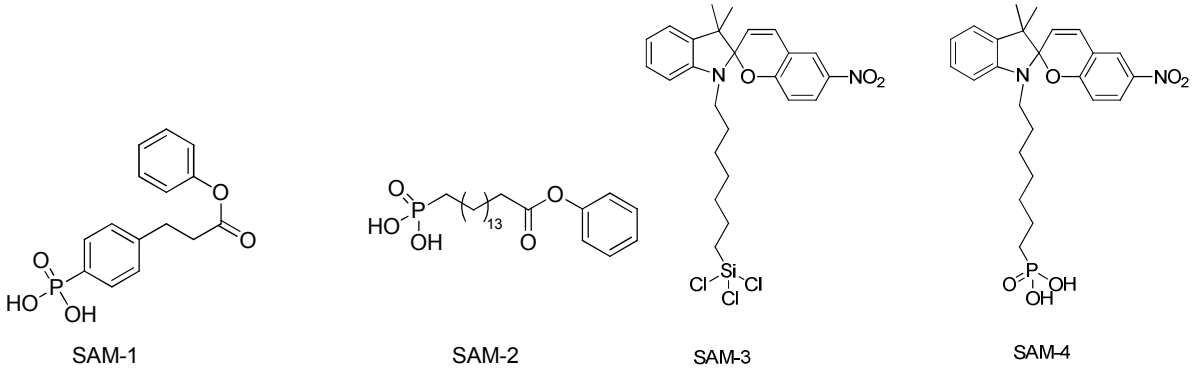

Figure 36. The four synthesized SAM molecules

To achieve these molecules, different reaction methods and steps have been investigated. The first difficult part was the introduction of the anchor group, the phosphonic acid group, into the molecule. Several methods have been tested to realize this reaction in a good purity and yield. Figure 37 shows the final reaction step with a yield of over 80%.

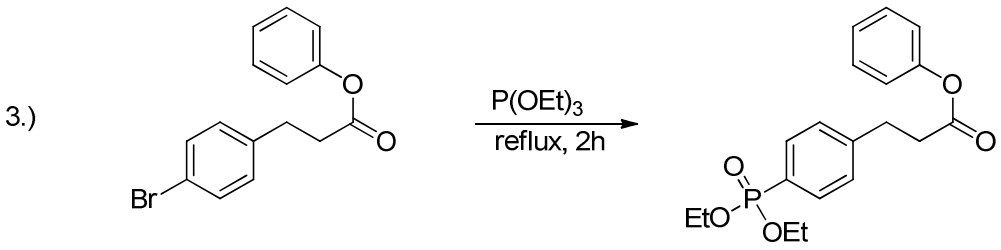

Figure 37. Last reaction step for the introduction of the anchor group

In a second step, the photoreactive part, the photo-Fries group, has to be introduced into the molecule. Finally the following reaction type was chosen due to its good yield.

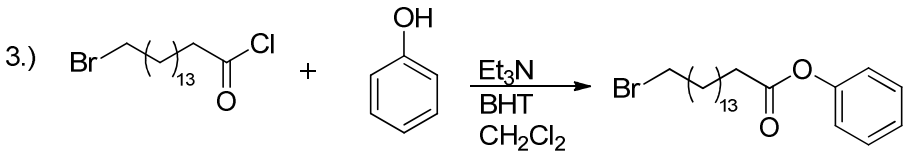

Figure 38. Introducing of the photo-Fries group

For the characterization of the synthesized molecules, ^{1}H-, ^{13}C- and ^{31}P- NMRs have been performed and compared with the literature.

In a next step, these molecules have been investigated for their use as self assembling monolayers. Self assembled molecules should form highly ordered and oriented monomolecular layers that assemble spontaneously on suitable solid surfaces. As already mentioned, in this work mostly phosphonic acid-group based SAM-molecules have been investigated. Figure 39 shows how they should bind on the desired surface.

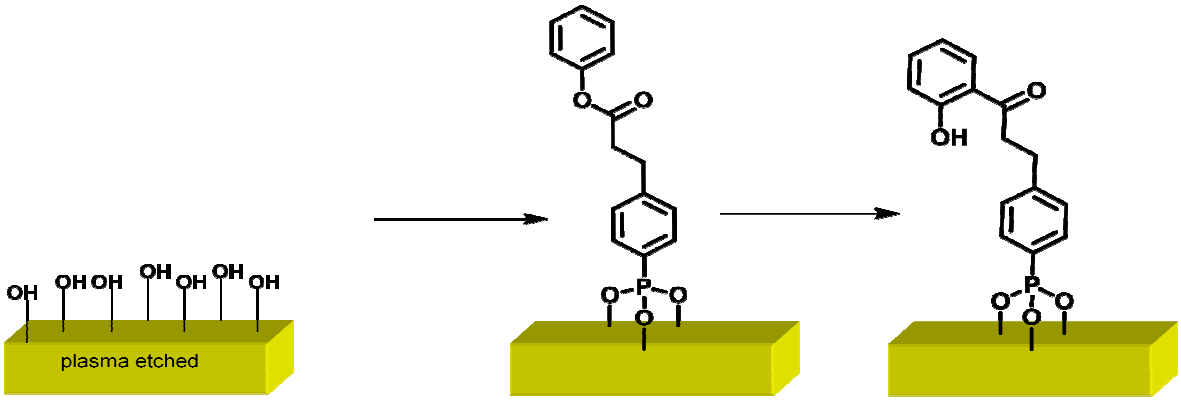

Figure 39. Coupling of phosphonic acid based SAMs on metal surfaces

The building of the SAMs as well as the photoreactions have afterwards been proved by CA, FTIR, XRR, AFM and XPS measurements. Table 8 shows the summarized contact-angle measurement results of the four SAM molecules, always before and after illumination. For the spiropyran molecules, also the reversible backreaction is shown.

Table 8. CA measurement results of the four synthesized SAM molecules

	H_2O	CH_2I_2	$IFT_{s,D}$ [mN/m]	$IFT_{s,P}$ [mN/m]	IFT_s [mN/m]	Polarity [%]
Photo-Fries -SAMs						
Untreated SAM-1	78.4 ±1.1	38.1 ±0.4	40.6±0.1	3.8±0.0	44.4±0.1	8.6
Illuminated SAM-1	63.7 ±0.6	44.4 ±1.8	37.3±1.2	11.3±0.7	48.6±1.9	23.3
Untreated SAM-2	76.6 ±0.7	36.8 ±1.1	41.2±0.0	4.3±0.0	45.5±0.0	9.4
Illuminated SAM-2	59.8 ±1.4	49.7 ±0.8	34.4±0.1	14.6±0.1	49.0±0.2	29.8
Spiropyran-SAMs						
Untreated SAM-3	96.3 ±1.1	17.0 ±0.4	48.6±0.2	0.0±0.0	48.6±0.2	0.0
Illuminated	80.5 ±1.3	24.8 ±1.3	46.2±0.1	2.2±0.2	48.5±0.3	4.5

SAM-3						
Illuminated (VIS) SAM-3	95.7 ±1.8	20.7 ±0.4	47.6±0.1	0.0±0.0	47.6±0.2	0.0
Untreated SAM-4	90.9 ±0.1	17.8 ±0.4	48.4±0.2	0.2±0.0	48.6±0.2	0.0
Illuminated SAM-4	79.8 ±0.5	26.6 ±0.5	45.6±0.3	2.5±0.1	48.1±0.4	5.2
Illuminated (VIS) SAM-4	92.9 ±1.2	22.8 ±1.9	46.9±0.5	0.1±0.0	47.0±0.5	0.0

As can be seen in Table 8, for each step a significant change in the surface polarity occurs after illumination and for the spiropyran based SAMs, SAM-3 and SAM-4, show after illumination with visible light almost the same contact angle and thus the same surface energy parameters proving the reversibility of the photoreaction. Due to the fact, that this monolayers are extreme thin films in nm range and that we have used highly doped silicon wafers, it was not possible to follow the photo-reaction by FT-IR spectroscopy. Thus, for this investigation, liquid films of each molecule have been drop coated onto CaF_2 discs. As can be seen in chapter 3.4.2 for SAM-1 and SAM-2 and in chapter 3.6.2 for SAM-3 and SAM-4, these FTIR measurements verify that these molecules undergo the photoreactions as expected. For the very good working photo-Fries monolayers, also XRR and AFM measurements have been performed, where a surface thickness of 1.35 nm was observed, close to the calculated molecule length of 1.35 nm.

In addition, in the case of SAM-2, different post-modification using the change of the surface polarity and of the chemical reactivity after illumination of the substrates, have been performed. For each modification, one half of the SAM-2 monolayer on a silicon oxide wafer was covered and the other half was treated with UV-light at 254 nm for a certain time. After this illumination, the wafers were engaged into a solution of the desired molecule and finally this molecule should only bind to the illuminated side of the wafer. Four different modifications have been investigated as shown in Figure 40. For all these modifications, CA and XPS measurements were carried out. The first modification using adopoyl chloride followed by ethylenediamine leads to high polar surfaces. The second one with perfluorobutyryl chloride leads to surfaces with relative low surface energy. In both cases, XPS detected on the illuminated and

on the non illuminated side a significant amount of nitrogen and fluorine, respectively, but the relative amount was higher on the illuminated side. The other two modifications use first CDI as mediator for the immobilization of hisitidin and iron oxide nanoparticles. However, in both cases, no differences in the XPS signal could be detected. Interestingly no iron signal was detectable, although there was a visible grey layer on the illuminated side.

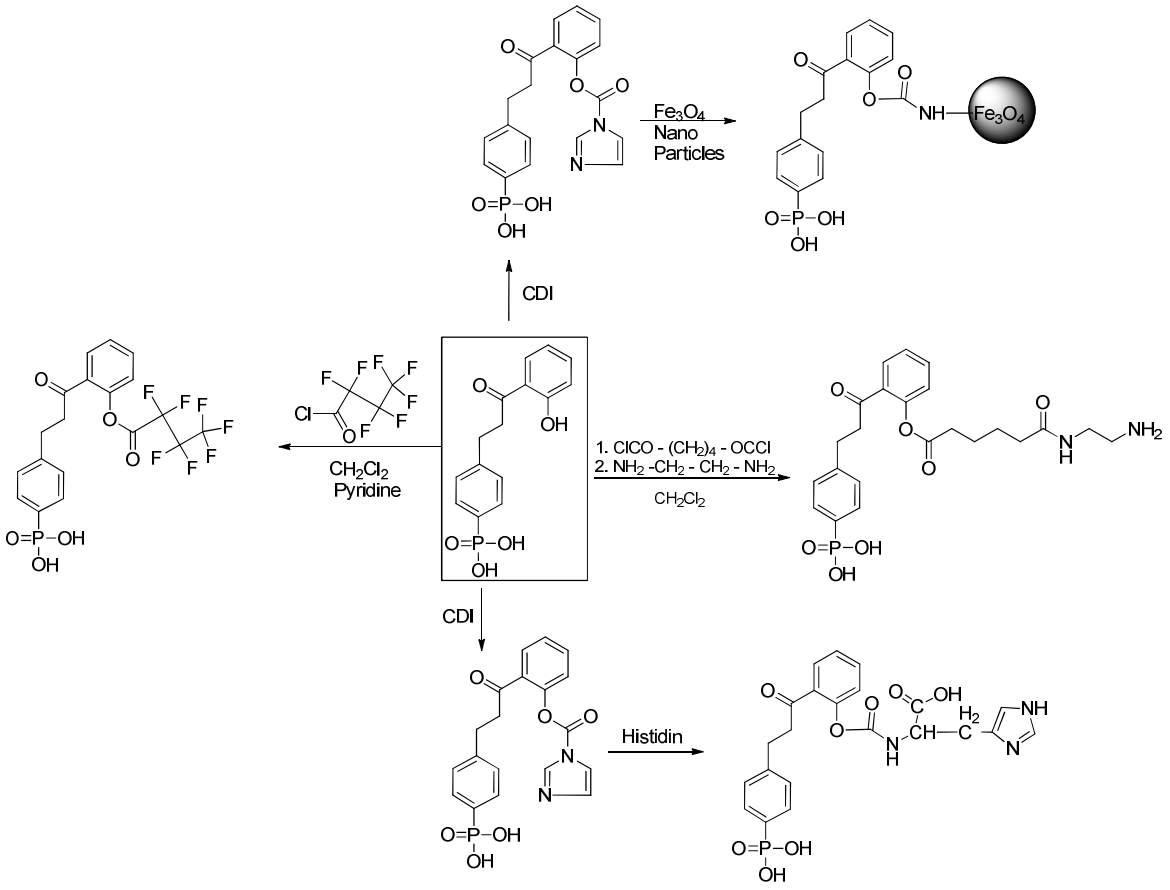

Figure 40. Scheme of the performed postmodifications

In the last part of the work a reversible photoreactive polymer based on the spiropyran-merocyanine photochemistry was synthesized. The idea behind it was to use this photochromic polymer as a switchable interfacial layer in an Organic Thin Film Transistor (OTFT). Figure 41 shows the last reaction step for the synthesis of the sp-polymer.

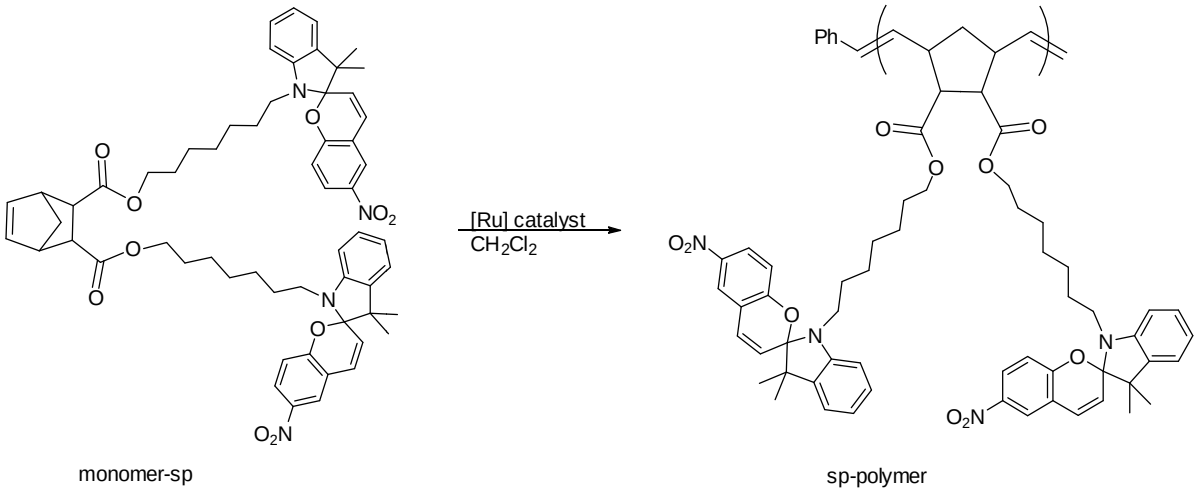

Figure 41. Polymerization of monomer-sp

This polymer was synthesized in a yield between 50-60 % with an average polydispersity index (PDI) of 1.84. For photochemical investigations a thin liquid film of the polymer was put either on a CaF_2 via spincoating or on a glass substrate using a doctor blade. Figure 42 is showing a part of a substrate, patterned with a mask with the sign of the University.

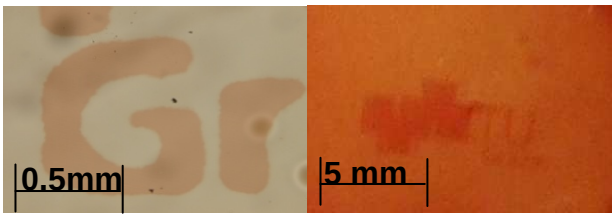

using sp-polymer

To prove the reversibility of this system, repeating UV-vis measurements were performed under nitrogen atmosphere. Figure 43 shows the results of the measurement, always the value at 557 nm. As can be seen, even after 20 cycles, the values are constant.

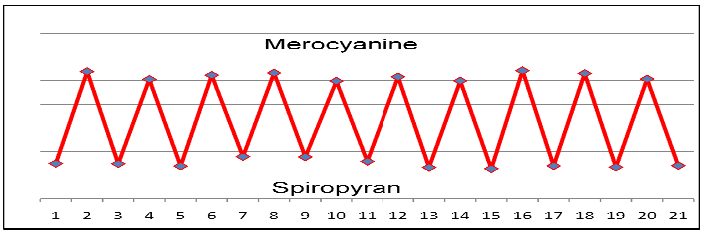

Figure 43. Measuring points out of the UV-vis spectra of sp-polymer

After the photochemical investigations, UV-vis and FTIR, the polymer was introduced into an organic field effect transistor (OTFT) as an interfacial layer. This was done in cooperation with Stefan Kirnstötter from the Institute of Solid State Physics of the Graz University of Technology. Figure 44 shows the setup for this transistor.

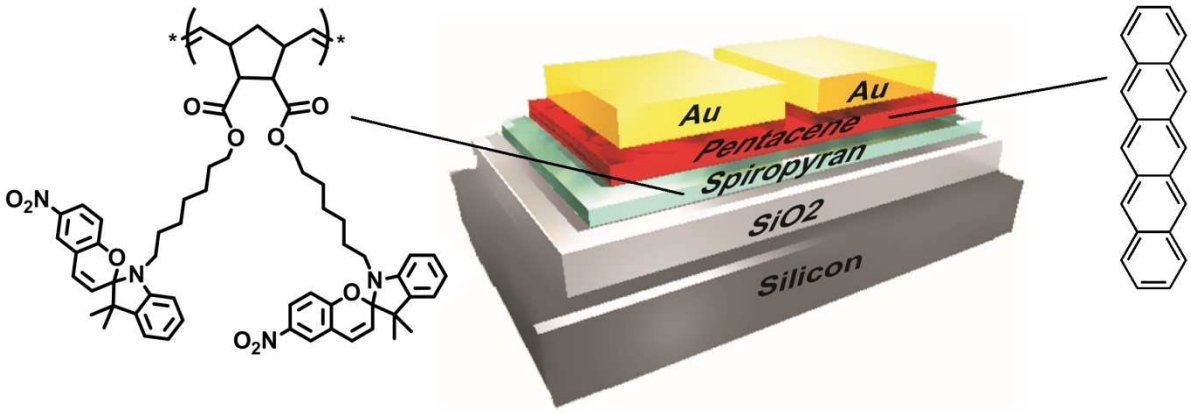

Figure 44. Setup for an OTFT with the sp-polymer as interfacial layer

After the setup was complete, the transfer characteristics of the transistor before and after illumination were measured. As can be seen in Figure 45, the curves show a reversible shift of the threshold voltage to even more negative values after illumination.

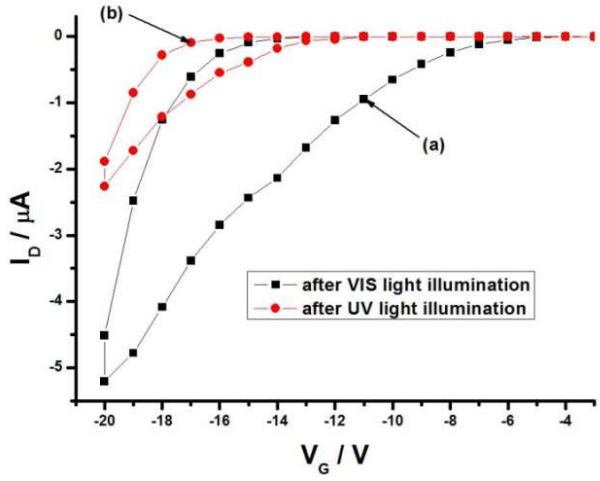

Figure 45. Transfer characteristics of the sp- polymer based OTFT

Also a huge bias stress occurs during long time measurements, which makes it clear that this polymer does not work in this transistor.

5 Experimental Part

5.1 Used chemicals and substrates

5.1.1 Chemicals

All experiments were performed under argon or nitrogen atmosphere, using Schlenk techniques. Solvents, like dichloromethane, tetrahydrofuran or diethyl ether, have been distilled and dried under ambient conditions. All chemicals were purchased from commercial sources and used without further purification.

Table 9. List of used chemicals

Substrate	Source	Purity
Acetic acid	Roth	100% p.a.
Acetonitrile	Aldrich	99.8%
Adipoylchlorid	Aldrich	>99%
Bicyclo[2.2.1]hept-5-ene-2,3-dicarbonyl dichloride	Aldrich	97%
Brine (satured NaCl solution in water)		
6-Bromo-1-hexanole, Aldrich	Aldrich	97%
3-(4-bromophenyl)-propionic acid	Aldrich	98%
Bromotrimethylsilane	Aldrich	97%
11-bromo-1-undecene	Aldrich	95%
Carbonyldiimidazole (CDI)	Aldrich	97%
Chloroform	Aldrich	99.9%
Chloroform-d1	Chemotrade	>99.9 % D
Cyclohexane	Roth	p.a.

1,7-dibromoheptane	Aldrich	97%
Dichloromethane	Aldrich	p.a.
Diethyl ether	Aldrich	p.a.
DMAP, 4-(dimethylamino)pyridine	Fluka	98%
BHT, 3,5-di-tert-butyl-hydroxy toluene	Fluka	99%
Ethanol	Aldrich	p.a.
Ethyl acetate	Roth	99.5%
Ethylene diamine	Fluka	>99.5%
Diiodomethane	Aldrich	99%
Histidin	Aldrich	99%
Hexachloroplatinic acid	Aldrich	99.9
Hexane	Roth	p.a.
Hydrogen bromide	Fluka	48%
Hydrogen chloride	Roth	37%
16-hydroxyhexadecanoic acid	Aldrich	98%
Grubb's Initiator 2nd generation	Aldrich	k.A.
Methanol	Roth	>99.5
5-Nitrosalicylaldehyde	Aldrich	99%
Phenol	Fluka	99%
Perfluorobutyrylchloride	Aldrich	98%
Potassium hydroxide	Roth	95%
Potassium permanganate	Roth	97%
Pyridine	Aldrich	99.5%
Silicagel	Fluka	
Sodium hydrogencarbonate	Fluka	99%
Sodium sulphate	Aldrich	>99%
Tetraethylammoniumtetrafluoroborate ($TBAPF_4$)	Aldrich	>99%
Tetrahydrofuran	Aldrich	p.a.

Thionyl chloride	riedel de häen	98%
Trichlorosilane	Aldrich	99%
Triethylamine	Sigma	>99.5%
Triethylphosphite	Aldrich	98%
2,3,3- Trimethylindolenine	Aldrich	98%

5.1.2 Substrates

Following type of substrate has been used in this work:

Single side polished silicon wafers with native silicon oxide (1.7 nm) from Infineon Technologies Austria AG.

For photochemical investigations, glass-substrates or CaF_2-discs were used.

5.2 Used equipment and methods

5.2.1 Thin-Film-Chromatography

Reactions were monitored by TLC (Silica gel 60 F_{254} on aluminium, Merck). Detection: UV-light (254 nm and 365 nm for fluorescent/phosphorescent compounds) and staining with molybdate/H_2SO_4 (dip: a solution of 10 g ammonium molybdate in 1000 mL 10% H_2SO_4 and a solution of 8 g cerium sulphate tetrahydrate in 80 mL 10% H_2SO_4 were mixed) or potassium permanganate (2% in H_2O dest.).

5.2.2 FTIR spectroscopy

All IR-spectra were recorded with a Fourier-Transformation-Infrared-spectrometer, a Perkin Elmer Spectrum One instrument (spectral range between 4000 cm^{-1} and 450 cm^{-1}), using a pyroelectrical DTGS-detector. (DTGS = DeuteratedTriglycine Sulphate). FTIR spectra of the samples were recorded in transmission mode (films on CaF_2 discs).

5.2.3 UV-vis spectroscopy

UV-vis spectra were measured with a Shimazu UV-vis-spectrophotometer. All UV-vis spectra were performed in absorbance mode, in a range of 800 to 300 nm, again using thin films on CaF_2 discs.

5.2.4 Size exclusion chromatography (SEC)

Weight and number average molecular weights (M_w and M_n), as well as the polydispersity index PDI=M_w/M_n, were determined by size exclusion chromatography (SEC) with the following set-up: Merck Hitachi L6000 pump, separation columns from Polymer Standards Service (8mm*300 mm, STV 5 µm grade size; 10^6, 10^4 and 10^3 Å pore size), refractive index detector (model Optilab DSP InterferometricRefractometer) from Wyatt Technology. Polystyrene standards from Polymer Standard Service were used for calibration. All SEC runs were performed with chloroform or THF as eluent.

5.2.5 NMR

NMR-measurements were performed on VARIAN INOVA 300MHz spectrometer. Deuterated solvents were purchased from Cambridge Isotope Laboratories and peak referencing was done according to literature.[142] ^{1}H-NMR spectra were recorded at 300 MHz, ^{13}C- NMR spectra were recorded at 125 MHz. Peak shape indication was done as followed: s (singlet), d (duplet), dd (doublet of doublets), t (triplet), q (quadruplet), m (multiplet), b (broad), bs (broad singlet).

5.2.6 Contact-angle measurements

Contact angle measurements were carried out with the Drop Shape Analysis System DSA100 (Krüss GmbH, Hamburg, Germany), using water and diiodomethane as test liquids (drop volume ~ 30 µL). The total surface tension of a solid, according to van Oss, Chaudhury and Good[143,144] is the sum of the dispersive (apolar Lifshitz-van der Waals) component γ^D and the polar (Lewis acid-base) component γ^D. The contact angles were obtained by means of the sessile drop method and they were measured within 2s.

5.2.7 Atomic Force microscopy

In this study atomic-force microscopy (AFM) in intermittent contact mode and lateral force mode-also called Friction Force Microscopy (FFM)-were used to characterize surface properties of the prepared films. During the FFM measurement, both topography and friction force data are record simultaneously: The topographical image shows surface morphological information (z-scale is nm) obtained from the vertical deflection signal. At the same time, two friction images (trace and retrace) are recorded. Using the simple arithmetic subtraction operation: real FFM = (trace FFM data – retrace FFM data) / 2, the topographic effects can be almost removed from the final FFM image. The real FFM image calculated shows the real friction contrast on the surface without artefacts induced by surface topographical changes. FFM measurements were performed on a DI Nanoscope Multimode IIIa Scanning Microscope using PPP-BSI-SPL probes from NanoSensors. The probes have a typical force constant of 0.01-0.5 N/m and a guaranteed tip radius of less than 10 nm. This tips are specially long and narrow (Length: 225±10 µm; Width: 28±7.5 µm) designed for biological applications. Therefore, this tip is sensitive for lateral force.

5.2.8 X-ray photoelectron spectroscopy

In this study measurements were performed in an ultrahigh vacuum (UHV) chamber at a pressure of $1x10^{-10}$ mbar and the samples were introduced into an ultrahigh vacuum (UHV) chamber at a pressure of $1x10^{-10}$ mbar and the samples were introduced via a fast entry load-lock. XPS experiments were carried out using Mg Kα radiation (1253.6 eV) and a hemispherical analyzer (Phoibos100), at an energy resolution of 1.2 eV. All spectra were acquired in normal emission and with a photon incident of 55°. To minimize possible photo rearran gement and irradiation damage caused by X-rays, a low excitation power of 100 W was use and the sequence of the measurements was considered. For fitting a standard Gaussian-Lorentzian line shape was used.

5.2.9 X-ray reflectivity

XRR measurements were performed on a Bruker D8-Discover diffractometer using Cu Kα radiation. The setup was set in a parallel beam configuration using 0.1 mm slits and a secondary side monochromator. Measurements were performed from 0.1° (0.007 $Å^{-1}$) up to 6° (0.42 $Å^{-1}$) with a step width of 0.005° using an integration time of 3 seconds. The Parrat algorithm was used to extract the layer thickness; roughness was included by a Nevot-Croce model.[145]

5.2.10 UV-lamps

Two different types of UV-lamps were used during this work:

For photo-Fries-rearrangement reaction the unfiltered light of a polychromatic medium pressure mercury lamp (Heraeus) was used. All UV irradiations of polymer samples were conducted under inert gas atmosphere (nitrogen with a purity >99.95%). For these experiments, the light intensity (power density) at the sample surface was measured with a spectroradiometer (Solatell, Sola Scope 2000TM, measuring range from 230 to 470 nm). The integrated power density for the spectral range 230 nm-400 nm was 20.9mW/cm^2.

The ring-opening UV-illumination, from spiropyran to the merocyanine form, was carried out under inert atmosphere (argon) by using an ozone-free mercury low-pressure lamp (EXFO EFOS Novacure), with an irradiation time of 30 sec. For ring-closure illumination a simple tungsten-lamp (60W) was used.

5.2.11 Parametric analyzer

Characterization of the Transistors was done by needle contact, using MDL positioners from Cascade electronics, and electrically characterized with an Agilent E5262A parametric analyzer.

5.3 Synthesis of the SAM molecules

5.3.1 SAM-1

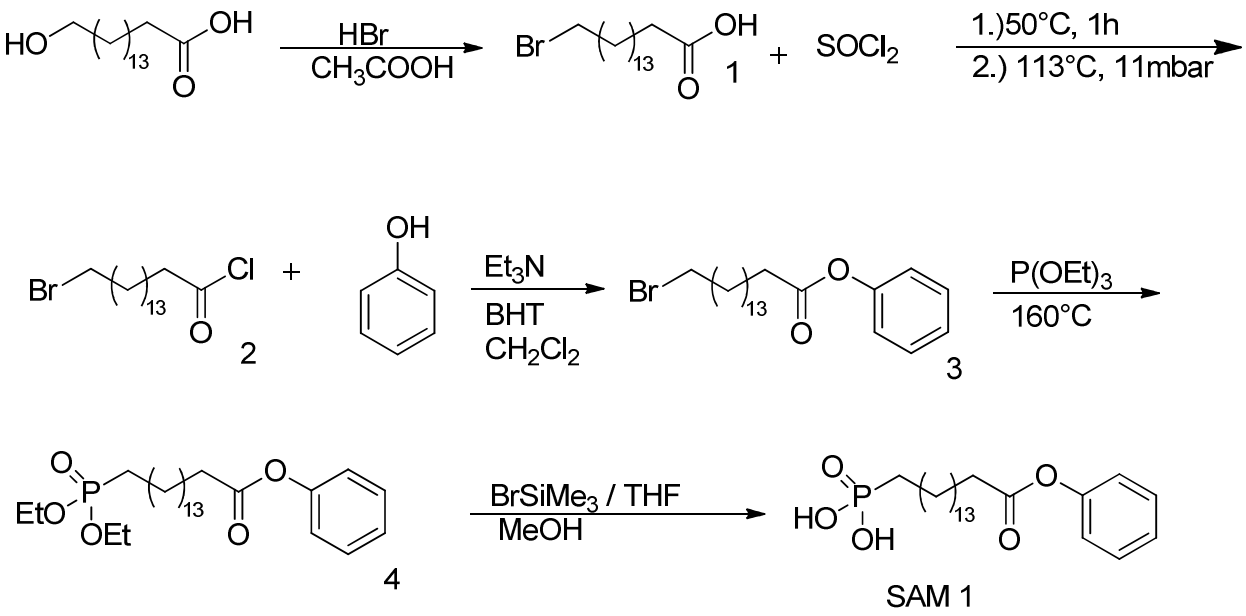

Scheme 16. Synthesis of SAM-1

A mixture of 16-hydroxyhexadecanoic acid (2.72 g, 10 mmol) in 15 ml conc. acetic acid und 15 ml hydrogen bromide was refluxed for 48 h. After complete conversion, proved by thin film liquid chromatography (TLC), it was cooled down to room temperature. The formed precipitate was filtered and recrystallized in cyclohexane. The white powder was treated with thionyl chloride (2.4 g, 20 mmol) and stirred at 50℃ for 1 h continued by a distillation at 113℃ a nd 11 mbar. The remaining product was dissolved in CH_2Cl_2, treated with phenol (0.94 g, 10 mmol) and triethylamine (1.55 g, 15 mmol) and BHT (~1 mg) as a catalyst. This mixture was stirred for 18 h, after whole conversion (TLC) quenched with water and extracted 3* with $NaHCO_3$ (3* 30 ml) and 3* with HCl (10%) (3* 30 ml). The combined organic phases were dried over $NaSO_4$, filtered and the remaining solvent was removed under vacuum. (2.28 g, 64.4 %)

A mixture of the product and excess triethylphosphite (3.24 g, 19.5 mmol) was heated slowly to 160℃ and the evolving ethyl bromide was distilled off simultaneously. After 4h, the excess triethylphosphite was distilled off for 30min under vacuum at 160℃. The resulting oil was cooled down to room temperature and recrystallized from diethyl ether. (4) The remaining oil in 100 ml THF was treated under ice-cooling with an excess of bromotrimethylsilane (12.24 g, 80 mmol) and stirred at room temperature for 24h. Afterwards the solvent was removed and the excess of bromotrimethylsilane was distilled of at 80 ℃ under vacuum. The residue was dissolved in 100 ml MeOH und 15 ml THF and refluxed for 23h. After this, the solvent was removed, dried under vacuum and finally cleaned via column chromatography (1.Ethylacetat, 2.MeOH), leading to a slightly yellow powder. (Yield: 1.5 g/ 40.1%)

4:

^{1}H-NMR (δ, 20℃, $CDCl_3$, 300 MHz): 7.37(t,2H,-$CH^{2,4}$); 7.20(m,1H,-CH^{3}); 7.07(d,2H,-$CH^{1,5}$); 4.05(m,4H,-OCH_2-); 2.48(t,2H, -CH2-COOR); 1.75(t,2H,P-CH_2); 1.36-1.23(m,26H,-CH_2); 1.19(t,6H,OEt) ppm.

^{13}C-NMR (δ, 20℃, $CDCl_3$, 125 MHz): 172(C=O); 151(C^{ph}-O); 130(C-P); 129($CH^{2,4}$); 125(CH^{3}); 121($CH^{1,5}$); 62(CH_2(PO**C**H_2CH_3)); 25-35(14*CH_2);15(POCH_2**C**H_3).

^{31}P- NMR (δ, 20℃, $CDCl_3$, 500 MHz): 33.775 ppm

SAM-1:

^{1}H-NMR (δ, 20℃, $CDCl_3$, 300 MHz): 7.37(t, 2H,-$CH^{2,4}$); 7.21(m,1H, -CH^{3}); 7.07(d,2H,-$CH^{1,5}$); 5.11(m,2H,-OH); 2.82-2.53(t,4H,-$C^{2,15}$); 1.81(m,4H,$C^{3,14}$); 1.65 (t,2H,P-CH_2); 1.33-1.21(m,22H,-CH_2) ppm.

^{13}C-NMR (δ, 20℃, $CDCl_3$, 125 MHz): 172(C=O); 151(C-O); 138(C-CH_2); 130(C-P); 129($CH^{2,4}$); 126(CH^{3}); 122($CH^{1,5}$); 25-35(15*CH_2) ppm.

^{31}P- NMR (δ, 20℃, $CDCl_3$, 500 MHz): 39.117 ppm

5.3.2 SAM-2

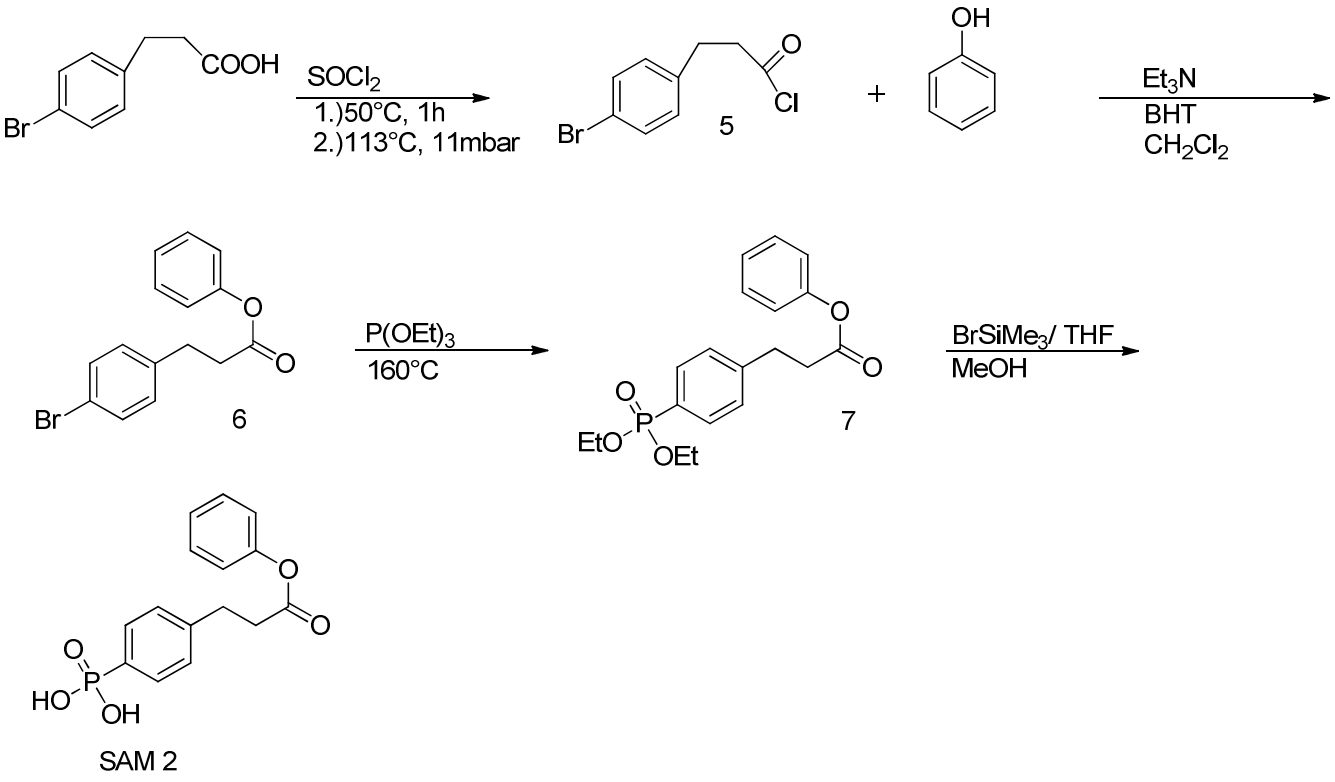

Scheme 17. Synthesis of SAM-2

3-(4-bromophenyl)-propionic acid (2.28 g, 10 mmol) was treated under argon atmosphere with thionylchloride (2.4 g, 20 mmol) and stirred at 50℃ for an hour. Then the solvent was distilled off at 11 mbar and 113℃.

The remaining oil was dissolved in ~30 ml CH_2Cl_2, 10 mmol of phenol (0.94 g) and 15 mmol of Et_3N (1.55 g) were added. As a catalyst BHT (1 mg) was used. This solution was stirred for 18 h. After this the reaction was quenched with water (~50 ml) and extracted with $NaHCO_3^-$ and HCl. The organic phase was dried over sodiumsulfite and after filtering the solvent was removed via vacuum. (2.69 g, 70%)

The slightly yellow powder was treated with triethylphosphite (3.5 g, 21 mmol) and refluxed at 160℃ for 2-3 hours. Then the solution was cooled to room temperature and the excessive triethylphosphite was removed by distillation (7)

The remaining powder was dissolved in 100 ml THF and 80 mmol of bromotrimethylsilane (12.24 g) was added under ice-cooling. The solution was stirred at RT for 24 hours. After this the solvent and the excessive bromotrimethylsilane were removed by oil-vacuum at 80℃. The remaining oil was dissolved in 100ml MeOH and 15 ml THF and refluxed for 23 h. Finally the product was dried and cleaned by column chromatography (Cy/AA 5:1), leading to the yellow powder in a yield of 1.47 g (48.3%)

7:

^{1}H-NMR (δ, 20℃, $CDCl_3$, 300 MHz): 7.48(d,2H,-$CH^{8,9}$); 7.41(t, 2H,-$CH^{2,4}$); 7.33(m,1H, -CH^{3}); 7.14(d,2H,-$CH^{6,7}$); 7.07(d,2H,-$CH^{1,5}$); 4.12(m,4H,-OCH_2); 2.98(t,2H,-CH_2); 2.81(t,2H,-CH_2); 1.41-1.24(t,6H,OEt) ppm.

^{13}C-NMR (δ, 20℃, $CDCl_3$, 125 MHz): 172(C=O); 151(C-O); 140(C-CH_2); 132($CH^{8,9}$); 130(C-P); 129($CH^{2,4}$); 126($CH^{6,7}$); 125(CH^{3}); 121($CH^{1,5}$); 62(CH_2(PO<u>C</u>H_2CH_3)); 31-35(2*CH_2);16(POCH_2<u>C</u>H_3) ppm.

^{31}P- NMR (δ, 20℃, $CDCl_3$, 500 MHz): 34.94 ppm.

SAM-2

^{1}H-NMR (δ, 20℃, $CDCl_3$, 300 MHz): 7.37(d,2H,-$CH^{8,9}$); 7.29(t, 2H,-$CH^{2,4}$); 7.18(m,1H, -CH^{3}); 7.05(d,2H,-$CH^{6,7}$); 6.98(d,2H,-$CH^{1,5}$); 2.95(t,2H,-CH_2); 2.78(t,2H,-CH_2); 2.09(s,2H,OH) ppm.

^{13}C-NMR (δ, 20℃, $CDCl_3$, 125 MHz): 172(C=O); 151(C-O); 139(C-CH_2); 133(C-P); 132($CH^{8,9}$); 130($CH^{2,4}$); 129($CH^{6,7}$); 126(CH^{3}); 121($CH^{1,5}$); 31(2*CH_2) ppm.

^{31}P- NMR (δ, 20℃, $CDCl_3$, 500 MHz): 27.98 ppm.

,

5.3.3 SAM-3

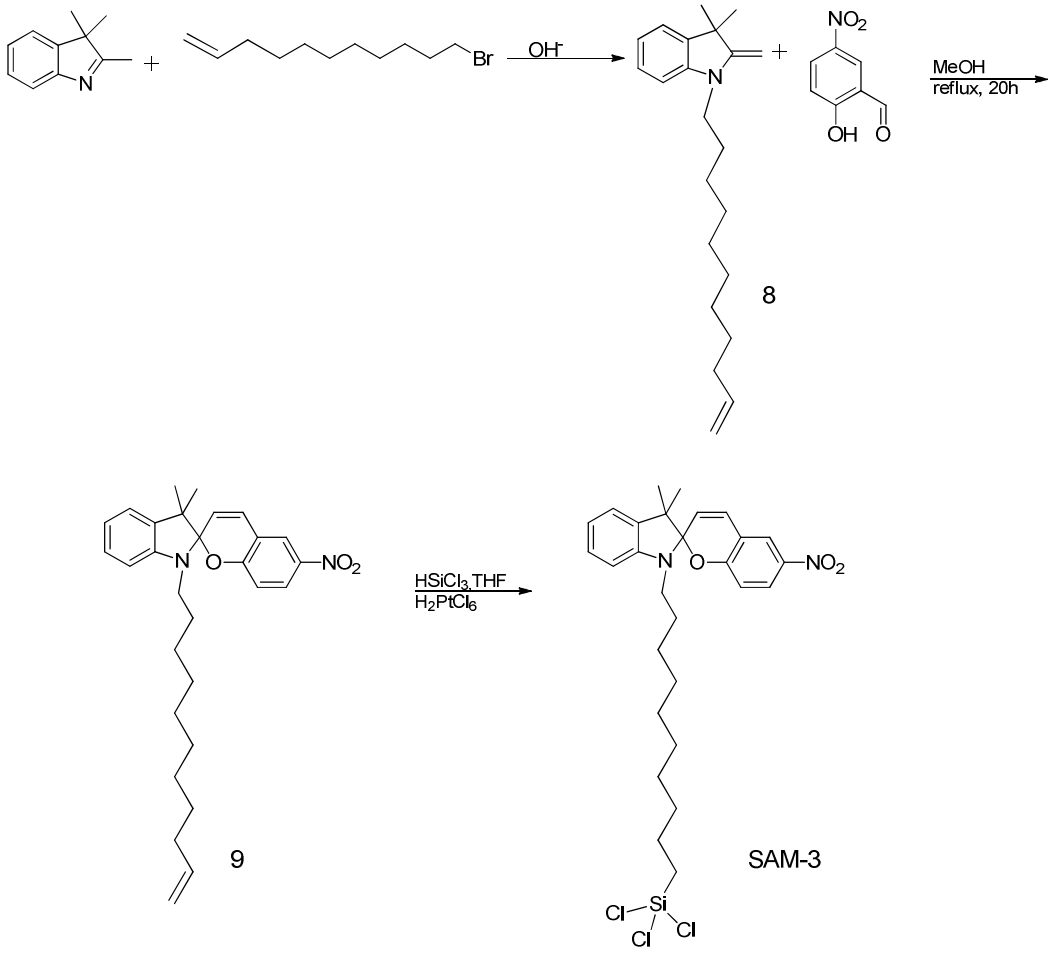

Scheme 18. Synthesis of SAM-3

A mixture of 2,3,3-trimethylindolenine (1.63 g, 11 mmol) and 11-bromo-1-undecene (2.33 g, 10 mmol) was refluxed for 72h. After cooling to room-temperature the excessive bromo-alkene was removed under vacuum. The remaining oil was dissolved in chloroform (50 ml) and extracted three times with water (3* 50 ml). The organic phase was dried with $NaSO_4$, filtered and finally dried under vacuum. The remaining product was dissolved in ethanol (30ml) and washed two times with aq. NaOH(2M). The organic phase was concentrated and extracted in ether three times (3* 30 ml). Finally the solution was dried with $NaSO_4$ and the solvent removed under vacuum.

The product was dissolved in 30 ml methanol and refluxed. During reflux, a mixture of 2-hydroxy-5-nitrobenzaldehyd (eq) in MeOH was added dropwise in a time range of

45 min and the whole mixture refluxed for 20 h. Afterwards it was cooled down to room temperature; the forming precipitate was filtered and washed with cold methanol. Recrystallization was performed in warm methanol (Yield: 2.55 g/ 71%)

To a solution of the product and H_2PtCl_6 (1 mg) in 50 ml THF, trichlorosilane (1.63 g, 12 mmol) was added dropwise. After complete conversion (TLC) the excessive trichlorosilane and solvent were removed under vacuum, leading to a red solid (Yield: 2.61 g/ 44.8%)

SAM-3:

^{1}H-NMR (δ, 20°C, $CDCl_3$, 300 MHz): 8.08(s,1H,spiro); 7.92(s,1H,spiro); 7.33(m,1H,spiro); 7.19(s,1H,spiro); 7.01(d,2H,spiro); 6.81(m,2H,spiro); 6.48(d,1H,spiro); 3.36(m,2H,N-CH_2); 1.47(t,6H,2*CH_3); 1.31-1.18(m,10H,-CH_2-); 1.11(m,2H,Si-CH_2) ppm.

^{13}C-NMR (δ, 20°C, $CDCl_3$, 125 MHz): 160.2; 148.4; 141.3; 135.7; 129.1; 128.4; 126.7; 125.6; 122.7; 120.4; 119.6; 116.6; 107.8; 53.6; 44.2; 34.0; 32.7; 31.8; 29.6; 28.9; 28.2; 27.1; 20.1 ppm.

5.3.4 SAM-4

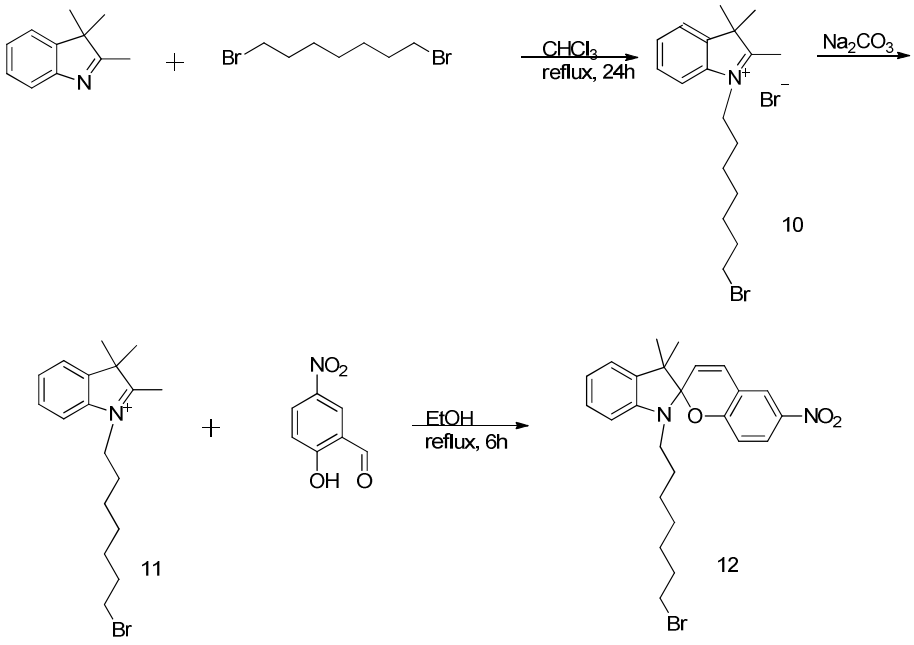

Scheme 19. Synthesis of 12

A mixture of 2,3,3- trimethylindolenine (0.8 g, 5 mmol) and dibromoheptane (1.29 g, 5 mmol) was refluxed for 24h. After cooling to room temperature, the obtained salt was washed three times with ether and dried under vacuum. Afterwards the salt was dissolved in 25 ml CH_2Cl_2 and stirred with 25 ml 0.2M NaOH for 30min. The organic phase was separated and the water phase extracted two times with ether (2* 30 ml). The combined organic phases were extracted with brine and water (50 ml), dried over $NaSO_4$, filtered and finally dried under vacuum. The product, dissolved in 30 ml THF, was mixed with 2-hydroxy-5-nitrobenzaldehyd (1 eq.) and refluxed for 16h. Afterwards the solvent was removed and the crude product was cleaned via column chromatography (hexane/dichloromethane 1:4). Finally the yellow powder was recrystallized in EtOH/$CHCl_3$. (Yield: 1.05 g/ 42.3 %)

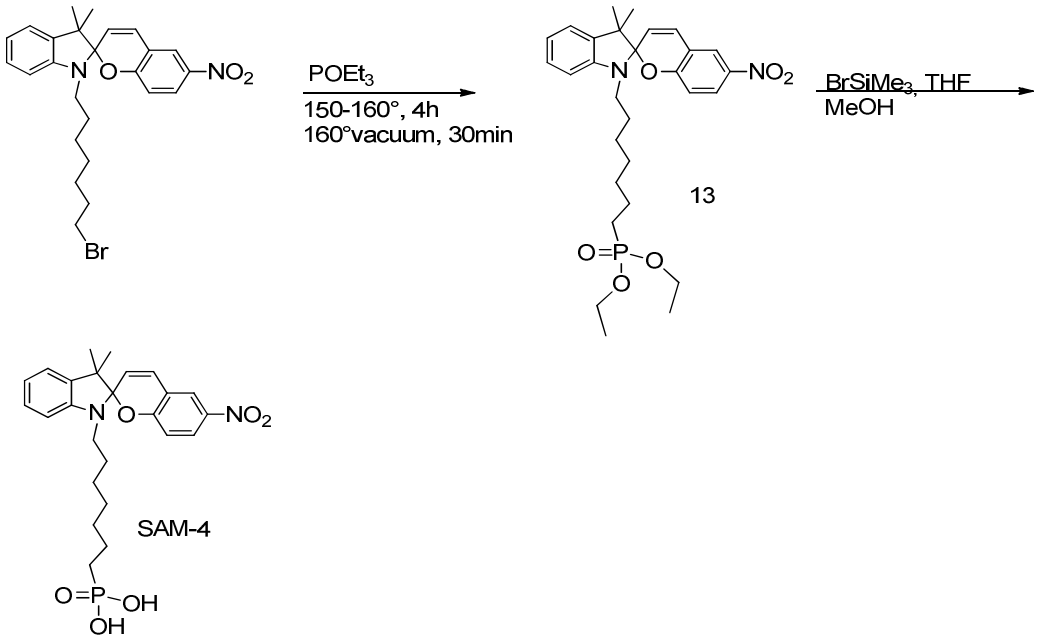

Scheme 20.Synthesis of SAM-4

The received product was treated with an excess of triethylphosphite (3 eq.) and slowly heated up to 150-160℃. The evolving ethylbromide was simultaneously distilled off. After 4 h the excess of triethylphosphite was removed under vacuum at 160℃. Afterwards the reaction was cooled down to room temperature and the product recrystallized in diethyl ether. The remaining oil in 100 ml THF was treated under ice-cooling with an excess of bromotrimethylsilane (8 eq) and stirred at room temperature for 24 h. After this the solvent was removed and the excess of bromotrimethylsilane was distilled of at 80℃ under vacuum. The residue was dissolved in 100 ml MeOH und 15 ml THF and refluxed for 23 h. Finally the solvent was removed, dried under vacuum and cleaned via column chromatography (1.Ethylacetat, 2.MeOH) to receive a red solid (Yield:1.3 g/ 25,6%)

SAM-4:

^{1}H-NMR (δ, 20℃, $CDCl_3$, 300 MHz):): 7.99(t,2H,spiro); 7.18(m,1H,spiro); 7.07(s,1H,spiro); 6.86(d,2H,spiro); 6.73(s,1H,spiro); 6.54(s,1H,spiro); 5.87(s,1H,spiro); 5.39(m,2H,OH); 3.40(m,2H,N-CH_2); 1.96(m,2H,CH_2-P); 1.56(m,2H, C^2); 1.50(t,6H,2* CH_3); 1.26-1.18 (m,6H,-CH_2-) ppm.

^{13}C-NMR (δ, 20℃, $CDCl_3$, 125 MHz):159.7; 147.1; 140.9; 135.9; 128.1; 127.8; 125.9; 122.1; 119.3.; 118.6; 115.7; 106.7; 52.7; 43.8; 33.9; 32.7; 31.0; 28.3; 28.2; 28.0; 27.1; 26.1; 19.9 ppm

^{31}P- NMR (δ, 20℃, $CDCl_3$, 500 MHz): 27.76 ppm

5.4 Synthesis of the Monomer

Step 1.

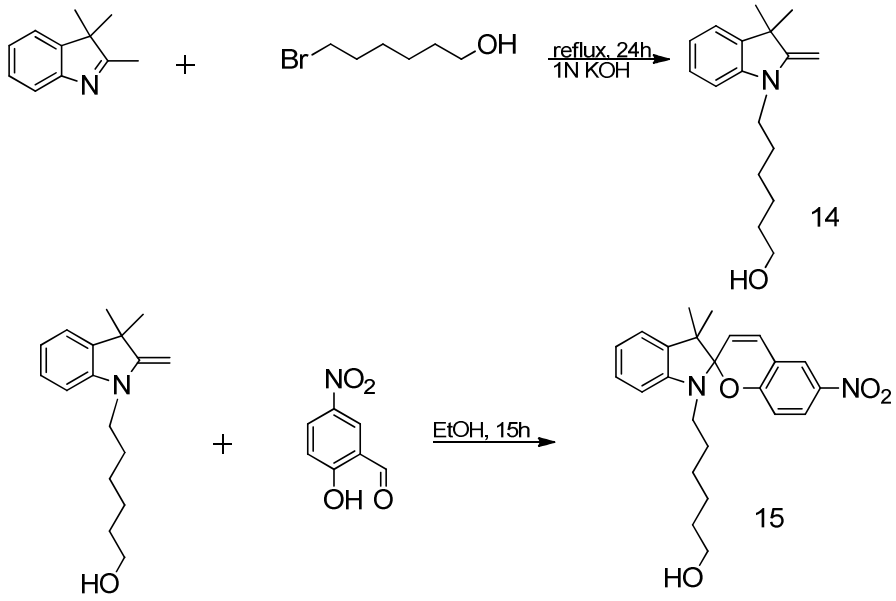

Scheme 21. Synthesis of the photochromic monomer, step 1

A mixture of 2,3,3- trimethylindolenine (0.8 g, 5 mmol) und 6-bromohexanol (1g, 5,5 mmol) in CH_3CN (0.21 g, 5 mmol) was refluxed for 24 h. After cooling to RT, the solvent was removed. The remaining product was dissolved in CH_2Cl_2 und extracted with water. The water phase was again extracted with CH_2Cl_2, 1N KOH was added to make the solution alcalic und finally extracted with Et_2O. The combined organic phases were again extracted by water and brine and finally dried with $NaSO_4$, filtered and dried under vacuum.

The remaining product was dissolved in abs. EtOH, 1eq. 5-Nitrosalicylaldehyde was added and stirred for 15 h at RT. After removing of the solvent, the product was cleaned via column chromatography. (75% EE/Cy). The dark red oil was recrystallized in a small amount of Et_2O by adding hexane till the solvent was getting cloudy.

Step 2.

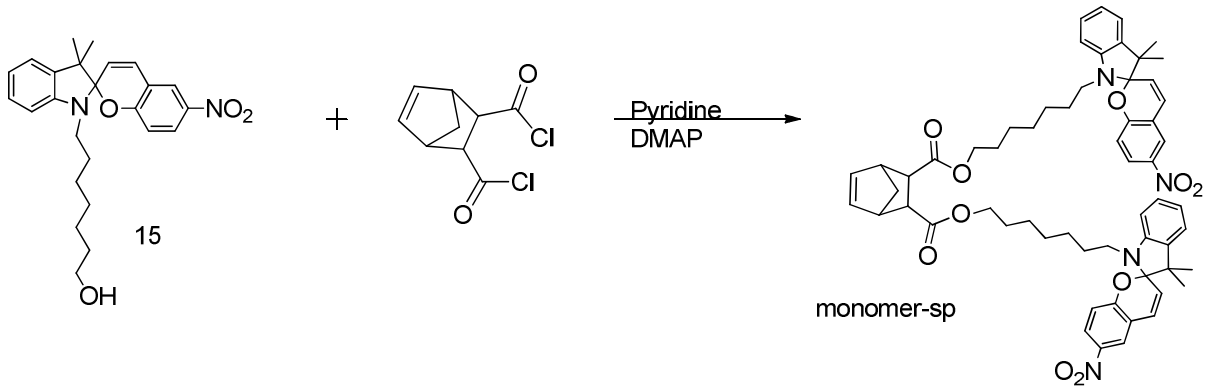

Scheme 22.Synthesis of the photochromic monomer, step 2

7-(3',3'-dimethyl-6-nitrospiro[chromene-2,2'-indoline]-1'-yl)heptan-1-ole (0.6 g, 1.5 mmol) was treated with bicyclo[2.2.1]hept-5-ene-2,3-dicarbonyl dichloride (0.15 g, 0.67 mmol) and pyridine (0.316 g, 4 mmol) in abs. CH_2CL_2 and a small amount of DMAP was added. The whole mixture was stirred overnight. After complete conversion (TLC), the product was extracted 3* with HCl und 3* with $NaHCO_3$ and dried over $NaSO_4$. After the solvent was removed, the product was cleaned through column chromatography (EE/Cy 1:10) leading to a red sticky product (Yield: 40-70%)

^{1}H-NMR (δ, 20℃, $CDCl_3$, 300 MHz): 8.19(m, 2H); 7.99(m, 2H); 7.76(d, 1H); 7.68(m, 1H); 7.31(d, 2H); 7.18(m, 2H); 7.09(s, 1H); 6,86(m, 2H); 6.79(d, 1H); 6.52(d, 1H); 6.34(d, 2H); 6.24(s, 1H); 6.03(s, 1H); 5.84(d, 1H); 4.09-4.01(m, 4H); 3.38(m, 6H); 3.08(d, 4H); 2.81-2.65(s, 2H); 1.65-1.15(m, 36H) ppm.

^{13}C-NMR *1* (δ, 20℃, $CDCl_3$, 125 MHz): 174.5; 155.1; 147.2; 140.9; 137.7; 135.1; 132.8; 128.1; 128.0; 125.9; 122.1; 121.7; 119.4; 118.5; 115.5; 106.7; 64.2; 52.7; 48.0; 47.3; 45.7; 44.1; 43.7; 43.5; 42.3; 41.8; 32.6; 30.9; 28.9; 27.8; 26.9;26.0; 25.16; 23.5; 19.9 ppm.

5.5 Synthesis of the Polymer

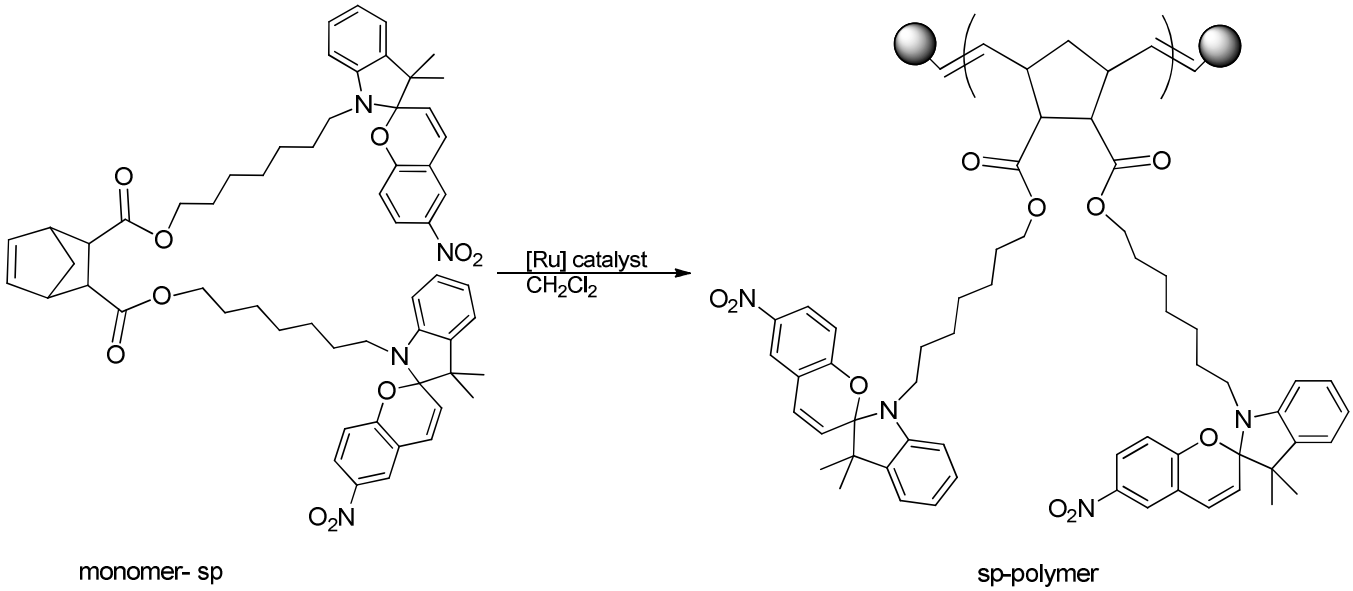

Scheme 23.Synthesis of the photochromic polymer

500 mg of monomer-sp were dissolved in 5 ml of dichloromethane and 1.22 mg of Initiator (Grubbs 3rd) were added and the mixture was stirred at RT for 20 h. After whole conversion (TLC), the reaction was stopped by adding of 0.15 ml ethylvinylether. Finally the polymer was recrystallized several times in cold methanol and dried under vacuum. The yield for the slightly red sticky polymer was between 30-60%.

^{1}H-NMR (δ, 20℃, $CDCl_3$, 300 MHz)

8.21(1H, spiro); 7.97(1H, spiro); 7.11-7.00(1H, spiro); 6.81-6.79(2H, spiro); 6.65-6.61 (2H, spiro); 6.51(1H, spiro); 5.76(1H, spiro); 5.68-5.10(m,4H, polymer); 3.97-3.95 (4H, -O-CH_2-); 3.38(4H, N-CH_2-); 3.26 -2.86(4H, nb^{1,2,3,5}); 1.84(2H, nb^4); 1.60-1.16(18H, spiro, -CH_2-) ppm.

5.6 Preparation of SAMs

The Silicon-Oxide and steel wafers were plasma etched in an O_2 atmosphere for 3 min and afterwards sonicated two times in Milli-Q water and finally in deionised water, to get as much hydroxyl anchor groups on the surface as possible. After drying in a nitrogen stream, the wafers were transferred into a glove-box and put into a 5 mmol solution of the synthesized molecule in 2-propanole for about 48 hours. Finally the substrates were dried at 60 ℃ for one hour.

5.7 Surface Patterning of SAMs

Flood UV-illumination was carried out under inert atmosphere (argon) by using an ozone-free mercury low-pressure lamp (Heraeus Noble Lamp; 254nm) with a power density of 1.35 mW/cm^2 and an irradiation time of 60 min. Patterned structures were obtained by using contact masks with lines and spaces. For postmodification reactions, wafers were half/half illuminated, shown in Figure 46.

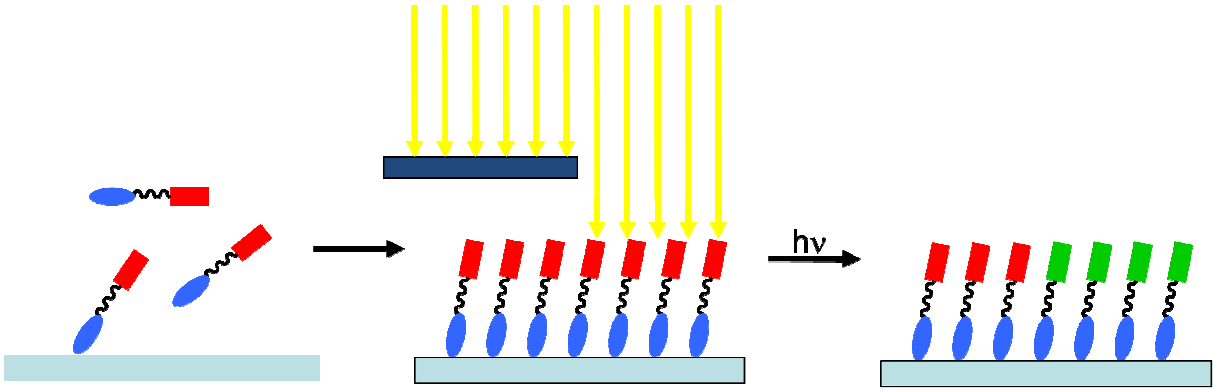

Figure 46. Scheme of half/half illumination of the substrates

5.8 Postmodification of SAMs

For postmodification reactions, the photo-Fries SAMs have been half-half illuminated for 30 min. After illumination, four different pathways were realized:

The first substrate was immersed in a solution of 200 µL adipoylchlorid and 50 µL triethylamine in 2 mL CH_2Cl_2 for 60 min and finally put in a solution of 100 µL ethylendiamine in 2 mL CH_2Cl_2 for 10 min. The second one was immersed in a solution of 200 µL perfluorobutyrylchloride and 400 µL pyridine in 5 mL CH_2Cl_2 for ten minutes, this time under anhydrous conditions, in a glove box. In a third try the wafer was modificated in a first step by 0.5 g carbonyldiimidazole (CDI) in 5 mL CH_2Cl_2 for 60 min and followed by immersing the substrate in a solution 0.2 g histidin in 2 mL CH_2Cl_2 for 30 min. For the last wafer, again CDI was used, but in difference to number three, iron-nanoparticles, synthesized by Dr.Thomas Rath, were capped to the surface.

5.9 Preparation of Thin Polymer Films

For photochemical measurements, a thin film of the polymer, dissolved in Chloroform, was spin coated onto CaF_2-discs. For some measurements a doctor blade was used to get the polymer as a homogeneous film on the surface.

5.10 Illumination of the Thin Films

The ring-opening UV-illumination, from spiropyran to the merocyanine form, was carried out under inert atmosphere (argon) by using an ozone-free mercury low-pressure lamp (EXFO EFOS Novacure), with an irradiation time of 30 sec. For ring-closure illumination a simple tungsten-lamp (60W) was used.

5.11 Cyclovoltammetry

The cyclovoltammetric experiments were performed in a three electrode configuration with an Autolab PGSTAT 100 potentiostat. A platinum disc was engaged as working electrode, platinum wire as the counter electrode and silver wire as pseudo-reference electrode. The measurements were performed using a $1*10^{-3}$ M solution of the photoreactive polymer in chloroform containing 0.1 M tetraethylammoniumtetrafluoroborate ($TBAPF_4$) as a supporting electrolyte. The scan rate was 0.2 $V.s^{-1}$ and the range from -1.8 V to 0.8 V. Figure 47 shows the setup of the measurement.

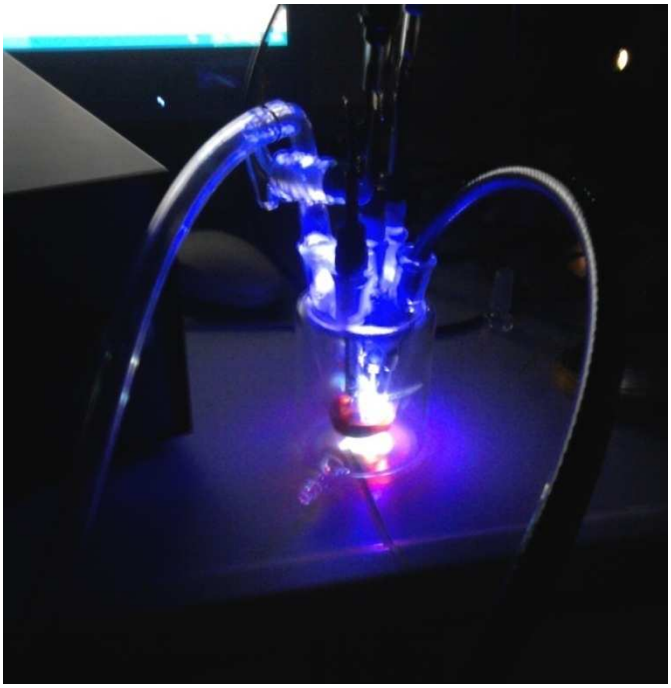

Figure 47. Setup for cyclovoltammogrammic measurements

5.12 OTFTs

Organic field effect transistors (OFETs) are using organic films instead of inorganic semiconductors. This new systems has a lot of advantages over the classic inorganic field effect transistors, like the silicon technology. The two most important one are the large area coverage and the low cost fabrication, an important factor for industry. These points made the OFETs to be one of the most studied systems and devices during the last decade.[146] Since they were first described in 1987[147], uncountable numbers of articles and papers are published every year, nice summarized in very good review articles.[148,149,150,151,152]

In this case, a special type of OFET was used, the so called Organic Thin Film Transistor (OTFT). Here the semiconductor, insulator, and the electrodes are thin layers on a supporting substrate. Figure 48 shows a typical setup of an OTFT.

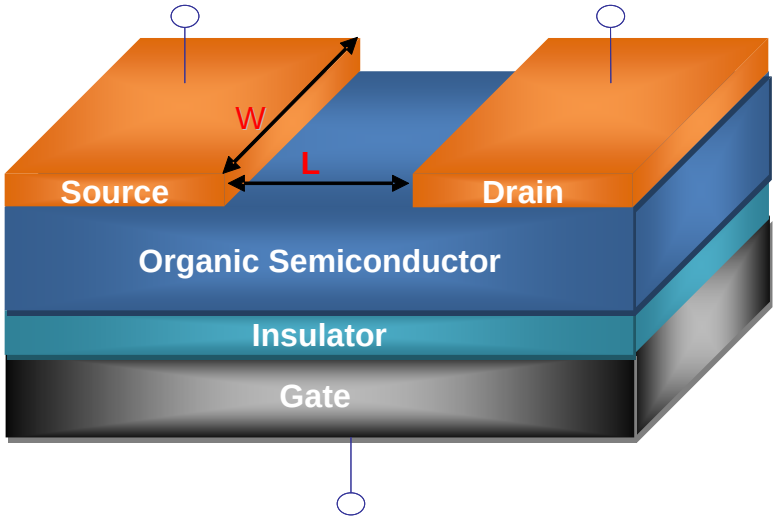

Figure 48. Setup of a classic OTFT

Commonly for the base of a transistor, the gate dielectric, a thermally grown SiO_x surface on doped silicon wafer is used, which works as a gate electrode and substrate. This gate electrode is separated from the organic semiconductor by an insulator, the gate dielectric. As organic semiconductor typically highly conjugated polymers poly(3-hexylthiophene) (P3HT)[153], poly(9,9-dioctylfluorene-*co*-bithiophene)

(F8T2)[154], poly(9,9-dioctylfluorene)-co-[phenylene-(*N*-4-sec-butylphenyl)-imino-phenylene] (TFB)[155] or small molecules like pentacene[156] are used.

These materials are mostly vacuum deposited or spin coated onto the surface. For the top electrodes, the source and drain, normally gold is evaporated on the organic semiconductor with a certain width (W) and separated by a distance (L).This area between the source and drain electrode is called channel.

Through variable- fabrication setups, two different types of transistors are possible: Top and bottom contact transistors. They differ in the position of the source and drain electrodes, whether they are evaporated on the gate dielectric (bottom contact) or on the organic semiconductor (top contact). Also through the type of the devices they can be differentiated in n- and p-type channels. N and p describe the type of the mobile carriers, electrons or holes. In a p-type device, a negative bias between source and gate generates holes in the channel, whereas in a n-type device a positive bias accumulates electrons.

3.1.1. Characterizing of the transistors

For characterizing of an OTFT an electrical field is modulated. Normally the source electrode is grounded (V_S=0 V), whereas voltage is applied to the drain and the gate electrode. After applying negative voltage at the gate electrode (V_G), a conductive channel is generated between the semiconductor and the insulator. This conductive channel consists of accumulated mobile charges, the so called holes. The source drain current I_D is formed by applying an additional voltage at the drain electrode (V_D) and so a horizontal electrical between source and drain is built. To turn the transistor off, V_G has to be 0 because in this case I_D is too low. But by decreasing the gate voltage, which means more negative voltage, the conductive channel is build up and the transistor is working by increasing the mobile charges.

For characterization, two main types of measurements are performed: The output characteristics and the transfer characteristics. For the output characteristics, the drain current I_D is measured as a function of the source-drain voltage V_D for a fixed

gate voltage V_G. Figure 49 shows an output characteristic for a typical pentacene-FET, measured by M. Marchl.

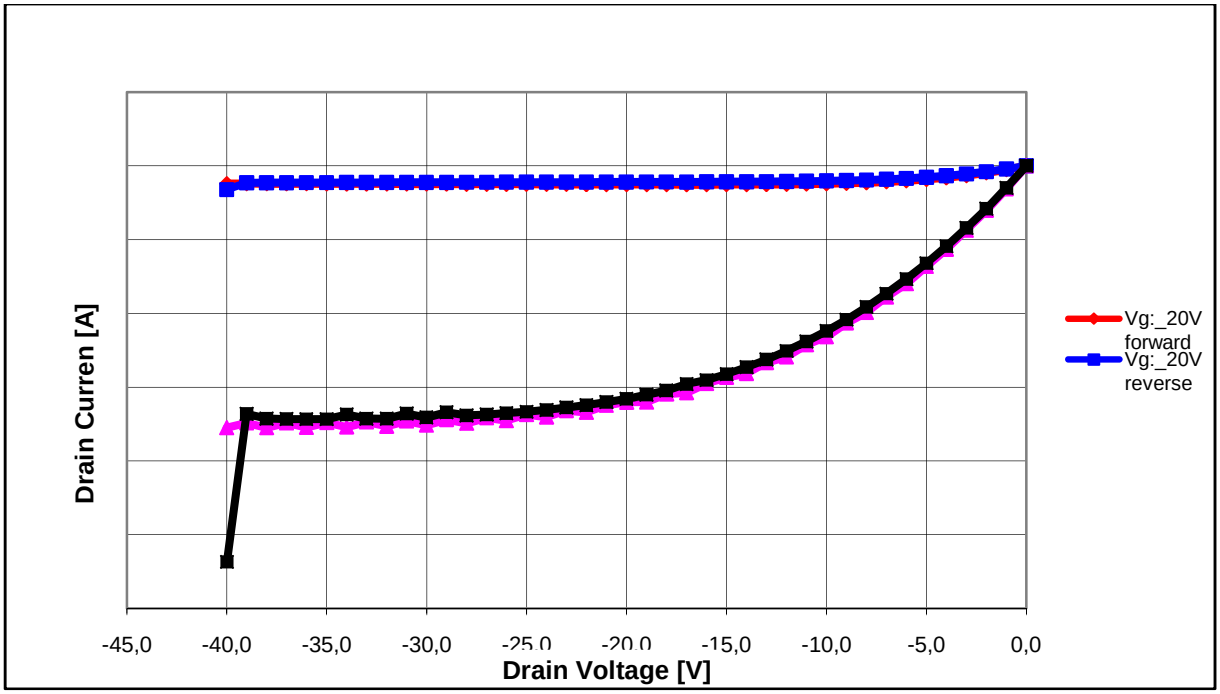

Figure 49. Classical output characteristic of an OTFT

The output characteristics show two regions, the linear and the saturation region. In the linear region, the gate voltage is larger than the drain voltage and the drain current increases linear with the drain voltage. When the drain voltage is bigger than the gate voltage and the drain current is saturated, the saturation regime is reached, caused by the so called pinch-off.

Figure 50 shows the transfer characteristic, again measured by M. Marchl, where the drain current is measured as a function of the gate voltage for a fixed drain voltage. This curves show, how the transistor can be switched by varying the gate voltage. Also the most important transistor facts can be extracted from the transfer characteristic: the threshold V_{TH} and turn-on V_{TO} voltages, the charge-carrier mobility μ or the on/off ratio. Turn-on voltage means the gate voltage when the drain current starts to flow. For determination of the charge-carrier mobility and threshold voltage some approximations are essential, which will not be discussed in this work.

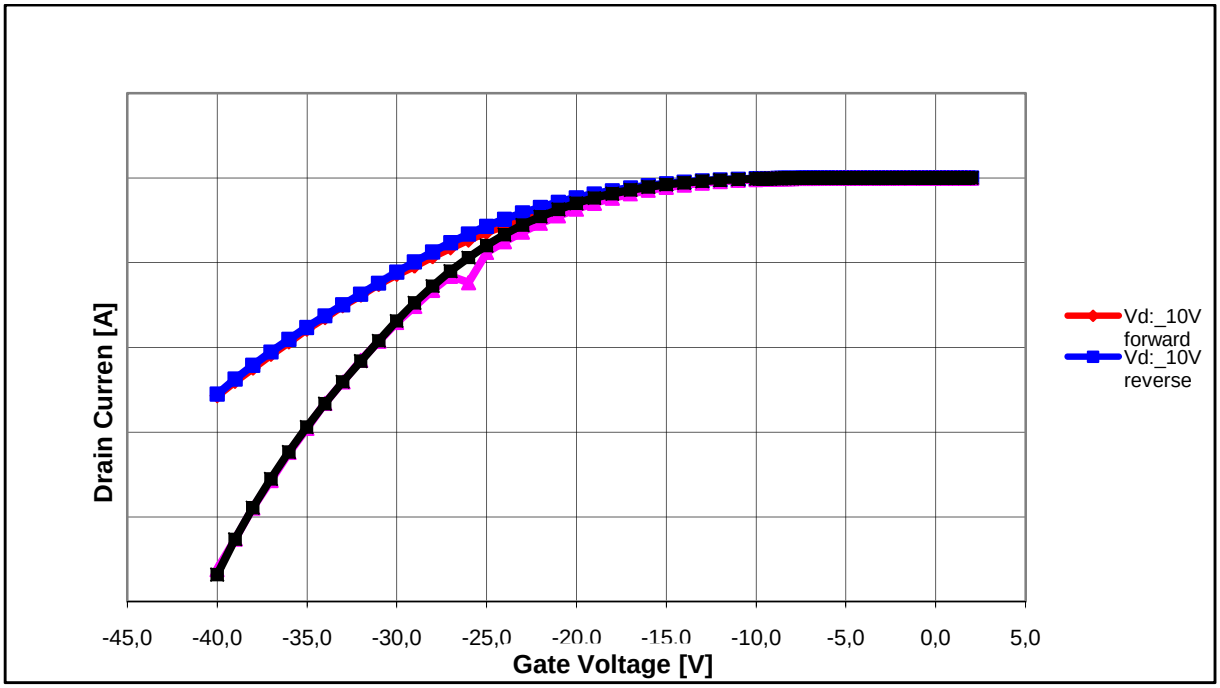

Figure 50. Classic Transfer characteristic of an OTFT

Another important fact during transistor characterization is the so called hysteresis effect. The hysteresis is the difference between the upward sweep, when the gate voltage increases, and the downward sweep, when the gate voltage decreases. Even when the same voltage is achieved, small differences in the current can be observed.

A lot of different studies have shown that the performance of the transistor is mainly controlled by the properties of the interface between the organic semiconductor (OSC) and the gate dielectric.[157] So the main focus of today's studies is to find the perfect semiconductor for each transistor type. Especially for OTFTs, self-assembling monolayers (SAMs) are one of the most interesting scientific fields at the moment. Although silan based molecules do not only form monolayers, more multilayers, as already mentioned in chapter 2.2, they seem to be predestined for transistor technology.[158]

The purchased SiO_2 wafers were unpacked in a laminar flow box, cleaned with a CO_2 spray and O_2 plasma etched for 2 min. After this step the wafers were treated in an ultrasonic bath in ultra-pure water to achieve a defined chemical composition on the surface. Now the polymer solution (10 mg Polymer/ml $CHCl_3$) was spin-coated onto the surface. Afterwards the wafers were locked in to a glove box, where the active material, pentacene, and the Au-source and drain electrodes were evaporated onto

the transistor. After this fabrication steps the transistors were ready for further characterization measurements. For comparison-measurements, a typical pentacene transistor was constructed in the same way.

6 Appendix

6.1 List of Figures

6.2 List of Schemes

6.3 List of Tables

6.4 Curriculum Vitae

Personal Details

Name	Hauser Lucas
Address	Moserhofgasse 25b
	8010 Graz
Mail	lucas.hauser@tugraz.at
Date of birth	19.08.1983
Citizenship	Austria

Education and Qualifications

1989-1993	Elementary school in Judenburg
1993- 2001	Secondary school BG/BRG Judenburg
2001-2002	Military service in Zeltweg, Fliegerhorst Hinterstoisser
2002-2008	Graz University of Technology- Technical Chemistry/ Chemical Engineering
	Diploma Thesis:
	“Cationic and dicationic zironocenes as isobuten catalysts”
2008-2011	PhD thesis at Graz University of Technology under supervision of Assoc.Prof. DI Dr. Gregor Trimmel
	PhD thesis:
	“New photoreactive materials for structured surface modification”

6.5 Publications

Talks:

2010

Hauser, L.; Kirnstötter, S.; Marchl, M.; Zojer, E.; Fian, A.; Kaltenböck, L.; Griesser , T.; Kern, W.; Trimmel, G.: **Reversible photoreactions in polynorbornenes bearing spiropyran side groups and their applications.** - in: NFN Meeting 2010. Schloß Röthelstein, Admont am: 29.09.2010

Außerlechner, S. J.; Ladinig, L.; Pressl, K. .; Flesch, H.-G.; Novák, J.; Hauser, L.; Zojer, E.: **Organic thin film-transistors – fundamentals and recent results.** - in: Physikalisches Oberseminar für DissertantInnen. Graz am: 14.12.2010

Hauser, L.; Kirnstötter, S.; Marchl, M.; Zojer, E.; Fian, A.; Grießer, T.; Kern, W.; Trimmel, G.: **Reversible Photoreactions in Polynorbornenes Bearing Spiropyran Side Groups and their Application in Organic-Thin-Film Transistors.** - in: 10th Austrian Polymer Meeting and 2nd Joint Austrian-Slovenian Polymer Meeting. Leoben am: 08.09.2010

2009

Hauser, L.; Jaeger, M.; Griesser, T.; Kern, W.; Resel, R.; Trimmel, G.: **Patterning and Tuning of Surface Properties with Photoreactive Molecules.** - in: NFN Meeting 2009. Schloß Röthelstein, Admont am: 16.09.2009

Poster:

2011

Hauser, L.; Kaltenböck, L.; Schmuck, M.; Kirnstötter, S.; Marchl, M.; Griesser , T.; Kern, W.; Zojer, E.; Trimmel, G.: **Changing the surface - Reversible photoreactions in polynorbornenes and their application in OFETs.** - in: E-MRS 2011 . Nizza, Frankreich am: 09.05.2011

2010

Kirnstötter, S.; Marchl, M.; Hauser, L.; Trimmel, G.; Haase, A.; Fian, A.; Grießer, T.; Zojer, E.: **Reversible tuning of the electronic properties of pentacene based Organic Thin-Film Transistors with an UV/VIS-light reactive interfacial spiropyran layer.** - in: International Conference on Organic Electronics. Paris, Frankreich am: 22.06.2010

Außerlechner, S. J.; Marchl, M.; Pacher, P.; Hauser, L.; Obermüller, T.; Golubkov, A.; Haase, A.; Stadlober, B. .; Buchner, M.; Edler, M. .; Flesch, H.-G.; Grießer, T. .; Trimmel, G.; Resel, R.; Zojer, K.; Schürrer, F.; Zojer, E.: **Understanding the Origin of Threshold-Voltage Shifts in Organic Thin Film Transistors Induced by Interfacial Layers.** - in: International Conference on Organic Electronics 2010. Paris am: 22.06.2010

Hauser, L.; Griesser , T.; Jäger, M.; Kern, W.; Trimmel, G.: **UV-patterning and surface modification using the photochemistry of spiropyrans .** - in: Winterschool on Organic Electronics. Planneralm, Donnersbach am: 06.03.2010

Kirnstötter, S.; Marchl, M.; Obermüller, T.; Haase, A.; Hauser, L.; Edler, M.; Grießer, T.; Zojer, E.: **Controlling the electronic properties and morphology of the active layer in organic thin film transistors by an interfacial photoreactive layer.** - in: Winterschool on Organic Electronics - Fundamental Properties of Devices - Sensors, Transistors, and Solar Cells. Planneralm, Austria am: 06.03.2010

2009

Hauser, L.; Trimmel, G.; Griesser , T.; Kern, W.: **Reversible photoreactions in polynorbornenes bearing spiropyrane side groups.** - in: EPF 2009. Graz, Austria am: 12.07.2009

Jaeger, M.; Hauser, L.; Edler , M.; Griesser, T.; Kern, W.; Trimmel, G.: **UV-patterning and surface modification using functional poly(norbornene)s bearing photoacidgenerator groups.** - in: European Polymer Congress 2009 (EPF09). Graz, Austria am: 12.08.2009

Obermüller, T.; Marchl, M.; Außerlechner, S. J.; Golubkov, A.; Haase, A.; Stadlober, B.; Hauser, L.; Trimmel, G.; Edler, M.; Grießer, T.; Kern, W.; Zojer, E.: **Temperature dependent bais-stress measurement in organic thin film transistors.** - in: International Conference on Organic Electronics. Liverpool am: 15.06.2009

Hauser, L.; Griesser , T.; Flesch, H.-G.; Resel, R.; Kern, W.; Trimmel, G.: **Design and application of tunable surfaces by photoreactive monolayers.** - in: MRS Fall Meeting 2009. Boston, USA am: 29.11.2009

Marchl, M.; Pacher, P.; Golubkov, A.; Haase, A.; Stadlober, B.; Possanner, S.; Schürrer, F.; Zojer, K.; Hauser, L.; Slugovc, C.; Trimmel, G.; Zojer, E.: **Controlling the temperature dependent electronic properties of Organic Thin Film Transistors by Self Assembled Monolayers.** - in: MRS Spring Meeting. San Francisco am: 13.04.2009

Kremser, G.; Hauser, L.; Flesch, H.-G.; Resel, R.; Trimmel, G.: **Synthesis of Monofunctionalized Electroactive Molecules and their Application in Surface Modification.** - in: MRS Spring Meeting 2009. San Francisco, CA am: 13.04.2009

2008

Hauser, L.; Trimmel, G.; Griesser , T.; Höfler, T.; Track, A. M.; Ramsey, M. G.; Kern, W.: **Tuning of Si/SiOx surfaces by photoreactive monolayers.** - in: 58. Jahrestagung OEPG 2008. Montanuniversität Leoben am: 22.09.2008

6.6 Literature

1 http://goldbook.iupac.org/P04588.html, 25.07.2011 [18:53 Uhr]

2 http://www.uni-regensburg.de/EDV/Misc/Bilder/Spektrum.gif, 19.05.2011 [14:55 Uhr]

3 Kopecky, J. Photochemistry a visual approach, New York: VCH; **1992**: 4.

4 Horspool, W.; Armest, D. Org.Photochem. A: Comprehensive treatement. New York: Ellis Horwood Limited; **1992**: 1-2.

5 Horspool, W.M.; Synthetic Organic Photochemistry. In: Horspool WM, eds. Plenum Press; **1984**, Chapter 9.

6 http://www.chemiedidaktik.uni-wuppertal.de/alte_seite_du/material/lichtsp/jablt.gif, 19.05.2011 [15:07]

7 Prucker, O.; Naumann, C. A.; Rühe, J.; Knoll, W.; Frank, C. W. *J. Am. Chem. Soc.* **1999**, *121*, 8766.

8 Jeyaprakash, J. D.; Samuel, S.; Rühe, J. *Langmuir* **2004**, *20*, 10080.

9 Leshem, B.; Sarfati, G.; Novoa, A.; Breslav, I.; Marks, R. S. *Luminescence* **2004**, *19*, 69.

10 Prucker, O.; Habicht, J.; Park, I.-J.; Rühe, J. *Mater. Sci. Eng. C* **1999**, *8-9,* 291.

11 Prucker, O.; Rühe, J. *Langmuir* **1998**, *14*, 6893.

12 Tsubokawa, N.; Satoh, M. *J. Appl. Polym. Sci.* **1997**, *65*, 2165.

13 Liang, L.; Feng, X.; Liu, J.; Rieke, P. C.; Fryxell, G. E. *Macromolecules* **1998**, *31*, 7845.

14 Liang, L.; Rieke, P. C.; Fryxell, G. E.; Liu, J.; Enehard, M. H.; Alford, K. L. *J. Phys. Chem. B*. **2000**, *104*, 11667.

15 Jonas, U.; Del Campo, A.; Krüger, C.; Glasser, G.; Boos, D. *Proc. Nat. Ac. Sci.* **2002**, *99*, 5034.

16 Kodera, F.; Matsuzawa, Y.; Okano, K. ; Yamashita, T. *J. of Photopol. Scien. Techn.* ***2010****, 23*, 235-240.

17 Reichmanis, E.; Houlihan, F. M. ; Nalamasu, O.; Neenan, T. X. *Adv.Mater.* **1991**, *3*, 394-397.

18 Lex, A.; et al. *Chem. Mater.* **2008***, 20*, 2009-2015.

19 Bouas-Laurent, H.;Dürr, H. *Pure Appl.Chem.* **2001**, *73*, 639-665.

20 Natali M.; Soldi L. *Tetrahedron* **2010**, *66*, 7612-7617.

21 Kohno, Y.; Tamura, Y.; Matsushima, R. *J. Photochem. Photobiol. A,* **2009**, *201,* 98-101

22 Shibaev, V.P.; Bobrovsky, A.Y.; Boiko N.I. *Macromol.Symp.* **2001**, *174*, 319-332

23 Zhang, J.; Matsushita, M. M.; Kong, X. X.; Abe, J.; Iyoda, T. *J.Am.Chem.Soc.* **2001,** *123*, 12105-12106

24 Hvilsted, S.; Ramanujam, P.S. *Monatsh.Chem.*, **2001**, *132*, 43.

25 Fischer, E.; Hirshberg, Y. *J. Chem. Soc.* **1952**, 4522

26 Oda, H. *Dyepig* **1998**, *38*, 243-254

27 Shimidzu, I.; Kokado, H.; Inoue, E. *Bull.Chem.Soc.Japan* **1969**, *42*, 1730

28 Shimidzu, I.; Kokado, H.; Inoue, E. *Nippon Kagaku Zasshi* **1968**, *89*, 755

29 Hirshberg, Y.; *J. Am. Chem. Soc.* **1956**, 78, 2304

30 Berkovic, G.; Krongauz, V.; Weiss, V. *Chem. Rev.* **2000**, *100*, 1741-1753

31 Lukyanov, B.S.; Lukyanova, M.B. *Chem. Heterocycl. Comp*. **2005**, *41*(3)

32 Irie M., Menju A., Hayashi K. *Macromolecules;* **1979,** *12*, 1176

33 Menju A., Hayashi K., Irie M. *Macromolecules;* **1981**, *14*, 755-758

34 Delaire J.A., Nakatani K. *Chem.Rev.*, **2000**, *100*, 1817

35 Angiolini L. et al. *Macromol.Chem.Phys.*, **2008**, *209*, 2049-2060

36 Zelichenok A., et al. *Macromolecules*; **1992**, *25*, 3179

37 Dürr H., Ma Y., Cortellaro G. *Synthesis*, **1995,** *1,* 294

38 Bobrovsky A.Y., Boiko N.I., Shibaev V.P. *Adv.Mater.*, **1999**, *11,12,* 1025

39 Piech M., Bell N.S. *Macromolecules*; **2006**, *39,* 915

40 Samanta S., Locklin J.; *Langmuir*; **2008**, *24 (17),* 9558-9565

41 Angiolini, L.; Benelli, T.; Giorgini, L.; Raymo, F.M. *Polymer* **2009**, *50*, 5638-5646

42 Stitzel, S.; Byrne, R.; Diamond, D. *J. Mater. Sci*. **2006**, *41*, 5841-5844

43 Mysliwiec, J.; Sznitko, L.; Bartkiewicz, S.; Miniewicz, A.; Essaidi, Z.; Kajzar, F.; Sahraoui, B. *Appl. Phys. Lett.* **2009**, *94,* 241106

44 Zhu, L.; Zhu, M.Q.; Hurst, J. K.; Li, A.D.Q. *J. Am. Chem. Soc.* **2005**, *127*, 8968-8970

45 Feringa, B.L. *Molecular Switches*, 1st edition., Wiley-VCH, Weinheim, **2001**

46 Bouas-Laurent, H.; Dürr, H. *Pure Appl. Chem*. **2001**, *73*, 639-665.

47 Ohya, Y.; Okuyama, Y.; Fukunuga, A.; Ouchi, T. *Supramol. Sci.* **1998**, *5*, 21-29

48 Zhu, M.Q.; Zhu, L.; Han, J.J.; Wu, W.; Hurst, J.K.; Li, A.D.Q. *J. Am. Chem. Soc.* **2006**, *128*, 4303-4309

49 Schaudel, B.; Guermeur, C.; Sanchez, C.; Nakatani, K.; Delaire, J.A. *J. Mater. Chem.* **1997**, *7(1)*, 61-650

50 Andersson, J.; Li, S.; Lincoln, P.; Andersson, J. *J. Am. Chem. Soc.* **2008,** *130*, 11836-11837

51 Cho, M.J.; Kim, G.W.; Jun, W.G.; Lee, S.K.; Jin, J.-I. ; Choi, D.H. *Thin Solid Films* **2006**, *500*, 52-60

52 Testoni, F. M.; Ribeiro, E. A.; Giusti, L. A.; Machado, V. G. *Spectrochimic. Acta A* **2009**, *71*, 1704-1711

53 Kinashi, K.; Harada, Y.; Ueda, Y. *Thin Solid Films* **2008**, *516*, 2532-2536

54 Guerchais, V.; Ordronneau, L.; Le Bozec, H. *Coord. Chem. Rev.* **2010**, *254*, 2533-2545

55 Natali, M.; Aakeröy, C.; Desper, J.; Giordani, S. *Dalton Trans.* **2010**, *39*, 8269-8277.

56 Fries, K.H.; Driskell, J.D.; Samanta, S.; Locklin, J. *Anal Chem* **2010**, *82*, 3306-3314.

57 Natali, M.; Soldi, L.; Giordani, S. *Tetrahedron* **2010**, *66*, 7612-7617

58 Anderson, J.C.; Reese, C.B. *Proc. Chem. Soc. London* **1960**, *6*, 217-217.

59 Elad, D. *Tetrahedron Letters* **1963**, *14*, 873-875.

60 Finnegan, R.A.; Knutsen, D. *Tetrahedron Lett*. **1968**, *9*, 3429.

61 Barton,D. H. R.; Chow,Y. L.; Cox, A.; Kirby, G.W. *J. Chem .Soc*. **1965**, 3571-3 578.

62 Plank, D. A. *Tetrahedron Lett*. **1968**, *9* (42), 5423-5426.

63 Griesser, T.; Adams, J.; Wappel, J.; Kern, W.; Leggett, G.J.; Trimmel, G. *Langmuir* **2008**, *24*, 12420-12425.

64 Pockels, A. *Nature* **1891**, *43*, 437

65 Langmuir, I. *J. Am. Chem. Soc* **1917**., 39 (9), 1848-1906.

66 Langmuir, I. *Trans. Faraday Soc.* **1920**, 15, 62-74.

67 Bigelow, W.C.; Pickett, D.L.; Zisman, W.A. *J .Colloid Interface Sci.* **1946**, 1, 513.

68 Sagiv, J. *J. Am. Chem. Soc.* **1980**, 102, 92.

69 Nuzzo, R.G.; Allara, D.L. *J. Am. Chem. Soc.* **1983**, 105, 4481.

70 Onclin, S.; Ravoo, B.J.; Reinhoudt, D.N. *Angew. Chem. Int. Ed.* **2005**, 44, 6282-6304.

71 Ullman, A. *Chem. Rev.* **1996**, *96*, 1533-1554.

72 Aswal, D.K.; Lenfant, S.; Guerin, D.; Yakhmi, J.V.; Vuillaume, D. *Anal.Chim.Acta* **2006**, *568*, 84-108

73 Mayr, T. M.; de Boer, M. P. ; Shinn, N. D. ; Clews, P. J.; Michalske, T. A. *J. Vac. Sci. Technol. B* **2000**, *48*, 2433.

74 Hozumi, A.; Ishiyama, K.; Sugimura, H.; Takai, O. *Langmuir* **1999**, *15*, 7600.

75 Wu, K.; Bailey, T. C.; Willson C. G.; Ekerdt, J. G. *Langmuir* **2005**, *21*, 11795.

76 Karsi, N.; Lang, P.; Chehimi, M.; Delamar, M.; Horowitz, G. *Langmuir* **2006**, *22*, 3118.

77 Allara, D. L.; Nuzzo, R. G. *Langmuir* **1985**, *1*, 45.

78 Allara, D. L.; Nuzzo, R. G. *Langmuir* **1985**, *1*, 52.

79 Ogawa, H.; Chihera, T.; Taya, K. *J. Am. Chem. Soc.* **1985**, *107*, 1365.

80 Vercelli, B.; Zotti, G.; Schiavon, G.; Zecchin, S.; Berlin, A. *Langmuir* **2003**, *19*, 9351.

81 Sun, S.; Leggett, G. J. *Nano Lett.* **2007**, *7*, 3753.

82 Gao, W.; Dickinson, L.; Grozinger, C.; Morin, F. G.; Reven, L. *Langmuir* **1996**, *12*, 6429.

83 Textor, M.; Ruiz, L.; Hofer, R.; Rossi, A.; Feldman, K.; Haehner, G.; Spencer, N. D. *Langmuir* **2000**, *16*, 3257.

84 Spori, D. M.; Venkataraman, N. V.; Tosatti, S. G. P.; Durmaz, F.; Spencer, N. D.; Zuercher, S. *Langmuir* **2007**, *23*, 8053.

85 Tosatti, S.; Michel, R.; Textor, M.; Spencer, N. D. *Langmuir* **2002**, *18*, 3537.

86 Benitez, J. J.; Heredia-Guerrero, J. A.; Heredia, A. *J. Phys. Chem. C* **2007**, *111*, 9470.

87 Wang, L.; Jiang, J.; Song, Y.; Zhang, B.; Wang, E. *Langmuir* **2003**, *19*, 4953.

88 Benitez, J. J.; Kopta, S.; Diez-Perez, I.; Sanz, F.; Ogletree, D. F.; Salmeron, M. *Langmuir* **2003**, *19*, 762.

89 Dishner, M. H.; Hemminger, J. C.; Feher, F. J. *Langmuir* **1997**, *13*, 4788.

90 Huang, F. K.; Horton, R. C.; Myles, D. C.; Garrell, R. L. *Langmuir* **1998**, *14*, 4802.

91 Han, S. W.; Lee, S. J.; Kim, K. *Langmuir* **2001**, *17*, 6981.

92 Burgos, P.; Geoghegan, M.; Leggett, G. J. *Nano Lett.* **2007**, *7*, 3747.

93 Shaporenko, A.; Heister, K.; Ulman, A.; Grunze, M.; Zharnikov, M. *J. Phys. Cem. B* **2005**, *109*, 4096.

94 Silberzan, P.; Léger, L.; Ausserré, D.; Benattar, J. J. *Langmuir* **1991**, *7*, 1647.

95 Tripp, C. P.; Hair, M. L. *Langmuir* **1995**, *11*, 1215.

96 Wasserman, S. R.; Whitesides, G. M.; Tidswell, I. M.; Ocko, B. M.; Pershan, P. S.; Axe, J. D. *J. Am. Chem. Soc.* **1989**, *111*, 5852.

97 Ulman, A. *Chem. Rev.* **1996**, *96*, 1533.

98 Schreiber, F. *Prog. Surf. Sci.* **2000**, *65*, 151.

99 Love, J. C.; Estroff, L. A.; Kriebel, J. K.; Nuzzo, R. G.; Whitesides, G. M. *Chem. Rev.* **2005**, *105*, 1103.

100 Onclin, S.; Ravoo, B. J.; Reinhoudt, D. N. *Angew. Chem., Int. Ed.* **2005**, *44*, 6282.

101 Aswal, D. K.; Lenfant, S.; Guerin, D.; Yakhmi, J. V.; Vuillaume, D. *Anal. Chim. Acta* **2006**, *568*, 84.

102 Silberzan, P.; Leger, L.; Ausserre, D.; Benattar J.J. *Langmuir*, **1991,** 7, 1647.

103 Angst, D.L.; Simmons, G.W. *Langmuir* **1991**, 7, 2236.

104 Hanson, E.L.; Schwartz, J.; Nickel, B.; Koch, N.; Danisman, M.F. *J.Am.Chem.Soc.* **2003**, *125*, 16074-16080.

105 Hofer, R.; Textor, M.;Spencer, N.D. *Langmuir* **2001**, *17*, 4014-4020.

106 Brzoska, J.B.; Shahidzadeh, N.; Rondelez, F. *Nature* **1992**, 360 (6406), 719-721.

107 Carroro, C.; Yauw, O.W.; Sung, M.M.; Maboudian, R.J. *J Phys. Chem. B* **1998**, 102 (23), 4441-4445.

108 Bain, C.D.; Evall, J.; Whitesides, G.M. *J. Am. Chem. Soc.* **1989** 111, 7155.

109 Adden, N.; Gamble, L.J.; Castner, D.G.; Hoffmann, A.; Gross, G.; Menzel, H. *Langmuir* **2006**, *22*, 8197-8204.

110 Hahner, G.; Hofer R.; Klingenfuss, I. *Langmuir* **2001**, *17*, 7047.

111 Van den Brand, J.; Blajiev, O.; Beentjes, P.C.J.; Terryn, H.; de Wit, J.H.W. *Langmuir* **2004**, *20*, 6308

112 Mutin, P.H.; Lafond, V.; Popa, A.F.; Granier, M.; Markey, L.; Dereux, A. *Chem.Mater.* **2004**, *16*, 5670-5675.

113 Adolphi, B.; Jähne, E.; Busch, G.; Cai, X. *Anal.Bioanal.Chem.* **2004**, *379*, 646-652.

114 Hanson, E.L.; Schwartz, J.; Nickel, B.; Koch, N.; Danisman, M.F. *J.Am.Chem.Soc.* **2003**, *125*, 16074-16080.

115 Doudevski, I.; Schwartz, D.K. *Appl.Surf.Sci.* **2000**, *175-176*, 17-26.

116 Benitez, I.O.; Bujoli, B.; Camus, L.J.; Lee, C.M.; Odobel, F.; Talham, D.R. *J.Am.Chem.Soc.* **2002**, *124*, 4363-4370

117 Michel, R.; Lussi, J.W.; Csucs, G.; Reviakine, I.; Danuser, G.; Ketterer, B.; Hubbell, J.A.; Textor, M.; Spencer, N.D. *Langmuir* **2002**, *18*, 3281-3287

118 Armstrong, N.R. et al. *J. Phys.Chem. C* **2008**, *112*, 7809-7817

119 Ma, H.; Acton, O.; Ting, G.; Ka, J.W.; Yip, H.-L.; Tucker, N.; Schofield, R.; Jen, A.K.-Y. *Appl.Phys.Lett.* **2008**, *92*, 113303-1

120 Attavar, S.; Diwekar, M.; Linford, M.R.; Davis, M.; Blair, S. *Appl.Surf.Sci.* **2010**, *256* (23), 7146-7150.

121 Herisson, J.L.; Chauvin, Y. *Makromol.Chem.* **1971**, *141*, 161.

122 Slugovc, C. *Macromol. Rapid Commun.* **2004**, *25,* 1283-1297.

123 Leitgeb, A.; Wappel, J.; Slugovc, C. *Polymer* **2010**, *51*, 2927-2946.

124 Sanford, M.S.; Love, J.A.; Grubbs, R.H. *Organometallics* **2001,***20*(25), 5314-5318.

125 Griesser, T.; Adams, J.; Wappel, J.; Kern, W.; Leggett, G.J.; Trimmel, G. *Langmuir* **2008**, *24*, 12420-12425

126 Hoefler, T.; Track, A.M.; Pacher, P.; Shen, Q.; Flesch, H.G.; Hlawacek, G.; Koller, G.;

Ramsey, M.G.; Schennach, R.; Resel, R.; Teichert, C.; Kern, W.; Trimmel, G.; Griesser, T. *Mat.Chem.Phys.* **2010**, *119*, 287-293

127 Lex, A.; Pacher, P.; Werzer, O.; Track, A.M.; Shen, Q.; Schennach, R.; Koller, G.; Hlawacek, G.; Zojer, E.; Resel, R.; Ramsey, M.; Teichert, C.; Kern, W.; Trimmel, G. *Chem.of Mater.* **2008**, *20(5),* 2009-2015

128 Michaelis, A.; Kaehne, R. *Berichte* **1898**, *31*, 1048.

129 Arbuzov, A. E. *J. Russ. Phys. Chem. Soc.* **1906**, *38*, 687

130 De Leon, L.; Biewer, M:C.; *Tetrahedron Letters* **2000**, *41*, 3527-3530.

131 Frey, B.L.; Hanken, D.G.; Corn, R.M. *Langmuir* **1993**, *9*, 1815.

132 Dattilo, D.; Armelao, L.; Fois, G.; Mistura, G.; Maggini, M. *Langmuir* **2007**, *23*, 12945-12950

133 Ipe, B.I.; Mahima, S.; Thomas, K.G. *J.Am.Chem.Soc.***2003**, *125*, 7174-7175.

134 Galvin, J.M.; Schuster, G.B. *Supramol.Sci.* **1998**, *5* (1-2), 89-99

135 Bethell, G.S.; Ayers, J.S.; Hancock, W.S.; Hearn, M.T.W. *J.Biol.Chem.* **1979**, *254*, 2572.

136 Oda, H. *Dyepig*, **1993**, *23*, 1-12

137 De Mayo, P.; Safarzadeh-Amiri, A.; King Wong, S.; *Can.J.Chem.* **1984**, *62*, 1001-1002.

138 Keum, S.R.; Roh, S.J.; Ahn, S.M.; Lim, S.S.; Kim, S.H.; Koh, K. *J. Dyepig* **2007**, *74*, 343-347.

139 Rosario, R.; Gust, D.; Hayes, M.; Springer, J.; Garcia, A.A. *Langmuir* **2003**, *19*, 8801-8806.

140 Testoni, F.M.; Ribeiro, E.A; Giusti, L.A.; Machado, V.G. *Spectrochim.Acta A* **2009**, *71*, 1704-1711

141 Shen, Q.; Cao, Y.; Liu, S.; Steigerwald, M.L.; Guo, X. *J.Phys.Chem.C.* **2009***, 113* (24), 10807–10812.

142 Gottlieb, H.E.; Kotylar, A.; Nudelman, A. *J. Org.Chem.* **1997**,*62*, 7512-7515.

143 van Oss, C. J.; Chaudhury, M. K.; Good, R. J. *Chem. Rev.* **1988**, *88*, 927.

144 van Oss, C. J. *Interfacial Forces in Aqueous Media*; Marcel Dekker: New York, 1994.

145 Nevot, L.; Croce, P. *Rev. Phys. Appl.* **1980**, *15*, 761.

146 Sun, Y.; Liu, Y.; Zhu, D. *J. Mater. Chem.* **2005**, *15*, 53.

147 Koezuka, H.; Tsumura, A.; Ando, T. *Synth.Met.* **1987**, *18*, 699.

148 Horowitz, G. *Adv. Mater.* **1998**, *10*, 365.

149 Katz, H. E. *Electroanalysis* **2004**, *16*, 1837.

150 Dodabalapur, A. *Materials Today* **2006**, *9*, 24.

151 Zaumseil, J.; Sirringhaus, H. *Chem. Rev.* **2007**, *107*, 1296.

152 Facchetti A. *Materials Today* **2007**, *10*, 28.

153 Hamadani, B. H.; Corley, D. A.; Ciszek, J. W.; Tour, J. M.; Natelson, D. *Nano Lett.* **2006**, *6*, 1303.

154 Salleo, A.; Chabinyc, M. L.; Yang, M. S.; Street, R. A. *Appl. Phys. Lett.* **2002**, *81*, 4383.

155 Chua, L.-L.; Friend, R. H.; Ho, P. K. H. *Appl. Phys. Lett.* **2005**, *87*, 253512.

156 Kobayashi, S.; Nishikawa, T.; Takenobu, T.; Mori, S.; Shimoda, T.; Mitani, T.; Shimotani, H.; Yoshimoto, N.; Ogawa, S.; Iwasa, Y. *Nature Mater.* **2004**, *3*, 317.

157 Yoon, M.-H.; Kim, C.; Facchetti, A.; Marks, T. J. *J. Am. Chem. Soc.* **2006**, *128*, 12851.

158 Smits E.C.P. et al. *Nature* **2008**, *455*, 956-959